Heat Transfer at the Mold - Metal Interface in Permanent Mold Casting of Aluminum Alloys Project

Final Report

Professor R.D. Pehlke, Principal Investigator
Dr. John M. Cookson, Dr. Shouwei Hao,
Dr. Prasad Krishna, Kevin T. Bilkey

Department of Materials Science and Engineering
The University of Michigan
Ann Arbor, MI 48109-2136

December 14, 2001

Prepared for

THE U.S. DEPARTMENT OF ENERGY
AWARD NO. DE-FC07-97ID13559

Sponsored by:

Project Partners:

TABLE OF CONTENTS:

Executive Summary 5

1. Summary of Design Concepts 10

2. The HTC Programs 21

2.1 The Structure of the HTC Programs 21

2.2 The Interface of the HTC Programs 22

2.3 The File Description 22

2.4 The External Data Structure 24

2.5 The Internal Data Structure 24

3. The Experimental Study at CMI-Tech. Center 25

3.1 The Experimental Mold 25

3.2 The Objective of the Experiments 25

3.3 The Pressure Sensors 26

3.4 Experimental Plan 29

3.5 Literature Search 29

4. Experimental Study at Hayes-Lemmerz Tech. Center 30

4.1 Objectives of the Experimental Study 30

4.2 Experimental Data Sheet 31

4.3 Experimental Process Variables 31

4.4 Problems 31

4.5 Location of Measurements 32

4.6 Sample Experimental Data 32

4.7 Experimental Data Analysis 33

5. Squeeze Casting Metallographic Study at UM 40

6. Solidification Simulation at UM 44

7. Experimental Anslysis at Hayes-Lemmerz Tech. Center 51

8. Experimental Study at Amcast Automotive 54

9. LPPM Solidification Simulation at UM 57

10. Die Coating Analysis at UM 67

11. Metallographic Inspection of Wheel-Like Casting 84

12. Influence of Mold Coating Parameters on Interfacial Heat Transfer in the LPPM Casting Process 93

13. Influence of Air Gap Formation on Interfacial Heat Transfer in the LPPM Casting Process 94

14. CMM Measurement Results at Hayes-Lemmerz Tech. Center 95

15. References 99

Appendix A 104

Executive Summary:

This project on heat transfer coefficients in metal permanent mold casting has been conducted in three areas. They are the theoretical study at the University of Michigan, the experimental investigation of squeeze casting at CMI-Tech Center (Now Hayes-Lemmerz Technical Center) and the experimental investigation of low pressure permanent mold casting at Amcast Automotive.

At the University of Michigan, a sensitivity analysis was conducted. A brief analysis of the role of size on the temperature and fraction of solid distribution was performed for geometry approximating that of a wheel casting. This arose from the interest Amcast had expressed in fabricating a new mold, and the need to establish how closely the geometry of the experimental mold should match the geometry of molds in production. An initial geometry was defined for ProCAST to solve, and then a geometry half the size was defined and solved using the same boundary conditions. A conceptual mold geometry was examined and represented as an axisymmetric element. Furthermore, the influences of the localized heat transfer coefficients on the casting process were carefully studied. The evaluation of a 2-D interfacial heat transfer coefficient was undertaken.

In the initial year, the HTC Evaluator was proposed and initially prepared by the U-M team. The Reference and the Database Modules of the HTC Evaluator were developed, and extensively tested. The abstracts, key figures and conclusions of 68 papers related to this project were input. The relevant literature has been sorted and has been sent to the AFS Library. The distribution of 68 papers collected in terms of casting processes are Permanent mold casting: 26, Sand casting: 17, Continuous casting: 5, Investment casting: 4, Squeeze casting: 2, Die casting: 5, Other: 9. The development of a semi-automatic geometry recognizer has been undertaken. A series of technical barriers have been cited and potential solutions have been surveyed. The list of all the articles is presented in this report.

At the CMI-Tech Center, the Kistler direct cavity pressure measurement system was purchased and tested. The calibration was evaluated. The probe is capable of sensing a light finger pressure. An experimental mold was designed and modified. The first experiments were scheduled for October 14, 1998. The geometry of the experimental hockey-puck casting was given to the U-M team for numerical analysis.

At Amcast, an experimental mold was designed and prepared for fabrication. A thermal monitoring system was investigated. Some ambient temperature data were collected from a production mold. It was found that quite different heat transfer conditions exist on different parts of the exterior mold faces. A proposed ultrasonic gap formation measurement was regarded as promising. Three quotations for an ultrasonic gap formation measurement system were obtained. The quotations were forwarded to Amcast for review. Amcast reached a final stage for review of the cost of the system and its suitability for their purpose.

The first series of experiments at the Hayes-Lemmerz Tech Center (formerly CMI Tech Center) was successfully conducted on October 14 and 15, 1998 with the participation of the University of Michigan team (Prof. Pehlke, Dr. S.W Hao and Mr. Prasad Krishna). The Hayes-Lemmerz Tech Center team (Karl Voss, Don Roberts, Gregory Woycik, David Moore, Christopher Rohloff, Douglas Moran, and Mike Griff) had successfully designed the die, modified the die and instrumented the die with the help of the U-M team. We gratefully acknowledge their valuable contributions to the success of the experiments.

The preliminary experimental results indicated that the die surface temperature (or near the surface) influences the metal pressure profiles. If we consider the time difference in reaching the peak die temperatures, the higher melt temperature, and hence hotter die temperature for the high melt temperature and low pressure case would cause a longer solidification time and a slower decrease in the pressure than for low melt temperature and low pressure.

The slopes of the metal pressure profiles for the low pressure case were almost linear which would imply that the low metal pressure was not effective in keeping a pressure channel open. In other words, as temperature decreased, the solid fraction increased and the solidified shell strengthened, and the applied pressure, which could not overcome the resistance of the shell, would drop linearly. On the other hand, for the high pressure case, there were inflection points on the pressure curve. The inflection points occurred at about a pressure of 8500 psi for both the low and high melt temperature settings. This suggests that the metal pressure was sufficient enough to overcome the resistance of the solidified shell before the inflection point was reached. This also means that the pressure channel could be kept open longer and larger. In our case, when the inflection points were reached (at about 8500 psi), the solidified shell became strong enough to resist the intensification pressure. As a result, the slopes of the pressure profiles became steeper than before the inflection points.

At the high pressure setting, the higher melt temperature (1375 °F) slightly prolonged the time of pressure influence. The peak pressure values at the low melt temperature and at the high melt temperature settings were the same. However, at the low pressure setting, the melt temperature had a more significant influence on the pressure profile. This may also suggest that the low pressure was insufficient in our case. As a result, any change in other conditions, such as melt temperature and die temperature, would severely affect the quality of the castings.

Microstructural analysis shows that the dendrite arms at the location near the gate were much coarser than that at the top of the casting. Microstructures for both Low Pressure and High Pressure squeeze cast specimens were compared. The grain structure at the gate, close to the pressure sensor location, and away from the gate at the top of the casting, were also analyzed. A meeting was held on the 19th of March, 1999, at Climax Research Services to discuss the metallographic techniques for squeeze cast A356 alloys The meeting confirmed our method of specimen preparation and measurement of

Secondary Dendrite Arm Spacing. A few sample micrographs taken for the low pressure hockey puck-like shaped casting sample are enclosed in this report

A number of solidification simulations were conducted using various Interfacial Heat Transfer Coefficient (IHTC) values. The estimated IHTC, which provided the best fit between the computed and experimental cooling curve, were reported. The variations of heat transfer coefficient with solidification time and with cooling rate were also given, respectively.

Some observations made relating to the *Dendrite Arm Spacing* with the established relationship between the *cooling rate* and *local solidification time* are reported. The UM team had gone through the report from Dr. Ken Dolan of Lawrence Livermore which was delivered to the U of M by Hayes-Lemmerz Tech Center (HLTC) and observed that no immediate conclusion can be drawn from the testing of the newly developed fiber optic temperature sensor. It is learned from the report that, further testing and or calibration is required before the sensor can be commercialized. Some observations made while surveying journal articles on squeeze casting that are relevant to this project have been reported. UM compilations of literature on die coating and its effect on heat transfer are also reported.

Measurements of Secondary Dendrite Arm Spacing (SDAS) from the optical micrographs on the Hayes-Lemmerz squeeze casting indicated a very fine spacing, which are smaller than measurements reported in the foundry literature. Hayes-Lemmerz Tech Center conducted a spectrometric analysis of the squeeze casting samples for possible presence of grain modifying elements in the aluminum alloy.

A geometric model of the wheel-like test mold at Amcast was created and imported into MAGMAsoft for enmeshment. Low pressure PM experimental trials with the wheel-like test mold were conducted by Amcast Automotive on December 28, 1999 at their Fremont plant in Indiana. A detailed layout of the thermocouple locations inside the mold and the experimental parameters are presented. Temperature measurements from all the thermocouple locations were analyzed and used for estimating appropriate HTC values for each segment of the mold.

A new methodology to better simulate the experimental runs for the Low Pressure Permanent Mold (LPPM) casting experiments at Amcast Automotive, Fremont, Indiana is presented.

Some issues on die coatings and relative conductance values for the experimental trials conducted by Amcast Automotive on December 28, 1999 are reported.

The chemical composition of the alloy as reported by Amcast is comparable to that of the alloy used in the squeeze casting experiments

Results of fifteen simulations for the Low Pressure Permanent Mold (LPPM) casting experiments at Amcast Automotive, Fremont, Indiana with the segmented mold geometry data received from Amcast are compared in this report.

HTC distribution for the interface between the top core and casting has been modified in these simulations by adding a constant HTC period to better fit the experimental data. While the coating parameters were kept unchanged, the air gap for each simulation version was increased and the time for constant HTC decreased. The HTC distribution for the face core-casting interface is kept unchanged as it results in a very good match with the experimental data.

Comparison of experimental and simulated curves showed a large decrease in the HTC from 1765 to 500 W/m^2 K in about 40 seconds at the interfacial mold segments 1 (middle-inner) and 2 (top-inner), indicating a larger air gap formation than previously assumed.

It was observed from the simulations that the assumption of no air gap at the outer segments 4 and 5 between the mold and casting did not result in a good matching of the curves.

It is also seen from all of these simulations that the air gap does not influence the interfacial heat transfer after a lapse of about 300 seconds. The conductance and thickness of the die coatings as well as the surface roughness of the interfaces mainly control heat transfer at this stage.

Amcast sent five coating samples to UM, each representing the actual coating condition on the top and bottom die halves and the respective layers of coating, insulating as well as non-insulating. Optical micrographs of the die-coating samples received from Amcast are presented. Measured coating thickness data are shown. The average coating thickness of an insulating coating was found to be close to 43 μm compared to the earlier assumed value of 100 μm.

A different HTC distribution with an air gap of 50 μm and a reduced thermal conductivity of the die coating at outer segments 4 and 5 and inner segment 3 used in these simulations resulted in a better fit of the experimental data at these mold segments.

A temperature dependent HTC distribution for segments 1and 2 for these simulations in which the IHTC decreases from 1900 W/m^2 K to 300 W/m^2 K, when the temperature drops from the liquidus (613 °C) to the solidus (542 °C), resulted in a good match of the simulated and experimental cooling curves at mold segments 1 and 2. A corresponding time dependent HTC distribution indicated a large air gap of about 200 μm at these locations.

It is observed that a low coating thermal conductivity, and hence a lower overall HTC value at the interfacial mold segments 3, 4 and 5, seems to yield a relatively closer fit for every subsequent simulated version

Results of the fifteenth simulation show a comparatively good match at all the interfacial segments, and thereby identify the interfacial heat transfer coefficients for the present case study.

IT IS OBSERVED FROM THESE SIMULATIONS THAT THE METAL-MOLD INTERFACIAL HEAT TRANSFER AFTER AN AIR GAP FORMATION IS CONTROLLED PRIMARILY BY THE COATING PARAMETERS.

Results of the metallographic inspection of the wheel-like casting samples received from Amcast are presented.

Secondary Dendrite Arm Spacing (SDAS)-Cooling Rate Correlation developed for the LPPM casting is presented and compared with values reported in the literature.

1. SUMMARY OF DESIGN CONCEPTS

HEAT TRANSFER DESIGN IN PERMANENT MOLD CASTING
OF ALUMINUM ALLOYS

Introduction

In this investigation, two permanent mold casting processes were investigated: squeeze casting and low pressure permanent mold casting. The same alloy, modified aluminum alloy A356, was used in both studies. The characteristics of these casting processes are described in this report.

Squeeze Casting

In the squeeze casting process, a critical pressure (threshold pressure) is a key parameter in determining the maximum required pressure to reach the highest interfacial heat transfer coefficient. This pressure is on the order of 4200 psi, but may vary with alloy composition, and in the case of S. Okada, et al., "Development of a fully Automatic Squeeze Casting Machine", AFS Transactions, 82-16, (1982), pp. 135-146, the reported critical pressure was given in terms of the silicon content which for A356 alloy would be about 6600 psi. At pressures below this critical level, Y. Nishida and H. Matsubara, "Effect of Pressure on Heat Transfer at the Metal-Mould Interface", British Foundryman, V. 69, (1976), pp. 274-278, found from applying loads to solidifying castings that the increase in interfacial contact pressure rapidly rose to a maximum. Over a range of loads from 250 Kg to 30,000 Kg, these peak heat transfer coefficients ranged from 4,000 to 50,000 W/m^2-°K.

At the critical pressures obtained in this investigation, a maximum interfacial heat transfer coefficient of 4500 W/ m^2-°K provided the best fit between the simulated and experimental data. I.S. Cho and C.P. Hong, "Evaluation of Heat Transfer Coefficients at the Casting/Die Interface in Squeeze Casting", Int. J. Cast Metals Res. 1996, 9, pp. 227-232, reported an HTC value of about 4700 W/ m^2-°K for squeeze casting of Al-4.5% Cu alloys at a pressure of about 50 Mpa. The squeeze casting studied in this investigation is shown in Figure A.

Low Pressure Permanent Mold Casting

In low pressure permanent mold casting, the casting and mold may separate during the solidification and cooling process, leading to the formation of gaps which result in a dramatic decrease in heat transfer between casting and mold. This is reflected in the values of the interfacial heat transfer coefficients. With the complex shapes and various constraining configurations between mold and casting, the locations of gap formation as the casting cools and the mold surfaces increase in temperature will vary in every case. In addition, mold coatings also influence casting-mold heat transfer, even more so than in the case of squeeze casting where a mold release agent, rather than a thin refractory coating is used to separate the solidifying casting and the metal mold.

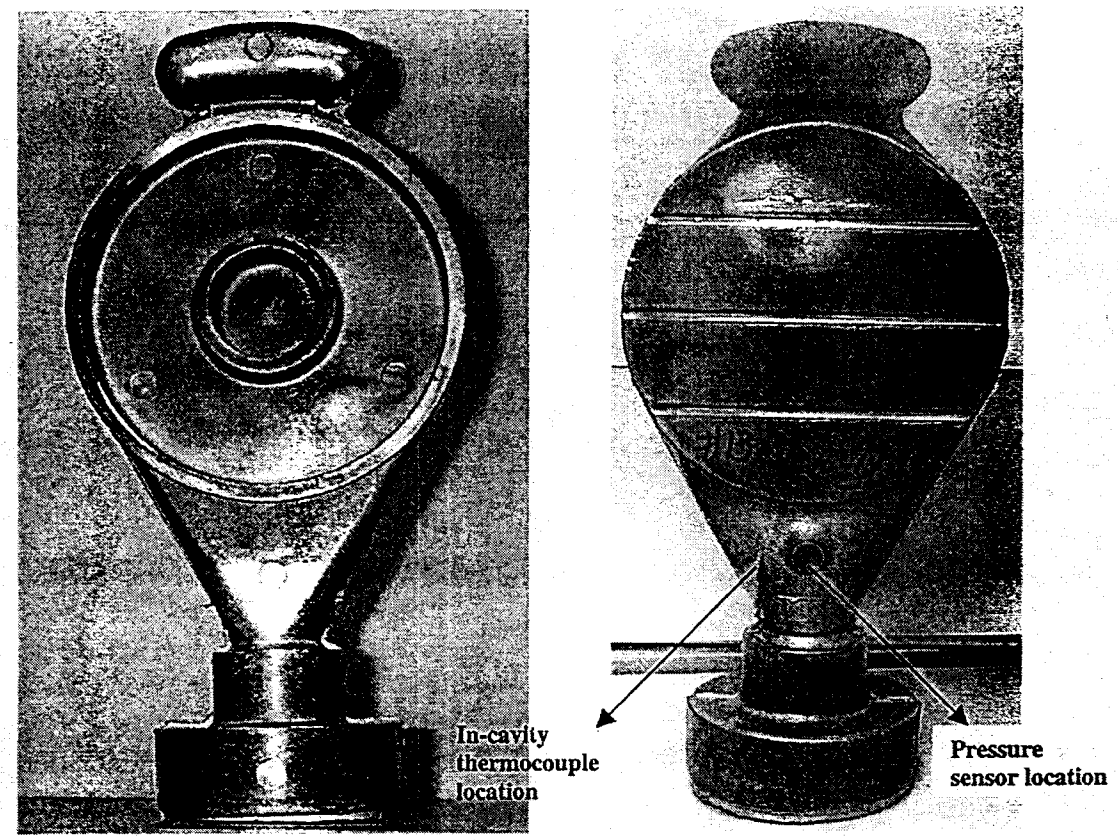

Figure A. Photograph of Hockey-Puck like Shaped Casting Showing Front and Rear

In this study, a wheel-like casting shown in Figure B was divided into several segments (Figures C and D) and the cooling traverses estimated (Ph.D. thesis of Prasad Krishna, University of Michigan, Ann Arbor, 2001). By analyzing thermal measurements taken during the casting process, the interfacial heat transfer coefficients for each segment were deduced using a straight-forward direct method involving interactions of the heat transfer coefficient profiles with time. The results of these analyses are summarized in Figures E-G. The interfacial heat transfer coefficient varied from 625-2000 W/ m^2-°K, depending the location, and eventually decreased to about 300-400 W/ m^2-°K due to an air gap formation with the limiting value depending on the mold coating.

Comparison of Squeeze Casting and Low Pressure Permanent Mold Casting

A comparison of the HTC distributions of the low pressure permanent mold casting process and the squeeze casting process is presented in Figure H. The heat transfer coefficient is much higher in the squeeze casting process because of the high pressure applied to the solidifying casting. A maximum value of 4500 W/ m^2-°K was

observed for the squeeze casting process versus maximum values varying from 625-2000 W/ m^2-^oK for the low pressure permanent mold casting process.

Influence of Mold Coating Parameters on Interfacial Heat Transfer in the LPPM Casting Process

In the LPPM casting process, a mold coating of 40 to 100 um thickness which has an insulating effect is applied to the mold and influences the casting to mold heat transfer. In the squeeze casting process, a very, very thin layer of "separating agent", usually an emulsion of graphite flakes in a carrier, is sprayed on the mold which has a minimum effect on heat transfer during the casting process.

The overall thermal resistance at the metal-mold interface, R_{total} (reciprocal of which is the overall HTC) during solidification in the LPPM process is the sum of the thermal resistance due to the mold coating, $R_{coating}$ and the thermal resistance due to the air gap formation R_{gap}. Considering conduction as the primary mode of heat transfer (radiation heat transfer can be neglected for metal mold casting of aluminum alloys), $R_{coating}$ is determined by the ratio of coating thickness to the thermal conductivity of the coating material.

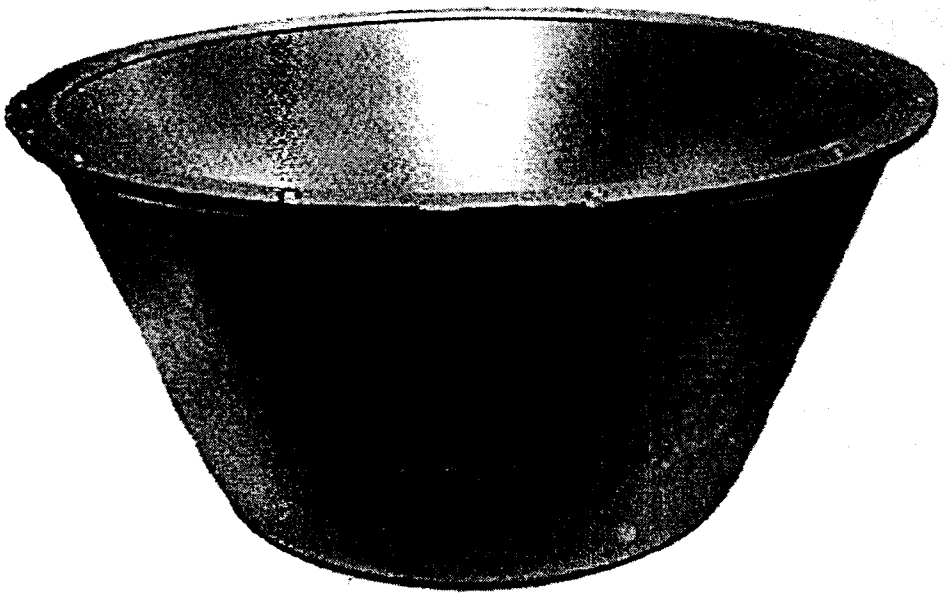

Figure B. Photograph of the Wheel-like Shaped Casting produced by LPPM Casting Process

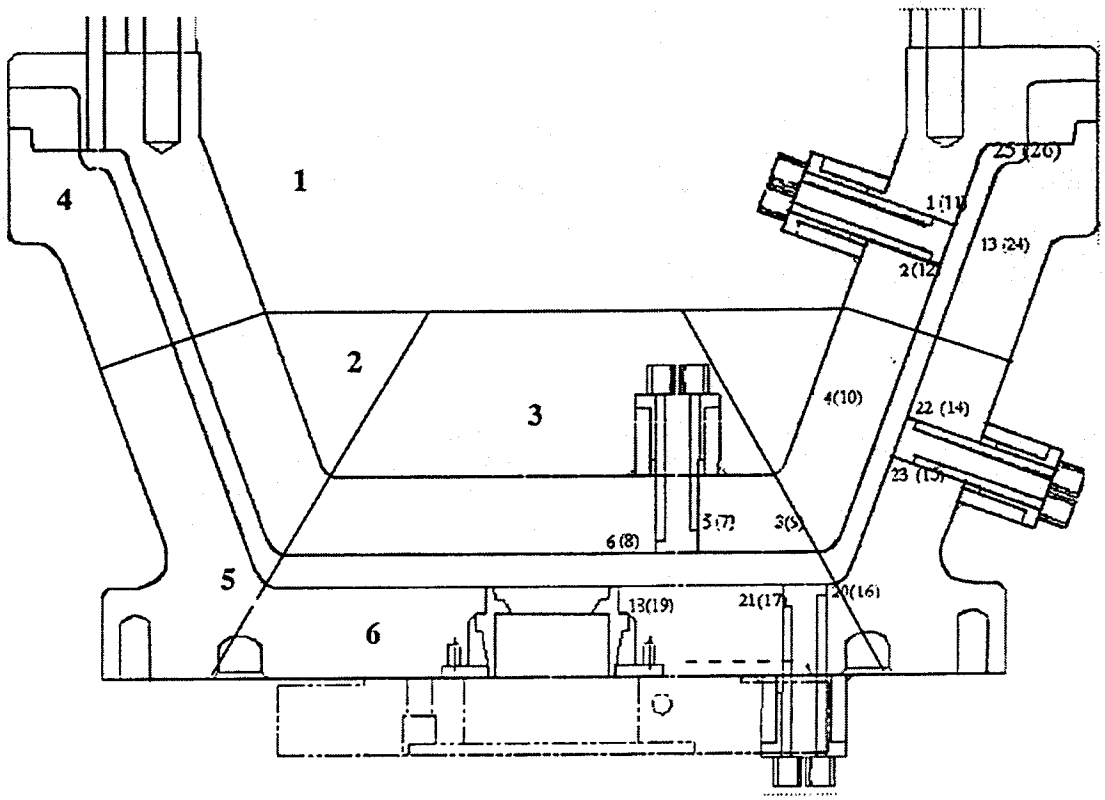

Figure C. A Cross Section of the Low Pressure Permanent Test Mold Showing Thermocouple Arrangement.

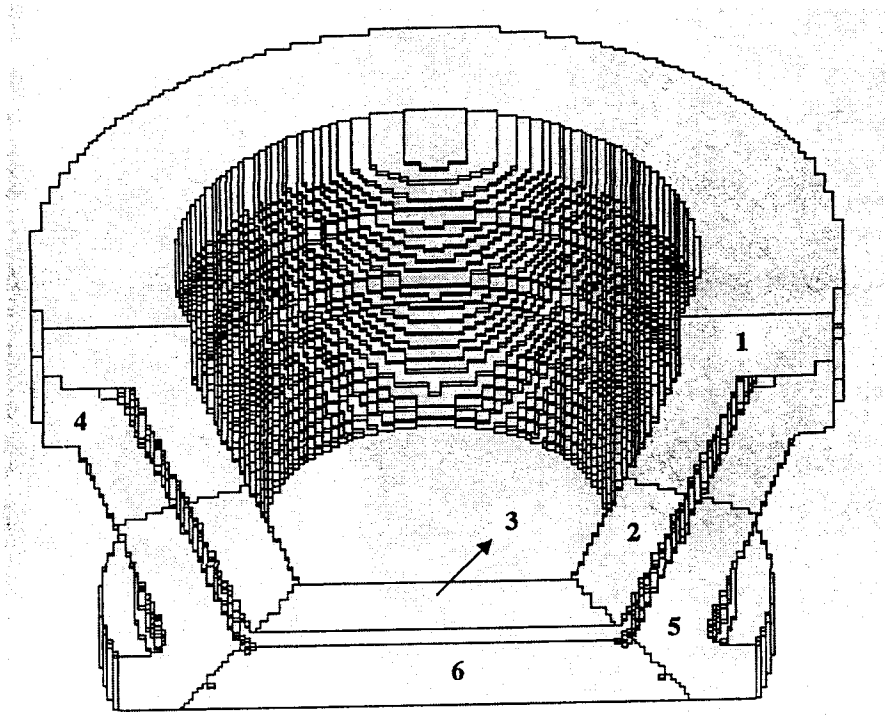

Figure D. A Section of the Segmented Mold for the Wheel-like Shaped Casting Showing all the Six Segments

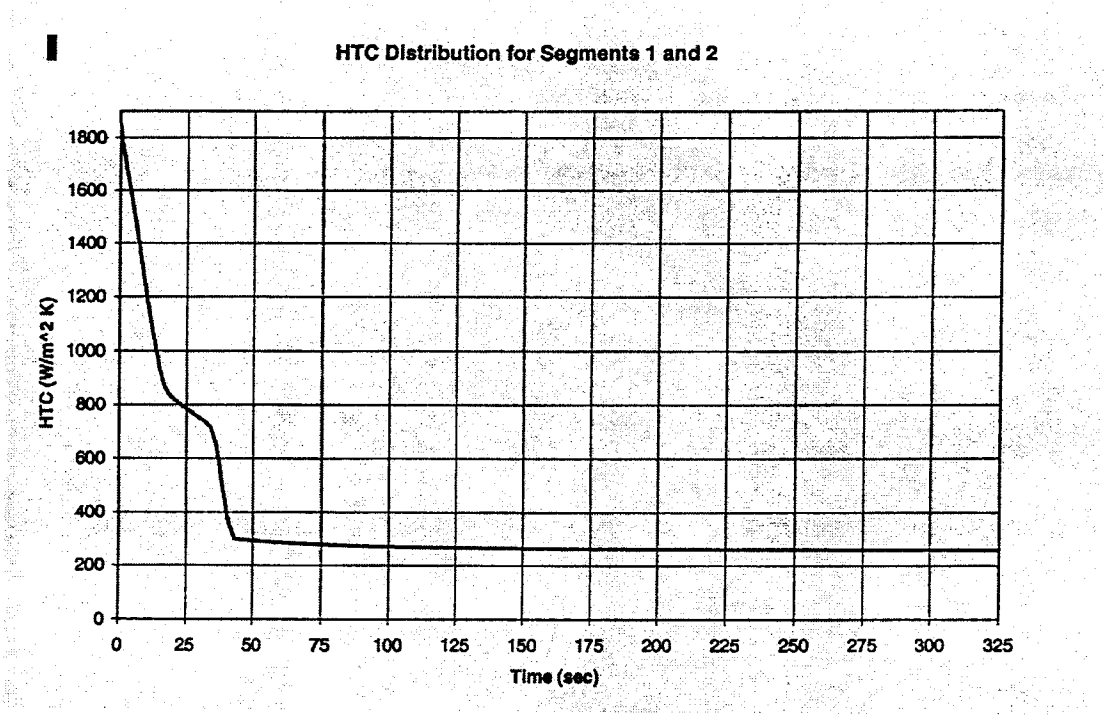

Figure E. HTC Distribution for Segments 1 and 2

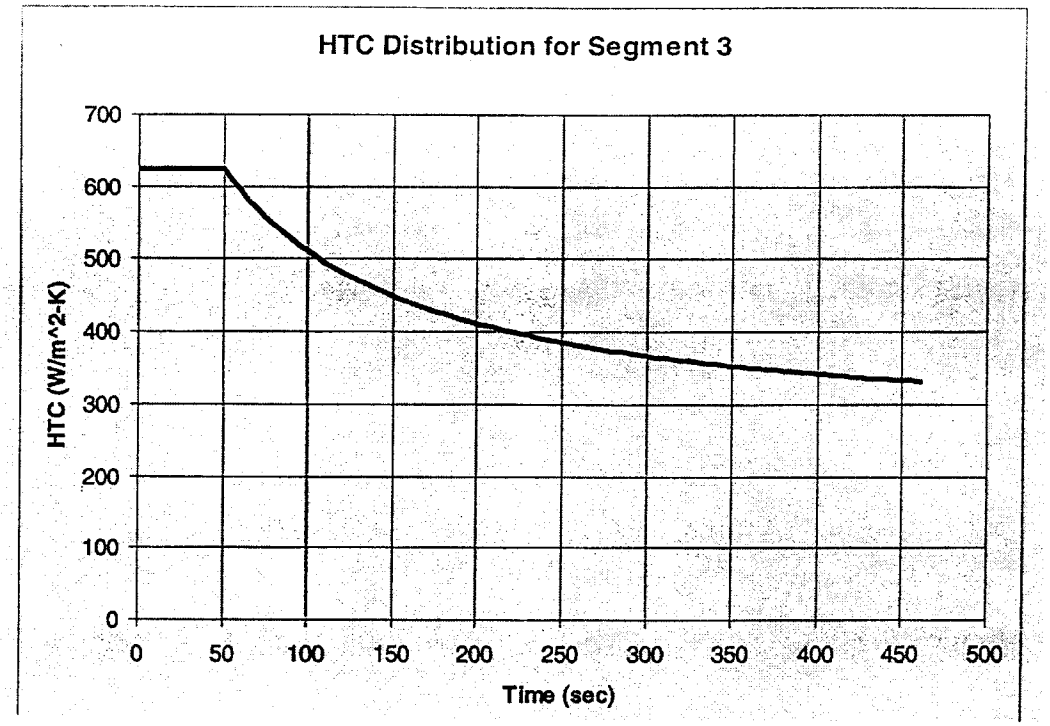

Figure F. HTC Distribution for Segments 3,4 and 5

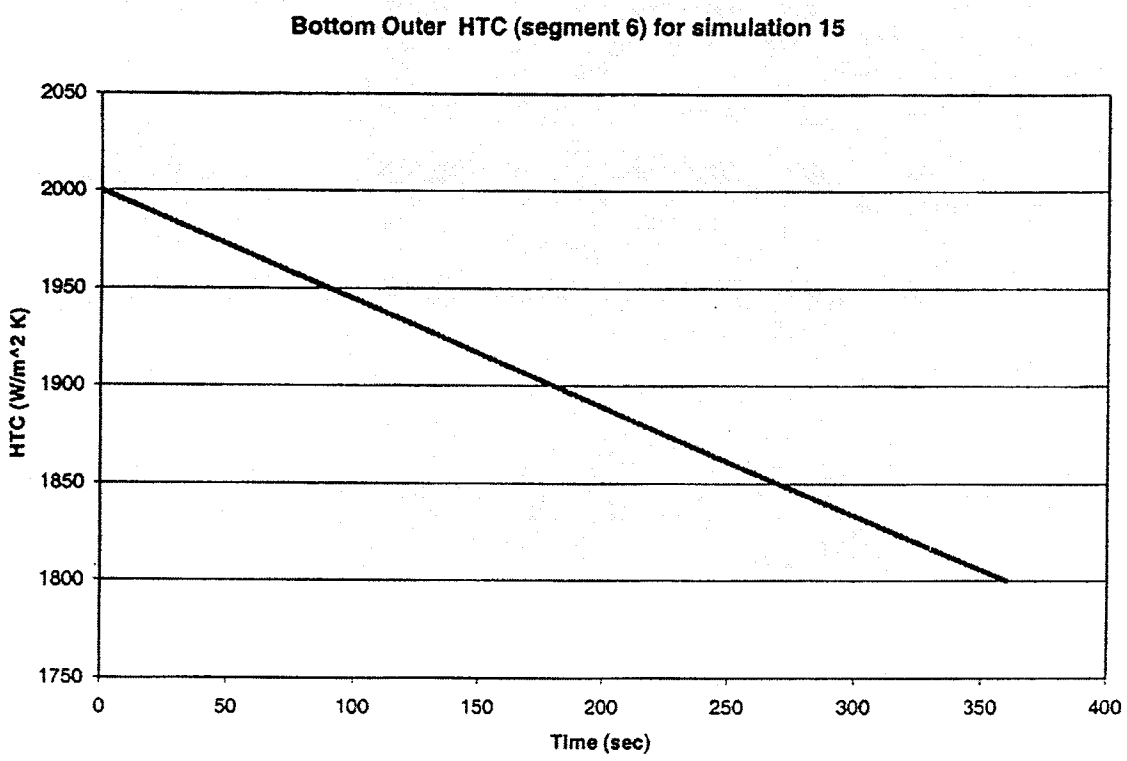

Figure G. HTC Distribution for Segment 6

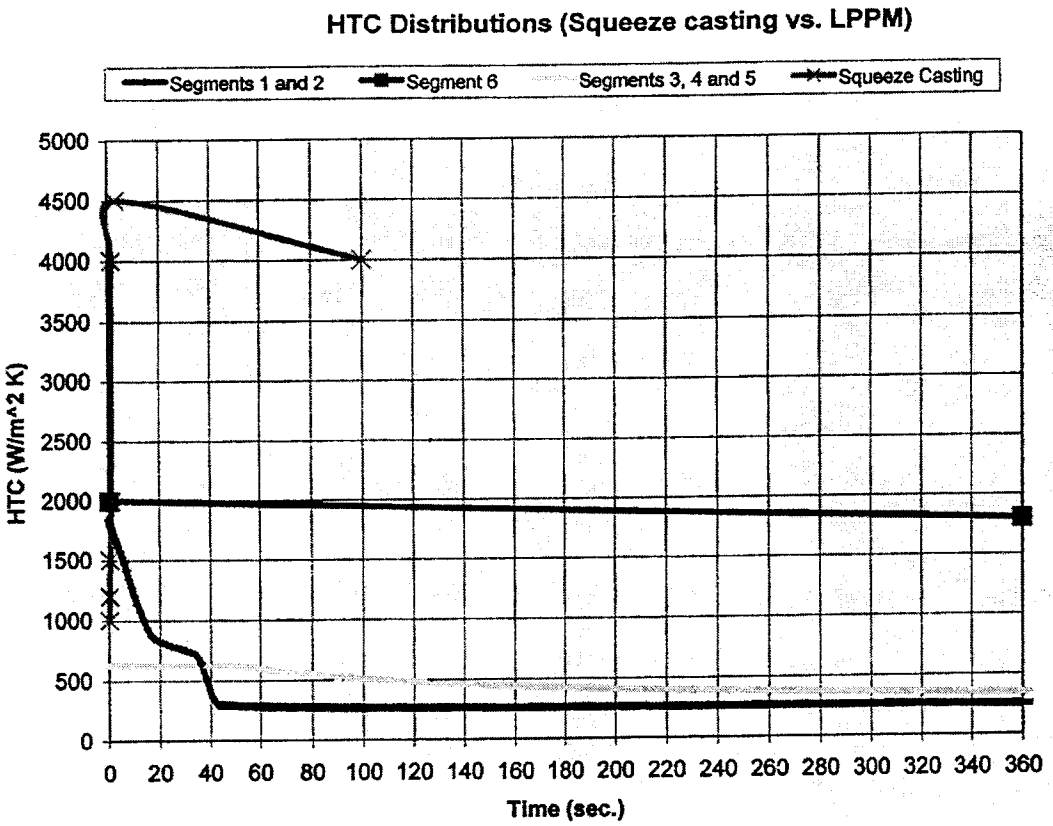

Figure H. A comparison of the HTC Distributions between the Squeeze Casting and LPPM Casting Processes

The conductivity is also found to vary with temperature and with the thickness and porosity of the coating as well. The compositional variations among different manufacturers of coating materials, as well as the influence of grain size, porosity and method of spraying the coating, influence the insulating performance, and further complicate their applicability of estimated thermal properties of the coating. Maintaining a uniform coating thickness on the mold surface is another problem. Frequent touch-up of the mold surfaces in between shots and the different methods of applying the coating materials on the mold surfaces result in large variations of coating thickness.

Considering all the above factors, the influence of coating parameters (thickness and thermal conductivity) on the cooling behavior of the casting were studied by varying these parameters in the simulations and analyzing the mold temperature history resulting from that change. To analyze the effect of thermal conductivity of the coating, K, in the overall HTC, values of K were varied from a maximum value of 0.46 to a minimum value of 0.08 W/m K, while keeping a constant thickness of 100 μm and a maximum air gap of 50 μm. The effect is shown in Figure I. The HTC values shown in the figure are the maximum values. The HTC eventually decreases to a minimum value of 300-400 W/m^2K during the solidification process. When the coating thickness was varied from 50 to 100 μm, keeping K=0.3 W/m K, the overall HTC decreased from 1938 W/m^2K for a thickness of 50 μm to 1465 W/m^2 K for a thickness of 100 um.

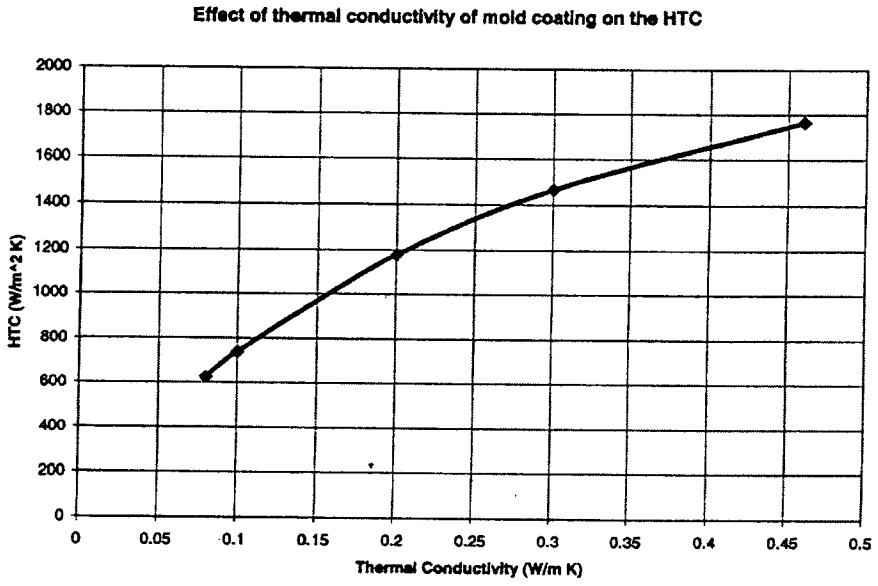

Figure I. Effect of Thermal Conductivity of Mold Coating on the HTC (Coating Thickness-100 um and Maximum Air Gap = 50 um)

Influence of Air Gap Formation on Interfacial Heat Transfer in the LPPM Casting Process

Determining and characterizing air gap formation in a permanent mold casting process is critical to the description of heat transfer. In the absence of measurements of the formation of an air gap at the interface, one can use the correlation developed by M. Trovant and S. Argropoulos, Metallurgical and Materials Transactions, Vol. 31B, February 2000, pp. 75-96 to relate the HTC with the air gap, based on an assumption of the gap behavior. The correlation developed by them is:

$H_{gap} = 1/(0.072)(A) + 0.000373 + 244$

where A is the air gap thickness in mm. The equation gives an initial h_{gap} value (with no air gap) of about 2900 W/m^2K. With a mold coating of K = 0.46 W/m K and thickness – 100 um, the overall HTC is as 1765 W/m^2 K. Thus on the onset of an air gap formation, if the coating properties remain unchanged, the overall HTC will be limited to a maximum value of 1756 W/m^2 K, no matter what may be the air gap. Assuming a linear distribution of air gap with the progress of solidification, the maximum assumed air gap in each simulation was distributed over a total period of about 400 seconds. To study the influence of air gap formation on the overall HTC distribution with time, different air gap thickness values ranging from 50 um to 500 um were used, keeping the coating parameters constant. The effect is presented in Figure J. Thus it can be seen that the air gap determines the rate at which the overall HTC decreases with time. A larger air gap at the interface will result in a rapid decrease of the HTC to a minimum value of 300-400 W/m^2 K. It is also observed from Figure J that the HTC approaches a minimum value of 350-500 W/m^2 K, independent of the air gap thickness. The HTC at this stage is governed by the coating properties.

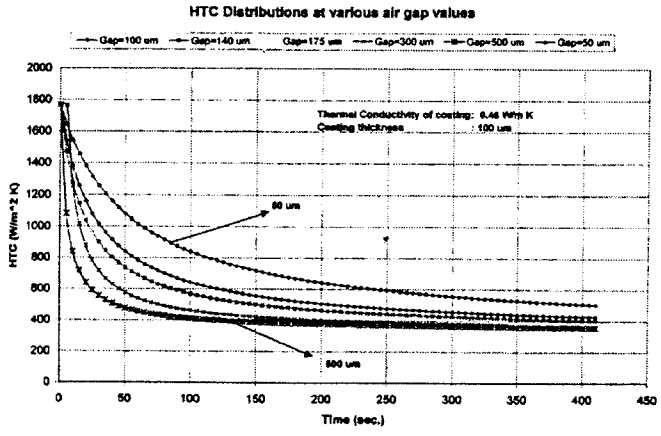

Figure J. Influence of Air Gap Thickness on the HTC Distribution

Guidelines for the Heat Transfer Designer

Given the uncertainties when one starts to design a casting and its related mold for permanent mold casting, the designer can proceed in the following manner.

First of all, for squeeze casting, the interfacial heat transfer coefficient depends on the pressure applied during solidification, with a constant HTC above a threshhold pressure. These relationships are reasonably well defined.

With regard to low pressure permanent mold casting, the following steps can be taken:

1. Break the casting-mold interface into segments, depending on whether a gap is unlikely to form, be delayed in the formation of a gap, or almost immediately form a gap after solidification has been initiated.
2. Characterize the gap behavior with time.
3. Include the mold coating in the heat transfer analysis.

While each of these steps is experience or intuition based, the heat transfer analysis can be parameterized to provide an overall view of the possible, and limiting, behaviors.

The preceeding analysis of the simulation of heat transfer in the low pressure permanent mold casting process should provide a range of heat transfer parameters which will aid in optimizing the design of the casting and mold.

2. THE HTC PROGRAMS

2.1. The structure of the HTC programs

The HTC program is implemented by Visual C++ on PC platforms. Object-oriented techniques and a document/view pattern are adopted in the HTC design.

The modules that the HTC includes are:

i) Reference Module

This module is related to the reference processing, which is divided into eight casting categories: squeeze, semi-solid, permanent, die, sand, investment, continuous and others. The functions include reference entering, browsing, finding, printing, modifying and deleting.

The graphics in references also can be processed, displayed and printed.

ii) Material Database Module

The material module is responsible for the processing of various materials. The material properties in this module include density, latent heat, solidus, volume shrinkage, liquidus, linear shrinkage, specific heat, solid fraction and thermal conductivity. Users can enter, modify, delete, browse and find any entry in the library with this module.

2.2 The interface of the HTC programs

Due to the program being based on the window platform, the interface of the HTC is very user friendly and easy to learn. When you enter the HTC program, the main window is displayed. In the client area of the window, the title, the project partner's mark and copyright will be displayed.

In the main window, there are the following menus and submenus:

File --- New, Open, Save, Save As, and Print view, Print, Print setting, Exit
DataBase --- New, Open
Reference --- Open, New, Find, Next, Previous, Delete
Exit
Option --- Toolbar, Status bar
Help --- Version, Description

2.3 The file description

The following gives the main programs in the HTC and their brief description:

. Htcc.h, Htcc.cpp

These are the main application source files that contain the application class CHtccApp.

. MainFrm.h, MainFrm.cpp

These files contain the frame class CMainFrame, which is derived from CFrameWnd and controls other frame features.

. HtccDoc.h, HtccDoc.cpp - the document

These files contain the CHtccDoc class, which implement file saving and loading.

. HtccView.h, HtccView.cpp - the view of the document

These files contain the CHtccView class.
CHtccView objects are used to view CHtccDoc objects.

. Base_open.h, Base_open.cpp

These files define a class CBase_open that are used to view and modify the Material Database.

. Data_base.h, Data_base.cpp

These files define a class CData_base which are used to renew a Material database entry.

. dibapi.h, dibapi.cpp, myfile.h, myfile.cpp, Frmfig.h, Frmfig.cpp

These files show the BITMAP graphs for reference.

. FileList.h, FileList.cpp

These files list the material category for reference.
Users can select one from the eight items.

. HelpText.h, HelpText.cpp

These files are used to display Help messages.

. MatList.h, MatList.cpp

These files list the material names which are already in the Data_base.

. RefDialog.h, RefDialog.cpp

These files define a Dialog box, which is used to view and modify the existing reference entry.

. RefInput.h, RefInput.cpp

These files define a Dialog box, which is used to add a new reference entry to the Database.

. RefList.h, RefList.cpp

These files define a class, which list the reference name in the current category.

. Temp_heat.h, Temp_heat.cpp

These files define a class which is used to enter heat and temperature and to show the corresponding diagrams.

. Warn.h, Warn.cpp

These files define a class which is used to give various warnings when an error occurs.

2.4 The external data structure

The external data are based in the hierarchy directory management. There are the following directories:

. $HtcRoot:

This variable defines the root directory in which the system will be installed.

. HtcRoot/Database

This directory contains material property information. Every material corresponds to a file. In this directory, the file <MaterialList.dat> contains all the existing material names.

. HtcRoot/Ref

This directory contains eight files, which are data files in correspondence to the eight casting categories, and eight sub-directories, which contain graphic files corresponding to the eight categories.

. HtcRoot/Projects

This directory includes many subdirectories, each of which is in correspondence to a project created by the File->New command.

. HtcRoot/Debug

The executable file is placed in the directory.

2.5 The internal data structure

The internal data structure can be divided into two kinds. The first one is related to the reference, the other one pertains to the material data.

(1) The reference data

```
class CRefEntry : public CObject
{
public:
```

```
  CString m_Title;
  CString m_Author;
  CString m_Abstract;
  CString m_Figure;
  CString m_Publ;
};

//reference data in htc
public:
  CObArray m_RefArray;
```

(2) The material data

```
class CDotEntry : public CObject
{
public:
  float m_Temperature;
  float m_Heat;
};

    // the material data in htc
public:
  CObArray m_DensityArr;
  CObArray m_LatentArr;
  CObArray m_SolidousArr;
  CObArray m_LiquidousArr;
  CObArray m_VolumeArr;
  CObArray m_LinearArr;
  CObArray m_SolidArr;
  CObArray m_SpecificArr;
  CObArray m_HeatArr;
```

---

3. THE EXPERIMENTAL STUDY AT CMI-TECH CENTER

3.1 The experimental mold

After meeting with U-M, CMI decided to use a "hockey puck" mold for the experiments. The mold required some minor modifications for the experiments. Pressure and temperature measurements will be conducted with pressure probes and thermocouples.

3.2 The objectives of the experiments

The objectives of the experiments at CMI were:

1) To predict the gate freezing time.

2) To predict whether a gap is formed.
3) To determine the correlation between pressure and porosity (if any).
4) To determine the HTC-pressure profile in squeeze and semi-solid casting.

3.3 The pressure sensors

There are two ways of measuring the cavity pressure in die casting and squeeze casting. They are indirect cavity pressure measurement and direct pressure measurement.

In indirect measurement, a movable pin is used to deliver the pressure from the cavity to a sensor outside the mold. In direct measurement, the sensor is installed to contact directly with the liquid metal. This can provide more accurate data with a shorter response time than the indirect pressure measurement.

The cost of a direct pressure sensor is high, roughly $2000/piece. There is feedback regarding a short lifetime for the direct pressure sensor in the application of squeeze casting from the industry. The reason for failure of the sensor is still unknown. It might be caused by high temperature during a relative long solidification time. Dr. S.W. Hao has experience in using the pressure sensors in Singapore for high pressure die casting and semi-solid casting experiments. He has not had problems with the pressure sensors up to 500 shots. The supplier of the pressure sensors has some experimental data showing that the direct pressure sensor can last for more than 100,000 shots.

After careful review and discussion with the vendors, CMI and U-M believed that the Kistler pressure sensor could fit the application for this project.

CMI purchased a system for direct cavity pressure measurement from Kistler based on suggestions from U-M. The system and pressure probes were delivered and checked item by item by both CMI and U-M. The hockey-puck casting was selected for this project.

The Kistler pressure sensor is shown in Fig.1 and it is the same type as those used at The Ohio State University [1] and the Gintic Institute of Manufacturing Technology, Singapore [2].

Fig. 1 The Direct cavity pressure probe for Die Casting (Type 6175A2)
(Courtesy Kistler, Switzerland)

A flow-chart of the direct cavity pressure measurement system is illustrated in Fig.2.

The hockey-puck casting used for the experiments is shown in Fig. 3 with the locations of temperature measurement and pressure measurement. At the beginning of a series of experiments, only one point was measured. It is just in front of the gate close to the centerline of the casting.

A series of experiments were designed at U-M and proposed to CMI-Tech Center for the first round study conducted at the CMI-Tech center. The plan of the experimental study was worked out together with CMI-Tech center team members, including Karl Voss, Don Roberts, Gregory Woycik, David Moore and Christopher Rohloff.

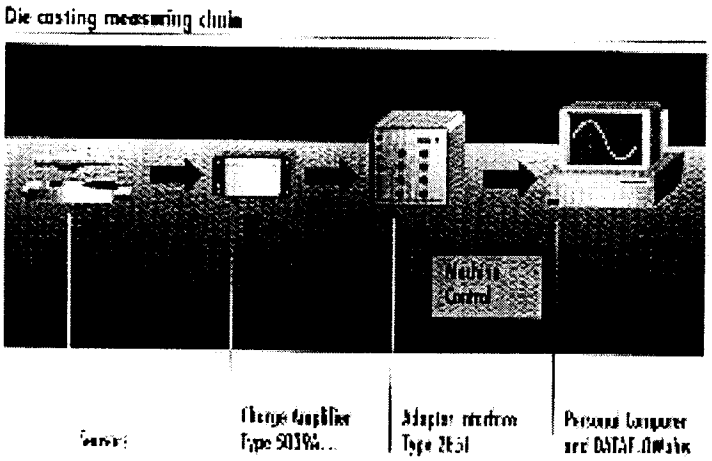

Fig.2 The flow-chart of direct cavity pressure measurement
(Courtesy Kistler, Swizerland)

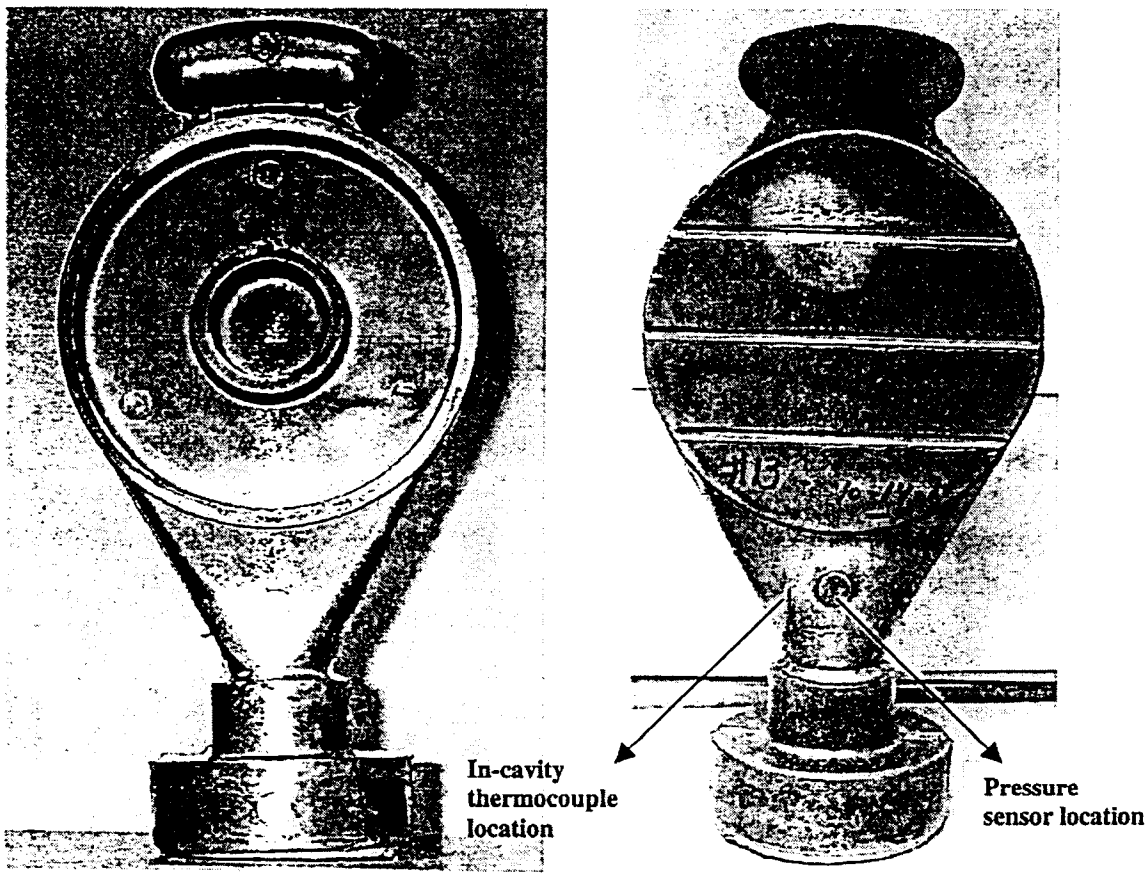

Fig.3 The hockey-puck casting for this project
(Courtesy CMI International)

3.4 Experimental Plan

Objectives

i. To study the feasibility of the Kistler Pressure Probe and the OMEGA temperature probe.
ii. To investigate the influence of intensification pressure on gate freeze time.
iii. To investigate the influence of the pouring temperature on gate freeze time.
iv. To collect data for predicting the proper heat transfer coefficient near the gate.

Number of Measurements

Each setting should be measured five times after 5 warm-up shots.

The Melt Temperature

Two melt temperatures to be experimentally used, the lower one at 1300 F and a higher one at 1390 F.

The Intensification Pressure

Two pressure settings are to be utilized, a high pressure and a low pressure. The setting should be measured later after the experiments. Targeted pressures were 15000 psi and 7000 psi, respectively.

The Plunger Speed

The gate velocity should be kept at 1 m/s. This can be calculated from the ratio of the gate area and the area of the shot sleeve.

Cycle Time

The cycle time for the first 5 shots should be as usual. For the five shots which are monitored, it was suggested to prolong the cycle time to 60 seconds for data collection purposes.

Die Temperature

If possible, the die would be preheated to 400 F.

3.5 Literature Search

An extensive search of the available literature concerning interfacial heat transfer coefficients (IHTCs) turned up a sizable number of papers. These papers address either the experimental determination of IHTCs or methods to manipulate the experimental data using various computational methods. The literature found appears in the list below in chronological order. It has been difficult to identify data from both smaller conferences

as well as internal documentation, such that the literature may not be complete. However, it seems reasonable to suggest that there are no glaring omissions from this list, as these papers tend to cross reference each other, with no relevant references to work with which are not already on this list. The pertinent information can be extracted from these papers and presented in the tabulated format shown in part below:

Table I: Heat Transfer Data from the Published Literature

Author(s)	Mold/Metal combination	Geometry	Experimental Interfacial Heat Transfer Coefficient (W/m^2-°K)	Simulation/ Computation Methods used
Ho & Pehlke	Copper chill/ Aluminum	Cylindrical, planar chill	initially... fell to	Finite diff.
Chiesa	Steel/Aluminum	Wheel mold	solidification front plots	Finite diff. (Magma)
Gunasegaram & Nguyen	composite: H13/Aluminum BeCu/Aluminum	Cylindrical with varying diameter	initially .... fell to	Finite diff. (Magma)

The article by Anderson et al. below represents a very comprehensive treatment, with an attempt made to correlate the geometry of the die with time dependent heat transfer coefficients, as well as the mold coating thickness (3).

This collection of papers has been sent to the American Foundry Society and a listing is presented as an Appendix to this report.

4. EXPERIMENTAL STUDY AT HAYES-LEMMERZ TECH CENTER

The series of experiments at the CMI Tech Center (now known as Hayes-Lemmerz Tech Center) were successfully conducted on October 14 and 15, 1998 with the participation of the University of Michigan team (Prof. Pehlke, Dr. S.W Hao and Mr. Prasad Krishna). The CMI-Tech team (Karl Voss, Don Roberts, Gregory Woycik, David Moore, Christopher Rohloff, Douglas Moran, and Mike Griff) successfully designed the die, modified the die and instrumented the die with the help of the UM team. Their contributions to the success of the experiments is gratefully acknowledged.

4.1 **Objectives of the experimental study**

v. To study the feasibility of the Kistler Pressure Probe and the OMEGA temperature probe.

vi. To investigate the influence of intensification pressure on gate freeze time.

vii. To investigate the influence of pouring temperature on gate freeze time.
viii. To collect data for estimating the appropriate heat transfer coefficient near the gate.

4.2 Experimental Data Sheet

Name of the casting produced: Hockey Puck-like shaped casting.
Machine: UBE-350 (vertical sleeve).
Alloy: A356 Pouring Weight: 1275 g.
Melt Temperatures (°F): 1290-1310 (low temp.), 1374-1387 (high temp.)
Mold temperature (°F): 300 - 387 (after warm-up shots)
(Measured by contact thermocouple)
Targeted Intensification Pressure (psi): 7000 (low), 15000 (high).
Gas Level: Level 2.
Coating: Graphite powder.
Cycle Time (recorded): 70 - 100 seconds.

4.3 Experimental Process Variables

1) Low melt temperature, Low intensification pressure (11 shots)
2) Low melt temperature, High intensification pressure (10 shots)
3) High melt temperature, High intensification pressure (14 shots)
4) High melt temperature, Low intensification pressure (10 shots)

4.4 Problems

Before the experimental results are discussed, problems, which occurred during the experiments, are cited.

1) Negative outputs of cavity pressure were recorded in the low intensification pressure condition. After discussion with Kistler, the vendor of the pressure probe, it was suspected that contaminated connectors might cause an erratic or drifting signal on the output device. To overcome this problem, a special solvent was needed to clean the cables and connectors in the measuring chain. Later, Kistler confirmed that the problem was in the ADA converter of the data acquisition system.

2) Due to the shielding effect of the thermocouples, the peak in-cavity temperature and the peak in-mold temperature were offset, and response times were delayed. It may be noted that this offset was accounted for in simulation runs.

4.5 Locations of measurements

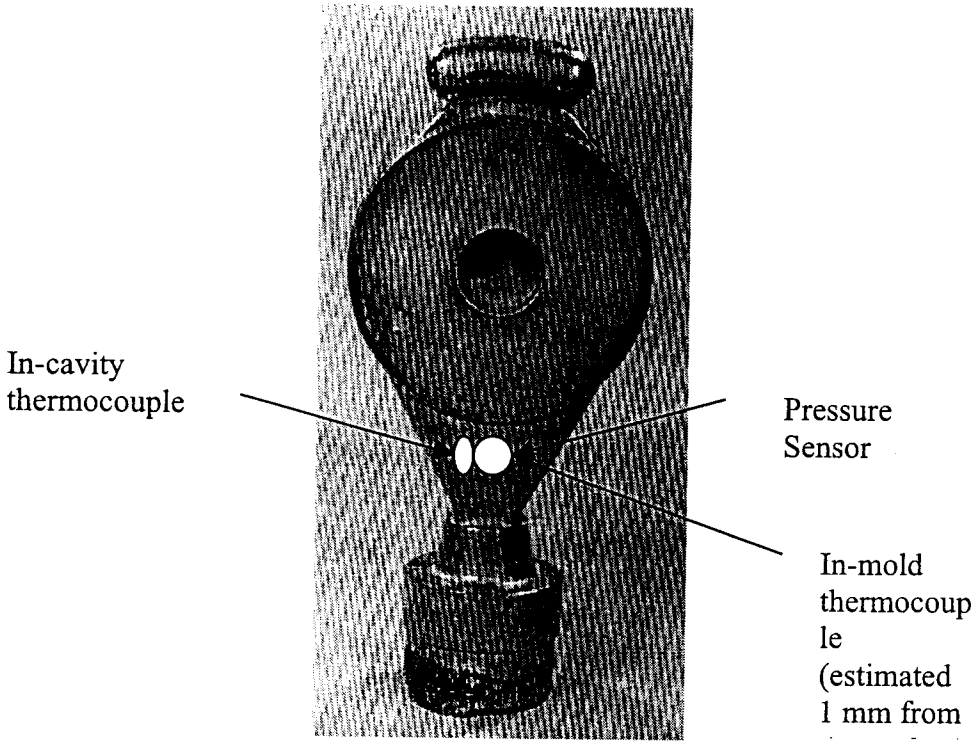

Figure 4: Locations of temperature and pressure measurements

As shown in Figure 4, both pressure probe and thermocouples were located before the gate. The in-cavity temperature measurement was aborted after the fifth shot, due to the failure of the thermocouple.

4.6 Sample experimental data

The result of an experiment at low intensification pressure and low melt temperature is presented in Fig. 5.

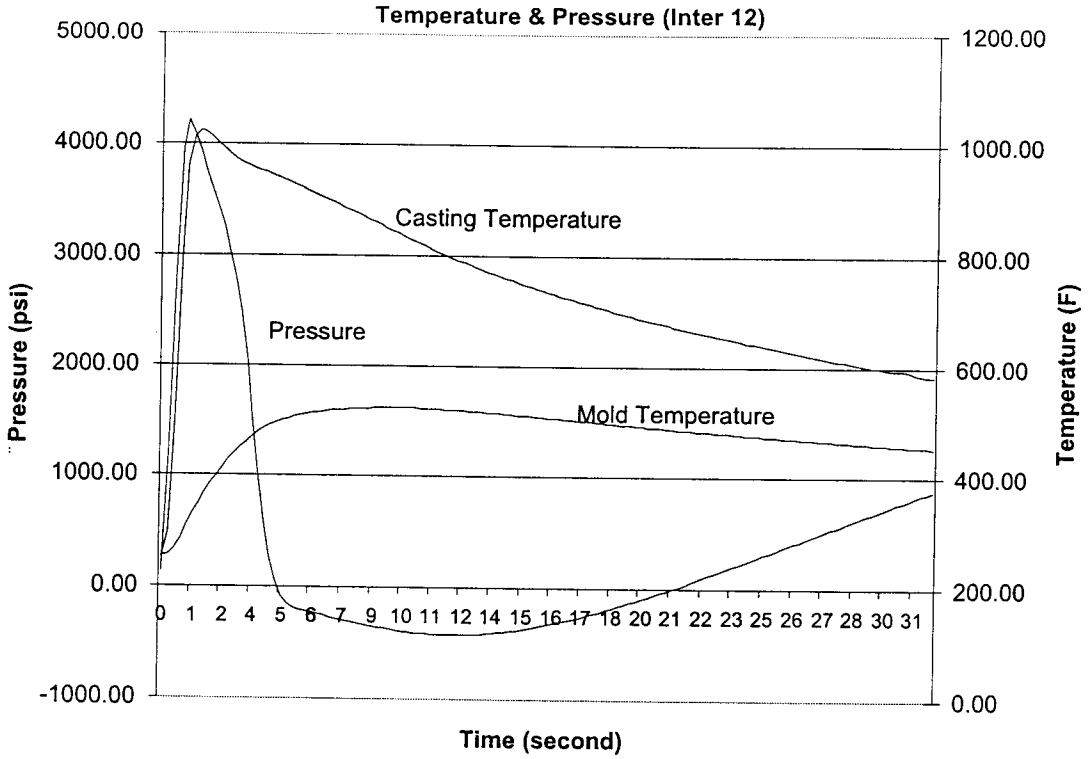

Figure 5: *Metal pressure, casting temperature and die temperature at low intensification pressure and low melt temperature condition*

It is noticed that the peak casting temperature in Fig. 5 is just about 1010 ° F. It is believed that the shield of the thermocouple offsets the peak in-cavity temperature.

Also, the pressure decreased to a negative value at the 5th second after sensing a positive pressure signal. Based on the explanation of Kistler, the vendor of the pressure probe, this might have been caused by contaminated connectors or cables in a casting workshop, which would result in an erratic output. Later, Kistler confirmed that the problem was in the ADA converter of the data acquisition system.

4.7 Experimental Data Analysis

4.7.1 Temperature measurement

As shown in Figure 5, the thermocouple with protection could not match the dramatic in-cavity temperature change. However, for the in-mold temperature measurement, due to the relatively slow change of the mold temperature, the thermocouple could measure the mold temperature with a certain degree of accuracy and reliability, as shown in Figure 6. However, this offset was accounted for while estimating the appropriate heat transfer coefficient.

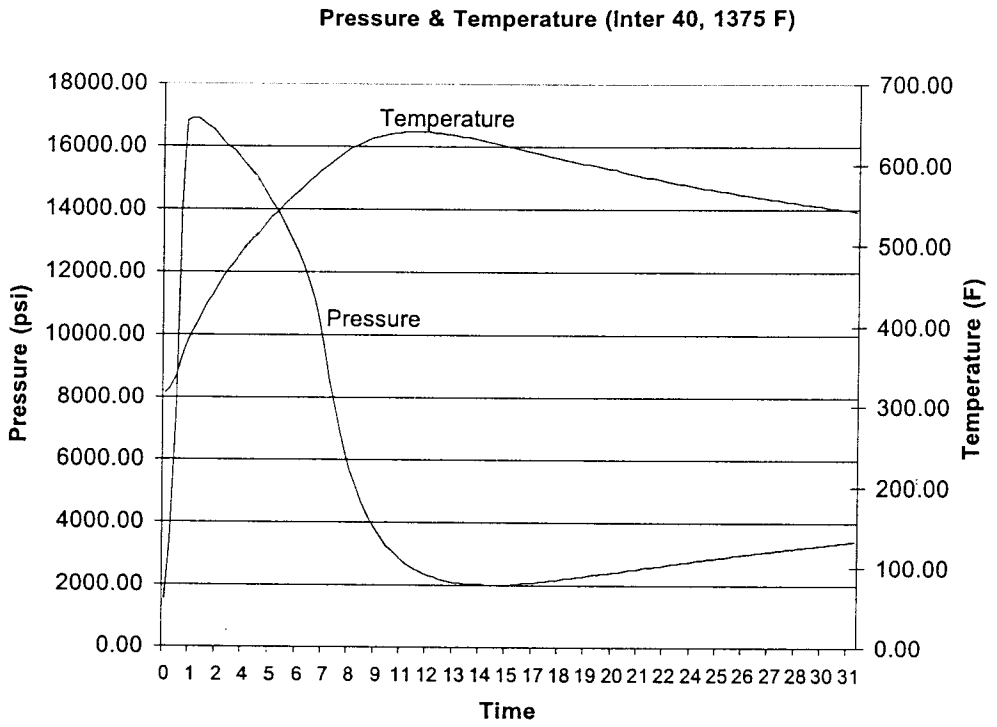

Figure 6: *Metal pressure, die temperature at high intensification pressure and high melt temperature condition*

It is noticed that no matter how long it takes to reach the peak die temperature, for example, 8 seconds in Fig.5, 11 seconds in Fig.6 and 9 seconds in Fig.7, die temperatures start to decrease when the pressure just reaches the valley. This can be explained in two ways. The first, as the interfacial contact situation worsens, the interfacial heat transfer coefficient decreases dramatically. As a result, the rate of the heat transfer across the interface is reduced, and the mold temperature starts to decrease. The second consideration is that, at this moment, most of the casting has been solidified, and the latent heat released. As a result, less heat is transferred to the mold. At this point, it is not possible to predict whether a gap was formed at the interface.

This observation strongly indicates that the die surface temperature (or near the surface) has a close correlation with the metal pressure profiles. For the difference in the timing of the peak die temperature in Fig.5 and Fig.6, the higher melt temperature and higher die temperature for Inter 54 might cause a longer solidification time, and the pressure will decrease more slowly than for Inter 12.

However, it is difficult to explain why it took 11 seconds for a high pressure condition to reach the peak die temperature shown in Figure 6, which was longer than for the low pressure setting. High pressure should enhance interfacial heat transfer, and then the die temperature must increase faster than for the lower pressure condition. One possible explanation is that if metal pressures at the interface were higher than a certain

threshold level, any increase in pressure would not significantly enhance heat transfer across the interface.

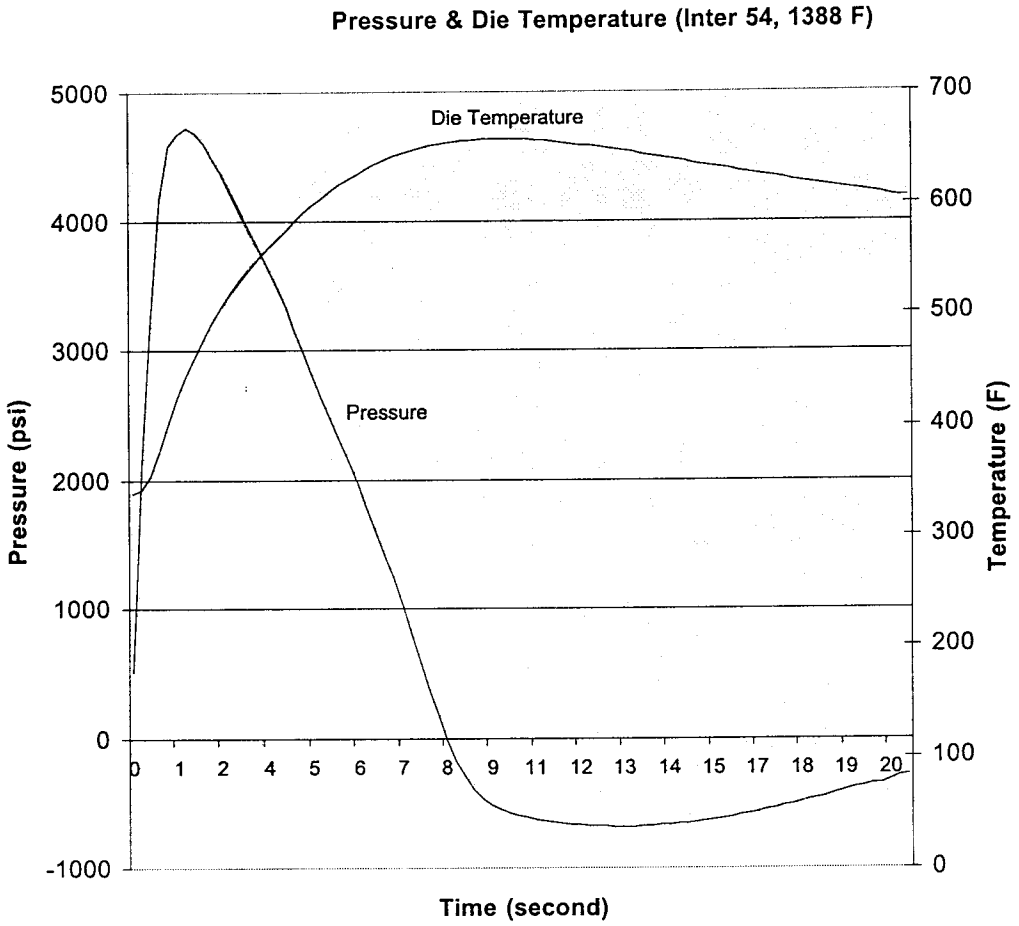

Figure 7: *Metal pressure and mold temperature at low pressure and high melt temperature condition (Inter 54)*

4.7.2 Pressure Measurement

In order to simplify the analysis, the portion of a pressure profile between the first positive recording and the peak pressure can be called the "pressure establishment stage", and the portion between the peak and the valley of a pressure profile can be called the "shell establishment stage". The origin of the time axis is assigned at the time of the first positive pressure recording. The pressure recovery stage from the valley should be further explained.

1) Pressure establishment stage

In Figures 8-11, all peak pressures occurred at 1.18 seconds after the first positive pressure record. The response time of the Kistler pressure probe is within a milli-second.

This is probably caused by the hydraulic characteristics of the *Ube* machine. When the runner is partially filled, the metal pressure probe starts to sense pressure. As the cavity is filled and the intensification starts, the pressure increases to the peak.

2) Shell establishment stage

Assuming constant hydraulic pressure of intensification until the end of the measurement, then the reason for pressure decrease from the peak value is the strengthening of the solidified shell of the casting, which causes the surface of the casting to move apart from the mold surface.

In Figure 9, the slopes of the metal pressure profiles at the low pressure setting are almost linear. This may mean that the low metal pressure couldn't effectively keep a pressure channel opened. In other words, as temperature decreased, solid fraction increased and the solidified shell strengthened, and the pressure, which couldn't overcome the resistance, dropped linearly.

However, at the high pressure setting (Figure 8), there are inflection points in the pressure profiles. The inflection points are at about 8500 psi for both the low and the high melt temperature settings. This suggests that the metal pressure was sufficient enough to overcome the resistance of the solidified shell before the inflection point was reached. This also means that the pressure channel remained opened longer and larger. In cases, when the inflection points were reached (at about 8500 psi), the solidified shell became strong enough to resist the intensification pressure. As a result, the slopes of the pressure profiles became steeper than before the inflection points.

This knowledge may be helpful in setting the intensification pressure for the squeeze casting process, such that the pressure channel should remain open as long as possible.

3) *The Influence of Melt Temperature on Metal Pressure*

At the high pressure setting (Fig. 8), the higher melt temperature (1375 °F) could slightly extend the time of pressure existence. This is because of the longer solidification time of the casting at the higher melt temperature setting. However, the peak pressure values at the low melt temperature and at the high melt temperature conditions are the same.

At the low pressure setting (Figure 9), the melt temperature had a more significant influence on the pressure profiles. This may also suggest that the low pressure was insufficient in our case. It may thus be inferred that the melt temperature and the die temperature are at limits of normal practice and any change in their setting would be detrimental to the quality of the castings.

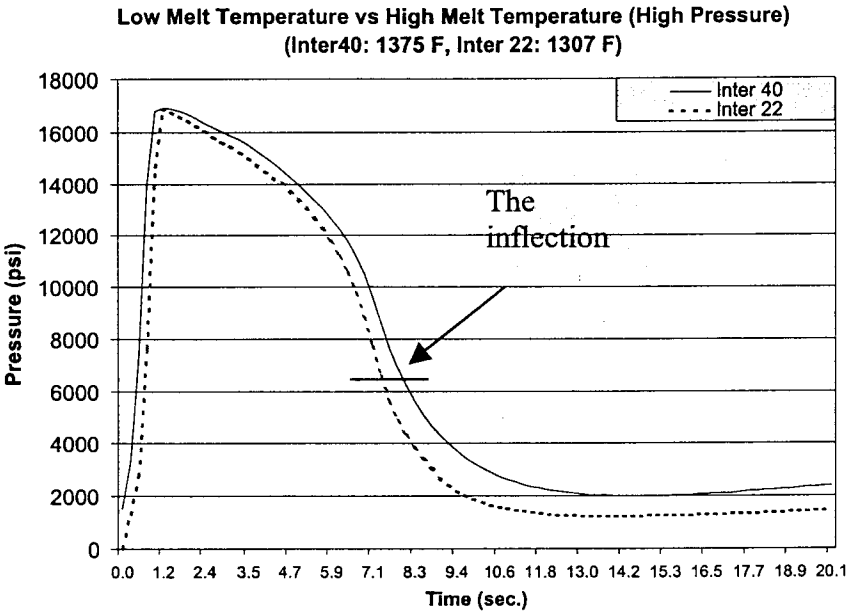

Figure 8: *The influence of melt temperature on pressure profiles at high intensification pressure condition*

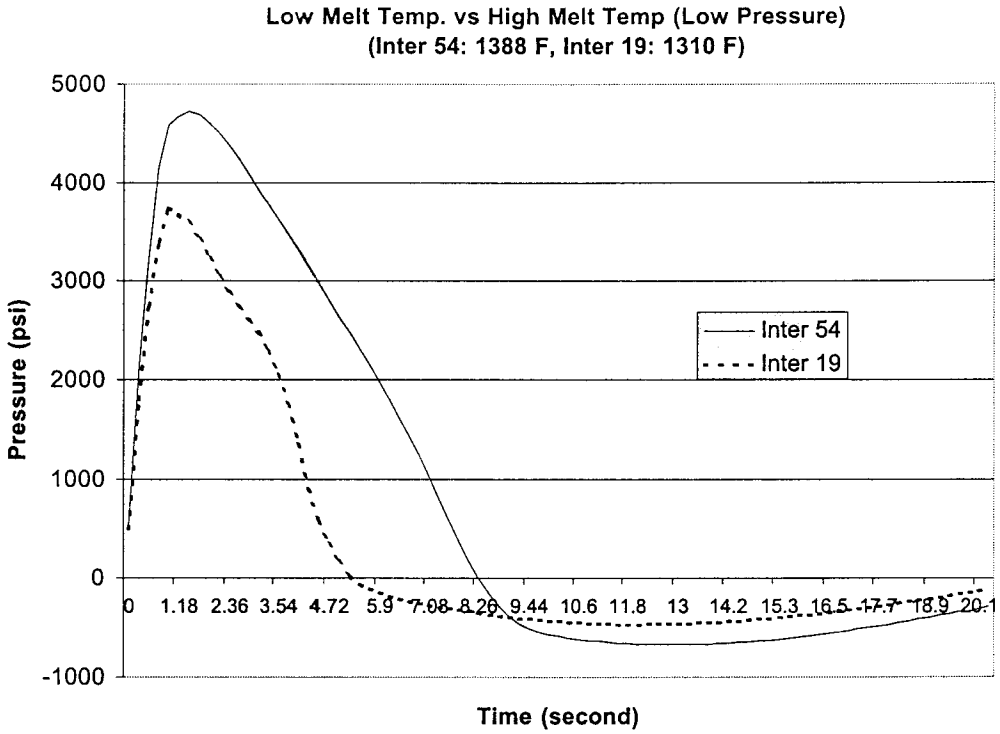

Figure 9*: The influence of melt temperature on pressure profiles at low intensification pressure condition*

4) *Pressure Profiles at High and Low Intensification Pressure Conditions*

At the higher melt temperature (Figure 10), the peak pressure values are 16900 psi and 4200 psi for high pressure and low pressure settings, respectively. At the low melt temperature (Fig.11), the peak pressure values are 16900 psi and 3720 psi for high pressure and low pressure settings, respectively.

In general, high pressure could keep a casting in contact with a mold surface for a longer period of time. It is believed this will result in a higher interfacial heat transfer coefficient for a longer period of time than at the low pressure condition.

It is believed that metal pressure will significantly affect the gate freezing time. This means that a gate will freeze at a higher solid fraction at a higher metal pressure condition. However, the correlation between gate freezing time and metal pressure is yet to be known.

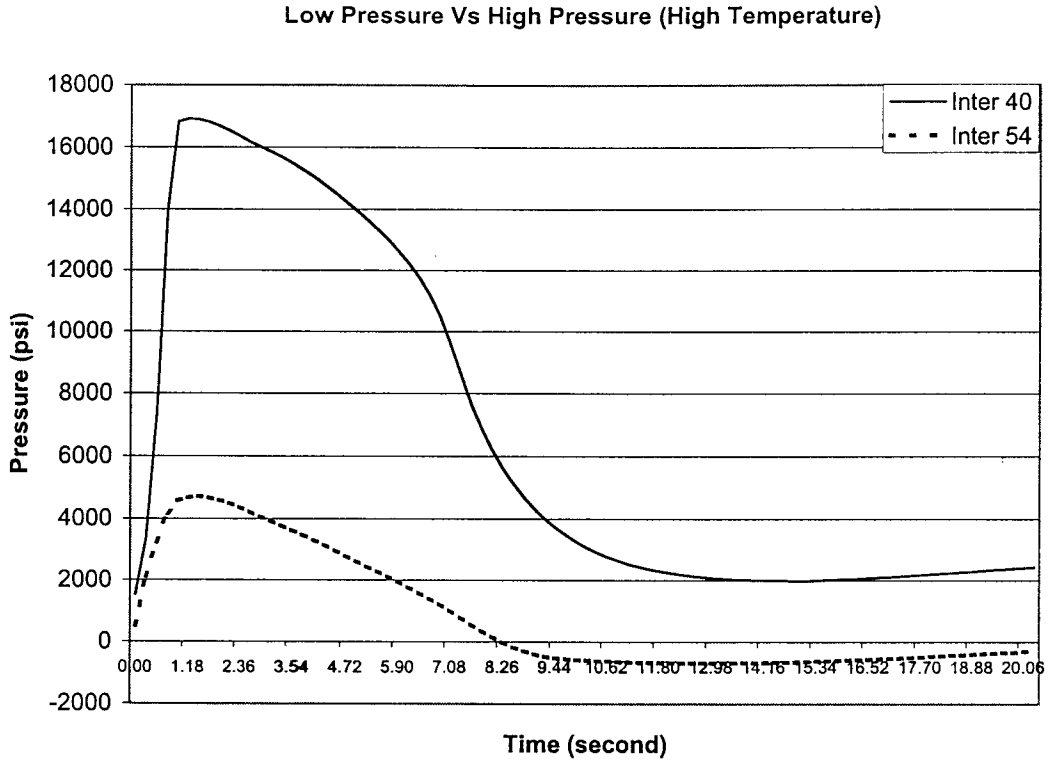

Figure 10: *Metal pressure profiles at high melt temperature condition*

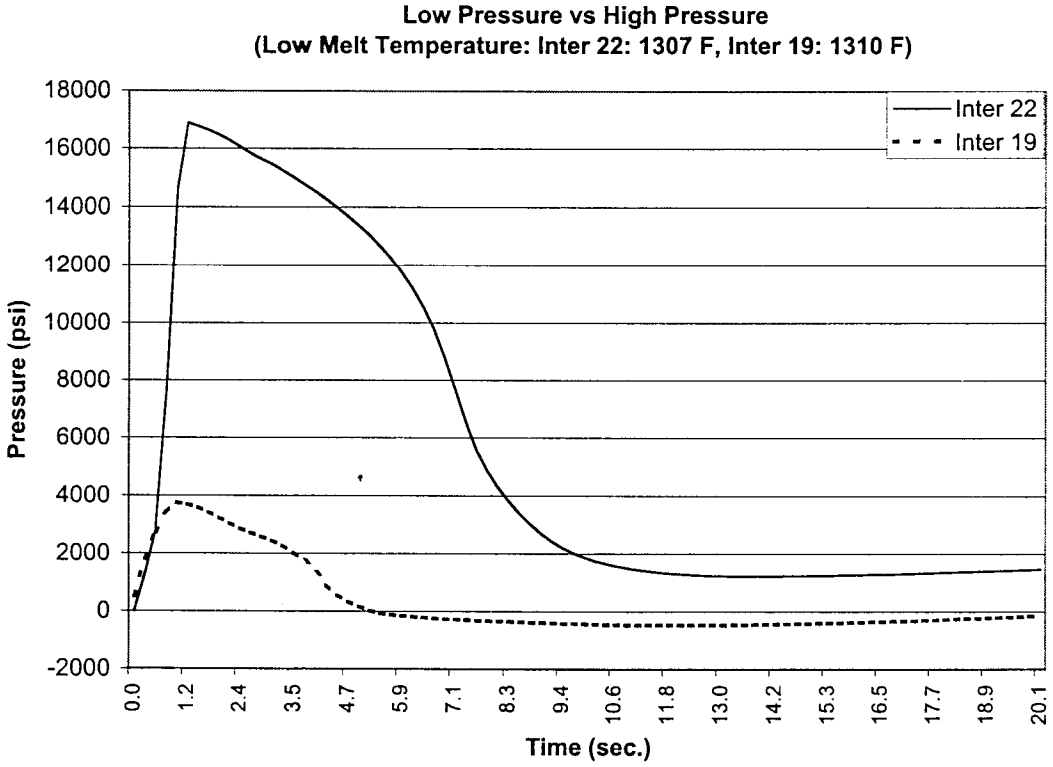

Figure 11: *Metal pressure profiles at low melt temperature condition*

A temperature probe, enclosing as many as four thermocouples in a row for monitoring die temperature has been designed and fabricated at the HLTC. The distances from the bare tips of the thermocouples to the die surface are 1 mm, 3mm, 5mm and 25 mm. A heating-and-cooling test was conducted and confirmed that the temperature probe is very sensitive to temperature changes.

Hayes-Lemmerz Tech Center has cleaned the pressure sensor cables with the recommended solution and completed the calibration. After recalibration, they used the pressure sensor for a semi-solid casting project. The problem was due to snags in the Kistler Data Acquisition System, which was later rectified by their engineers. As per their report, the pressure sensor has worked well, while using it for a *semi-solid Casting* project.

The HLTC team members also expressed their difficulty in controlling the die coating thickness and in measuring the thickness accurately. As such, HLTC do not use any permanent die coating in their experiments for squeeze casting, except for the spraying of graphite in a colloidal suspension at the beginning of each shot.

Although Hayes-Lemmerz Tech Center completed the design and fabrication of a new thermocouple carrier, the second set of experimental trials were not conducted, as the *Ube* casting machine was not available.

5. SQUEEZE CASTING METALLOGRAPHIC STUDY AT UM

All the squeeze cast samples were ground and the final polishing work completed for 15 samples. A few sample micrographs for the low pressure specimen are shown in this report. An image of the hockey puck-like shaped casting showing locations where the microstructure was taken is illustrated in Figure 12.

Tabulation of secondary dendrite arm spacing (SDAS) measurements for both high pressure and low pressure casting samples are also given in Table III and Table IV, respectively.

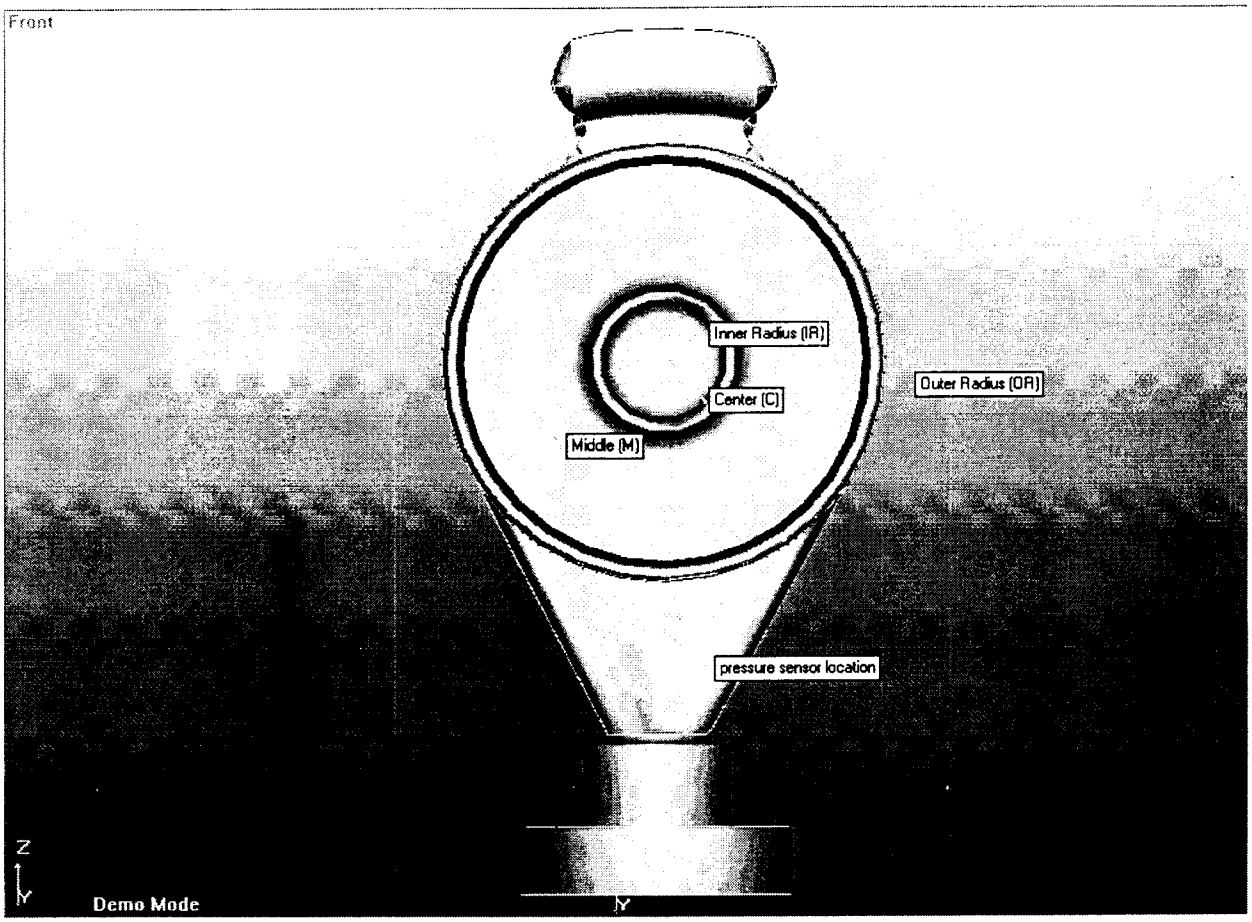

Figure 12 .Image of Hockey puck-like shaped casting, showing locations where microstructures were taken

The optical micrographs for a low pressure casting sample (Sample # 45 tested on 14th October, 1998) corresponding to Center(C), Middle (M), Inner Radius (IR) and Outer Radius (OR) positions, all at a location close to the 12 .00 clock position on the above image (Z axis), are presented on pages 42 and 43. The secondary dendrite arm spacing (SDAS) measurements using the intercept method for all these graphs are also tabulated and reported.

Figure 13 Optical micrographs of high pressure casting samples

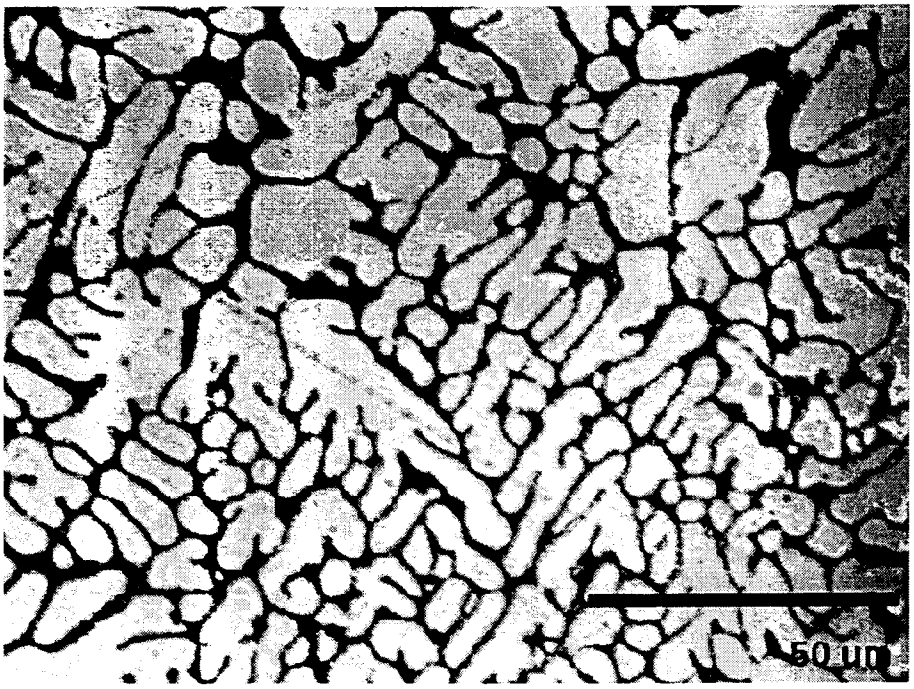

Microstructure of the outer ring at 12'O clock position for casting #34 (middle)

Microstructure of the outer ring at 6'O clock position (top)

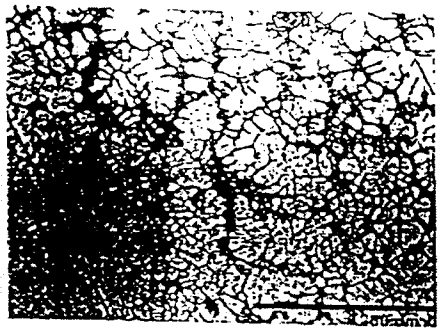

Segregation (IR)

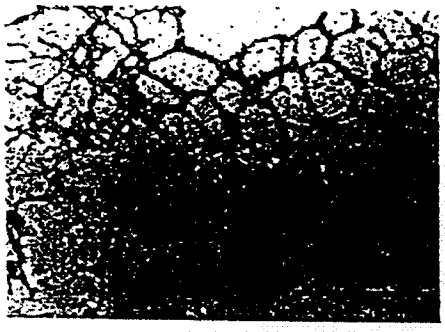

Bottom (IR)

Bottom (M)

Figure 14 Optical Micrographs of Low Pressure Casting Samples

Figure 15 Optical micrographs of low pressure casting samples

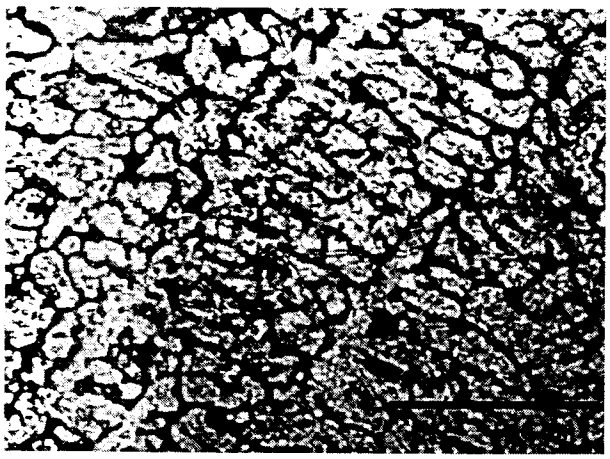

Top (OR)

Table III-Secondary Dendrite Arm Spacing for high pressure casting samples

Sample #34 (High Pressure)	Average SDAS (um)	Max SDAS (um)	Min SDAS (um)	Standard Deviation (um)
12-IR Top	6.9	16.2	3.1	2.5
12-IR Middle	9.6	13.1	5.4	2.1
12-IR Bottom	8.3	13.5	5.4	2.0
12-OR Top	4.6	8.9	2.3	1.6
12-OR Middle	7.1	15.4	3.1	3.1
12-OR Bottom	3.8	5.4	2.3	0.8
6-IR Top	5.8	16.9	3.1	2.7
6-IR Middle	10.5	22.3	4.6	3.4
6-IR Bottom	9.1	15.4	6.2	2.8
6-OR Top	5.6	9.6	3.8	1.6
6-OR Middle	13.0	15.4	10.0	1.8
6-OR Bottom	6.9	11.5	3.5	2.2

Table IV: Secondary Dendrite Arm Spacing for low pressure casting samples

Sample (Low Pressure # 45)	Average SDAS (μm)	Max SDAS (μm)	Min SDAS (μm)	Standard Deviation (μm)
Center Top	6.3	14.2	2.2	2.6
Center Bottom	7.1	11.2	4.5	1.8
12-IR Top	5.6	13.4	2.6	2.2
12-IR Middle	8.4	17.9	4.1	3.1
12-IR Bottom	6.9	12.7	3.7	2.3
12-M Top	8.5	14.2	4.5	2.5
12-M Bottom	8.0	18.7	3.0	3.3
12-OR Top	6.1	10.4	3.0	1.7
12-OR Middle	7.2	13.1	3.7	2.1

6. SOLIDIFICATION SIMULATION AT UM

Several simulations were run for the solidification of the hockey puck-like shaped casting using MAGMAsoft ver.3.5. Virtual thermocouples were placed inside the casting and die to output the cooling rates at those locations. While inputting the heat transfer boundary conditions, it is assumed that there is no gap formation in squeeze casting and that the HTC remains more or less constant during solidification except for a small drop as shown in the following graphs. This is in contrast to gravity die-casting where there is a marked decrease in the HTC value upon formation of an air gap between the casting and the mold during solidification. As reported earlier, pressure measurements at the Hayes-Lemmerz

Technical Center with a semi-solid casting process indicated no gap formation. Different HTC values were input for each of the simulations to study the effect of HTC on temperature distribution in the casting and the mold. A total of 1,567,808 control volumes were used to enmesh the hockey puck-like shaped casting. A die temperature of 100°C and a pouring temperature of 685°C were used for the initial run. Since the original ***stl*** file of the hockey puck-like shaped casting was generated by mechanically probing the actual cast sample using the special facility at the measuring room of Hayes-Lemmerz Technical Center, a few repairs were made before the model could be enmeshed in MAGMAsoft.

Simulations of solidification with the *MAGMApressurize* option of MAGMAsoft were also conducted. The estimation of the heat transfer coefficient (HTC) was carried out by successive computation of the temperature history in the die or in the casting, keeping interfacial HTC as a variable parameter. The heat transfer coefficient, which gave the best correlation between measured and calculated values, was taken as the correct one.

Figure 16 shows a cooling curve obtained from the solidification simulation by embedding virtual thermocouples at the bottom face of the hockey puck-like shaped casting. The local cooling rates were calculated from the cooling curves by dividing the temperature drop from liquidus to solidus by the local solidification time. Figure 17 compares the calculated and measured cooling rates. The results show good matching of the curves.

The variations of heat transfer with solidification time and with local cooling rates were plotted by running several simulations with HTC as a variable. Figure 18 shows cooling curves in the liquidus-solidus interval for six different values of HTC that were used in running the simulation. Figure 19 shows the corresponding time dependent HTC's referred to in Figure 18. Figure 20 shows the variation of HTC with local cooling rates. The results show that the HTC increases with cooling rate, as expected. Figure 21 shows how sensitive the HTC is with respect to the local solidification time.

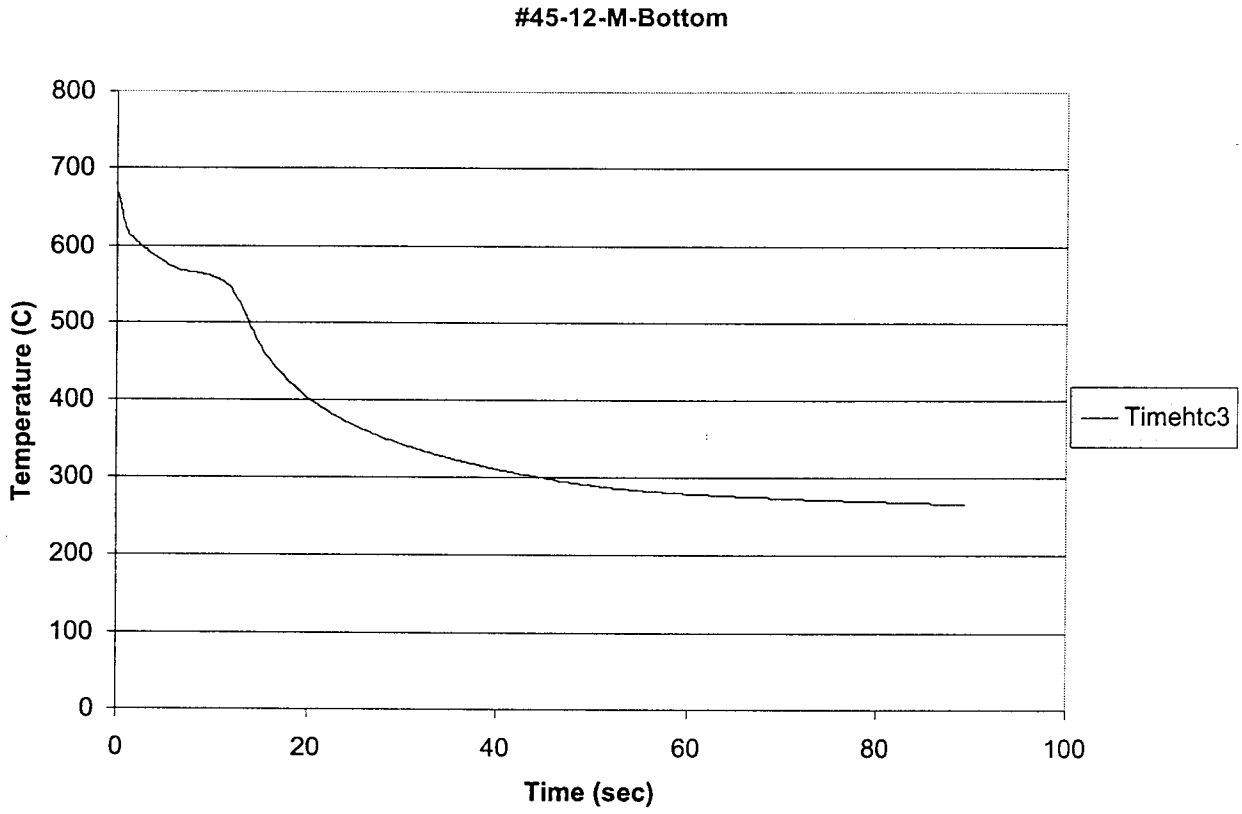

Figure 16:Computed cooling curve for low pressure sample #45 for HTC=4500 W/m^2.K

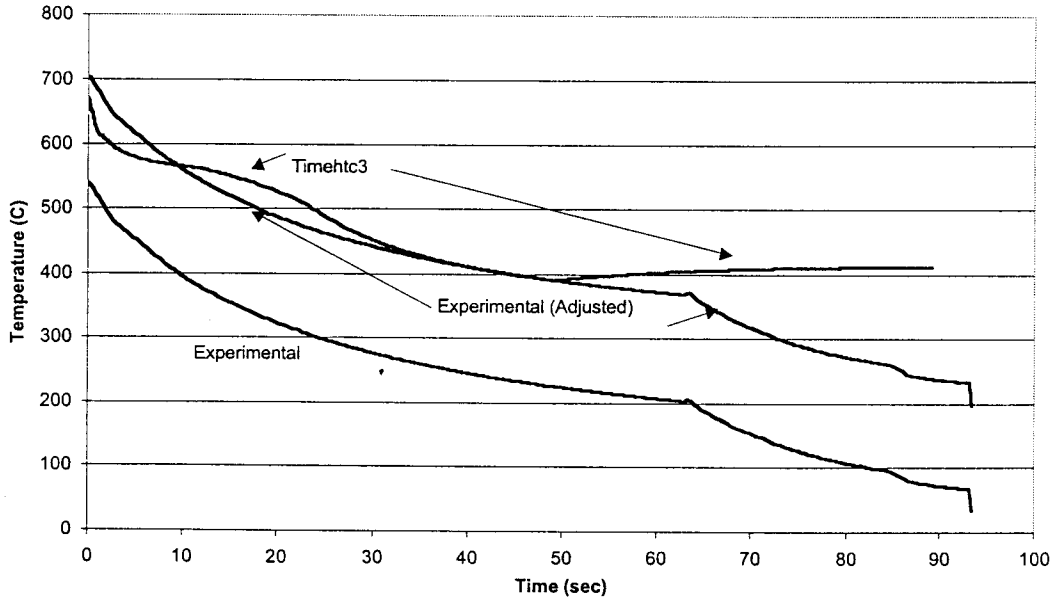

Figure 17:Comparison of simulated and experimental cooling curves

Note:

Experimental cooling curve was adjusted to account for the shielding effect of thermocouples used in the experiments.

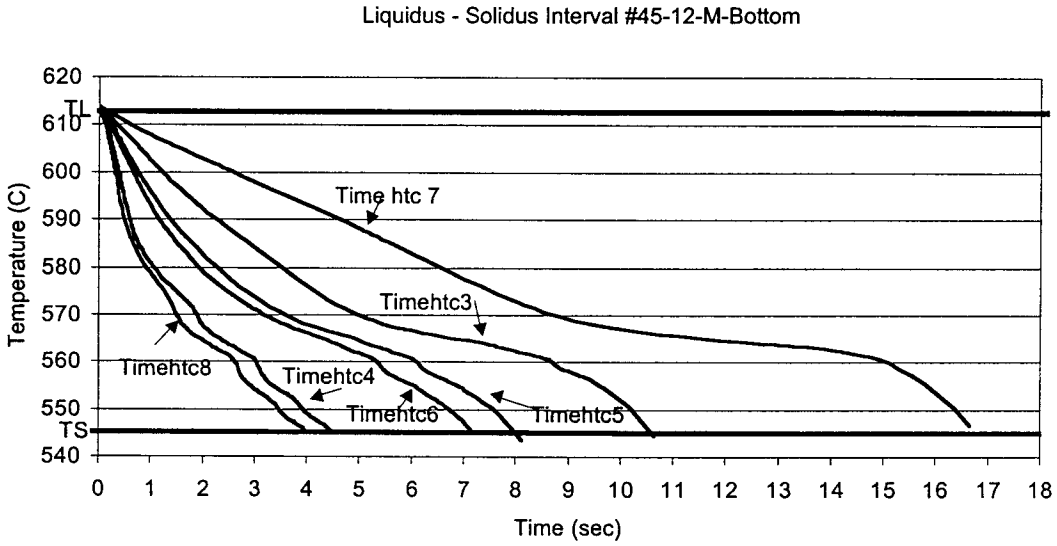

Figure 18:Cooling curves (liquidus-solidus interval) for various HTC values

Graphs below show time dependent HTC s used to simulate the cooling curves referred to in Figure 18.

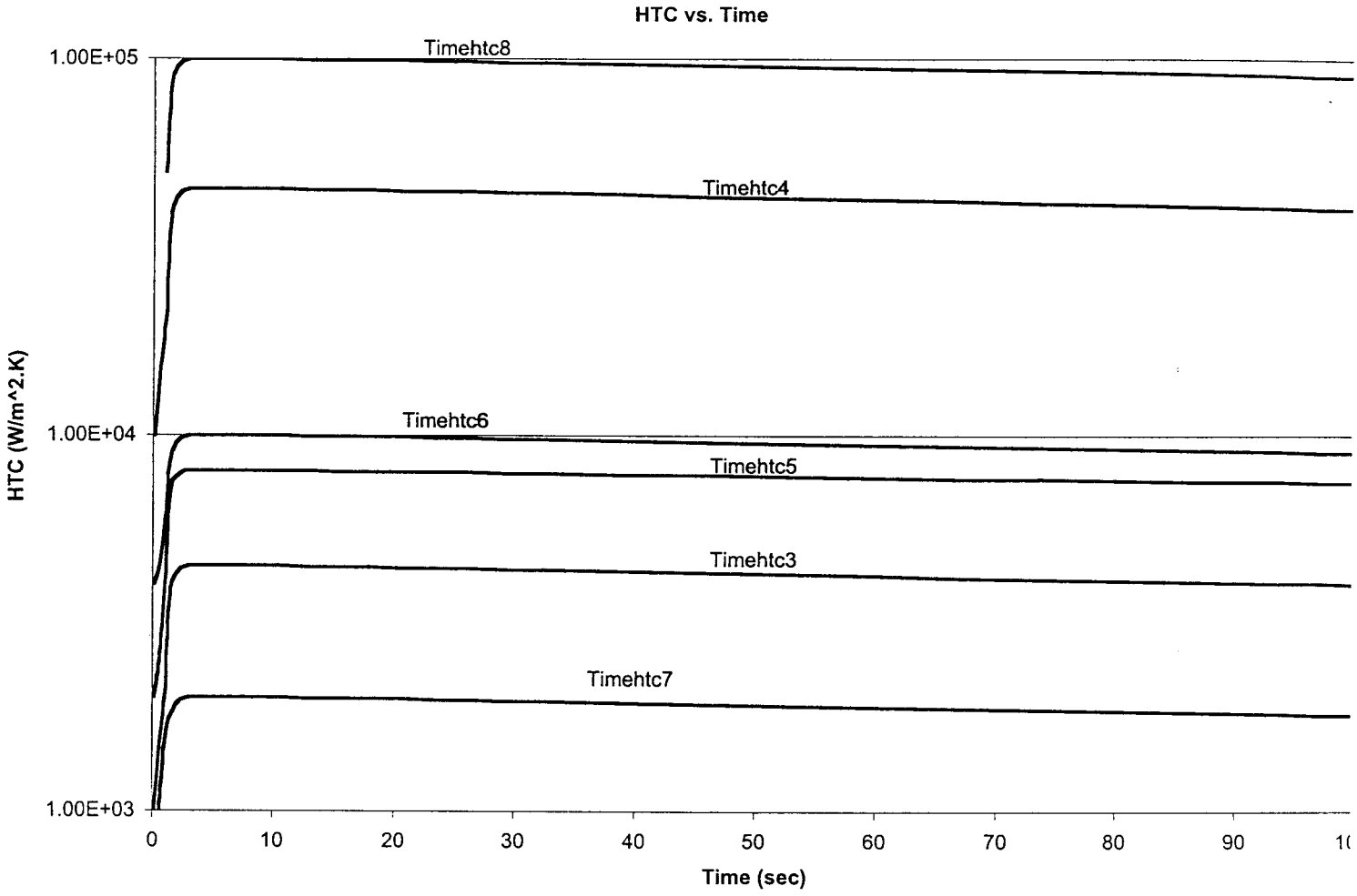

Figure 19:Time dependent HTC values used for simulations

Note:

For the casting sample we have used for study, the value of HTC that matched the theoretical and experimental cooling rate, was Timehtc3 as shown above.

I.S.Cho and C.P.Hong in their paper titled, *"Evaluation of Heat Transfer Coefficients at the Casting/Die Interface in Squeeze Casting", Int. J. Cast Metals Res., 1996, 9, pp. 227-232,* also reported an HTC value of about 4700 W/m^2.K, for squeeze casting of Al-4.5% Cu alloys at a pressure of about 50 MPa, using a cylindrical casting in a steel mold (4).

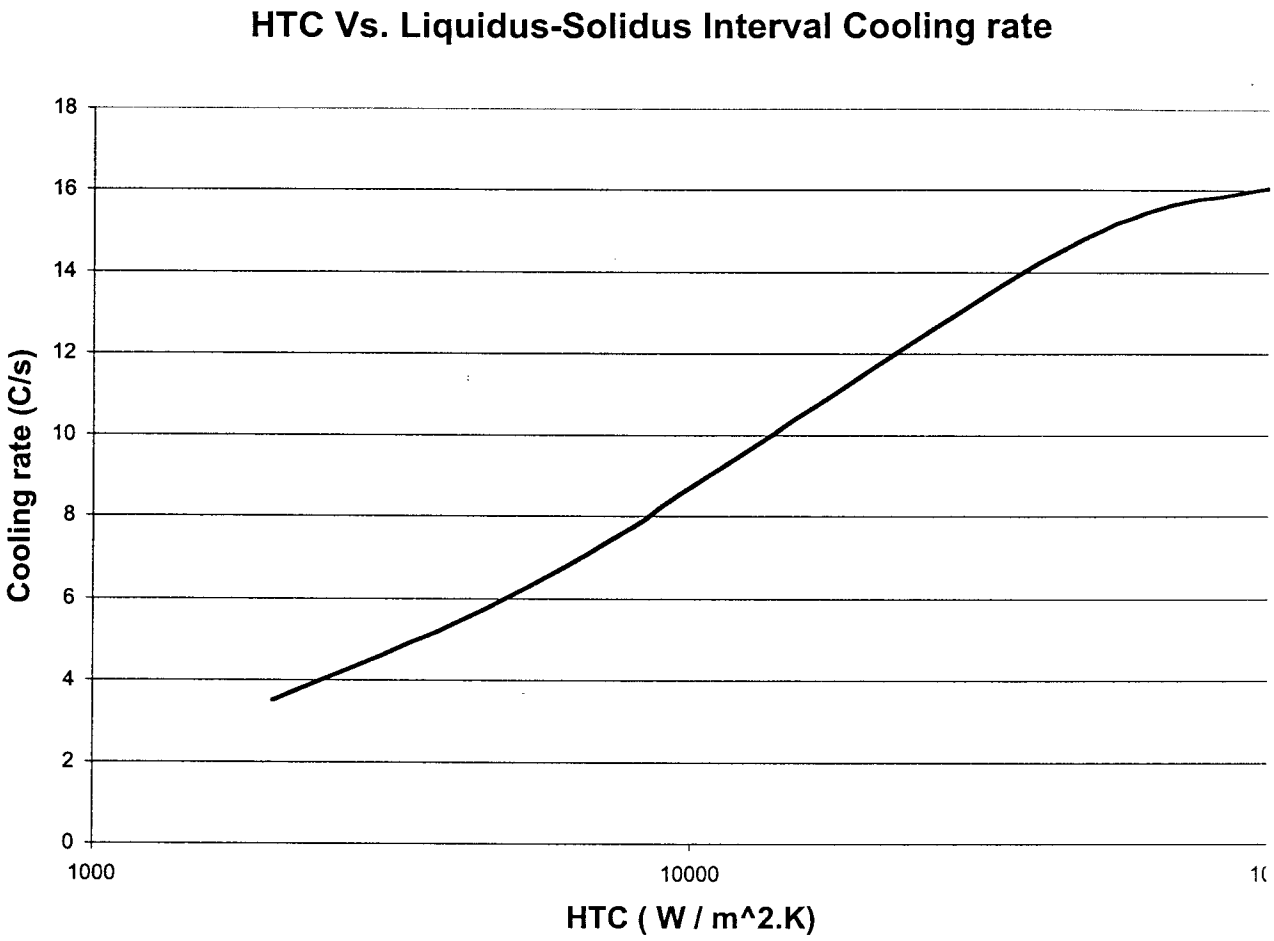

Figure 20:Graph showing variation of HTC with local cooling rates

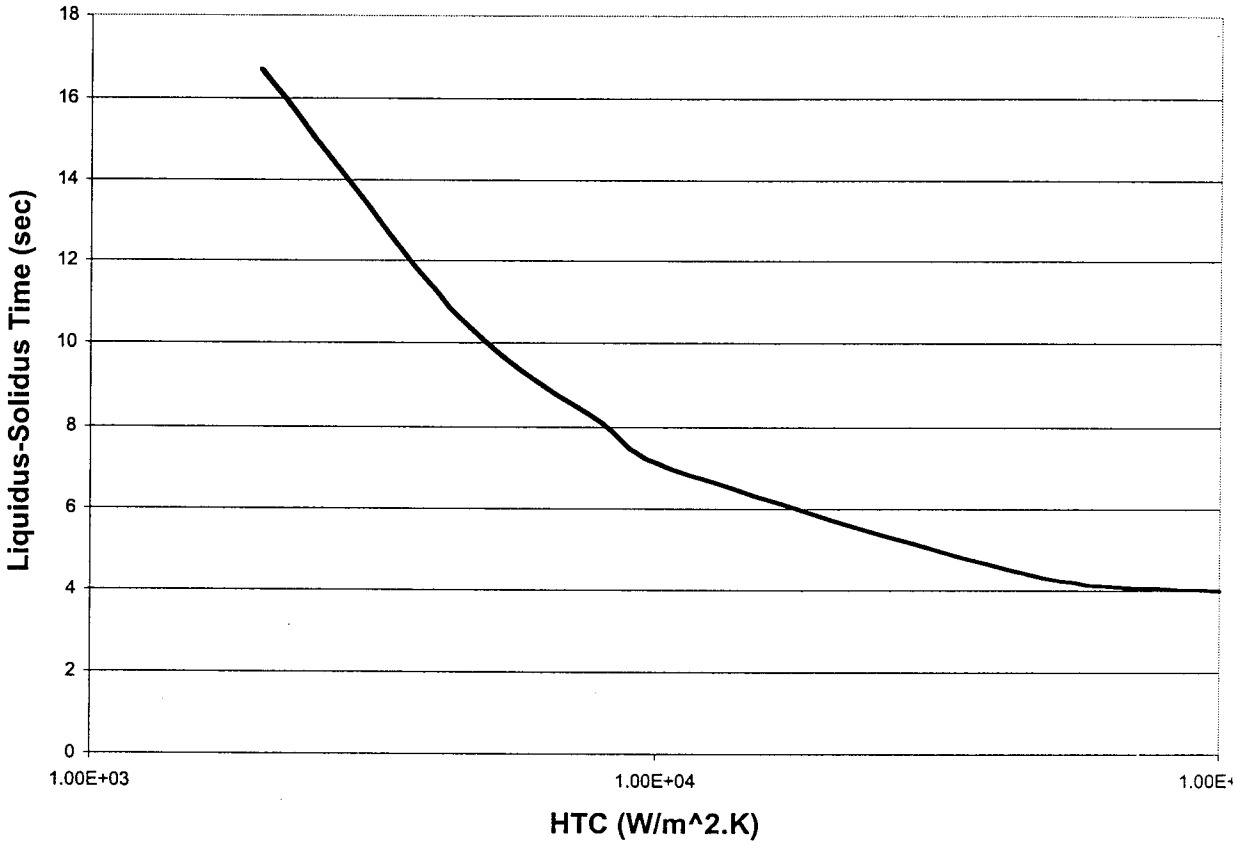

Figure 21:Sensitivity of HTC to the local solidification time

***Inference*:**

There seems to be an upper limit on the achievable heat transfer coefficient and the upper limit for this case study is about 1.00 E+05 W/m^2.K. Similar results were also reported by J.A.Sekhar and *et al.* in their paper titled, "*Effect of Pressure on Metal-Die Heat Transfer Coefficient during Solidification*", appeared in the Journal of Materials Science and Engineering, Vol.40, 1979, pp. 105-110 (1).

7. EXPERIMENTAL ANALYSIS AT HAYES-LEMMERZ TECH CENTER

A detailed metallographic inspection of the cast specimens at UM has revealed extremely small SDAS values, which are much smaller than the observations of other researchers. It is found that impractical cooling rates would be required to match such low SDAS values, if the SDAS-cooling rate correlation model of Rohatgi, P.K., et al., [5] is assumed for these A356 alloys.

Figure 22 shows the comparison of the experimental and theoretical models. This discrepancy has led to analyzing the chemistry of the alloy used for the experiments at Hayes-Lemmerz for possible grain refiners, especially the presence of titanium and boron, which are reported in the literature to be effective modifiers. Such grain refiners can cause very low SDAS, as reported in a journal article by Banghong Hu and Hang Li, 1996 [6].

Figure 23 shows the variation of the SDAS with local cooling rates, when average SDAS values for a specific location and cooling rate from the liquidus-solidus range were used. The figure also shows the comparison between the best power fit for the data and fitting a curve with the predicted exponent of -0.33.

Considering the above facts, it is obvious that modifying elements in the alloy have played a significant role in reducing the dendrite arm spacing. UM requested Hayes-Lemmerz to determine the exact composition of the aluminum alloy with which the earlier experiments with the hockey puck-like mold had been conducted. As reported by Hayes-Lemmerz Tech Center, they have checked the chemistry of the alloy from a section of the hockey puck-like casting. The sample was analyzed on their *ARUN* spectrometer (on two separate machined surfaces) and at their Howell casting facility (separate machined surfaces again) to be sure of the results. Reported results in wt.% were

Si 6.89, Fe 0.669, Cu 0.00974, Mg 0.202, Ti 0.109, Sr <0.006, Mn <0.0025, Zn 0.00926 %.

The iron (Fe) content of the alloy is high for the standard A356 composition (0.12 max. for the standard alloy). All other elements are in the standard operating ranges.
The material used mostly for refining is TiB (10% Ti 4% B). As per observations at the Hayes-Lemmerz Technical Center, the amount of Ti found in the castings (~0.109) may have been inactive due to fading, since no bump of TiB to reactivate the refining material was added in this case. To measure the amount of boron, the casting sample was sent to the Climax Research Services Laboratory, in Farmington Hills, Michigan. Climax Research Services reported the following composition in wt % for the A356 casting alloy

l used in tests at the Hayes-Lemmerz research laboratory (Table V). The report confirmed the presence of traces of boron in the alloy.

Table V: Composition of A356 alloy used for squeeze casting experiments at Hayes-Lemmerz Tech Center

Fe	Cu	Mn	Mg	Cr	Ni	Zn	Ti	Sn
0.75	0.01	0.01	0.17	<0.01	0.01	0.02	0.11	<0.01

Pb	P	Sr	Ca	Na	B	Ba
<0.01	<0.005	<0.001	<0.005	<0.005#	0.0012*	<0.005

The method used for the above analysis was *Inductively Coupled Argon Plasma Emission Spectrometry,* except for boron and sodium for which **Optical Emission Spectrometry* and *# Atomic Absorption Spectrophotometry* were used, respectively.

The presence of small amounts of boron in the sample tested and reported by Climax Research Services suggested some grain refinement of the basic A356 alloy, and subsequent reduction in the DAS. A systematic study conducted by Mohanty P.S. and Gruzleski J.E on the "*Mechanism of Grain Refinement in Aluminum* " [7] gives considerable insight into the role of titanium diboride (TiB_2) in the grain refinement process. As per their investigation [7], precipitation of a thin layer of $TiAl_3$ occurs on the boride, which undergoes a peritectic reaction and thereby nucleates the solid. TiB_2 plays an indirect role in grain nucleation. The optimum levels of titanium and or boron additions for grain size refinement and DAS refinement are discussed in reference [8].

Several useful discussions were held with Hayes-Lemmerz on the subject of grain refinement of aluminum alloys and the effect of boron additions on the reduction of Secondary Dendrite Arm Spacing (SDAS) of the alloy. The final conclusion is that boron additions with titanium do reduce the SDAS. Furthermore, UM presents several citations from the literature to support this fact, including [6-12]:

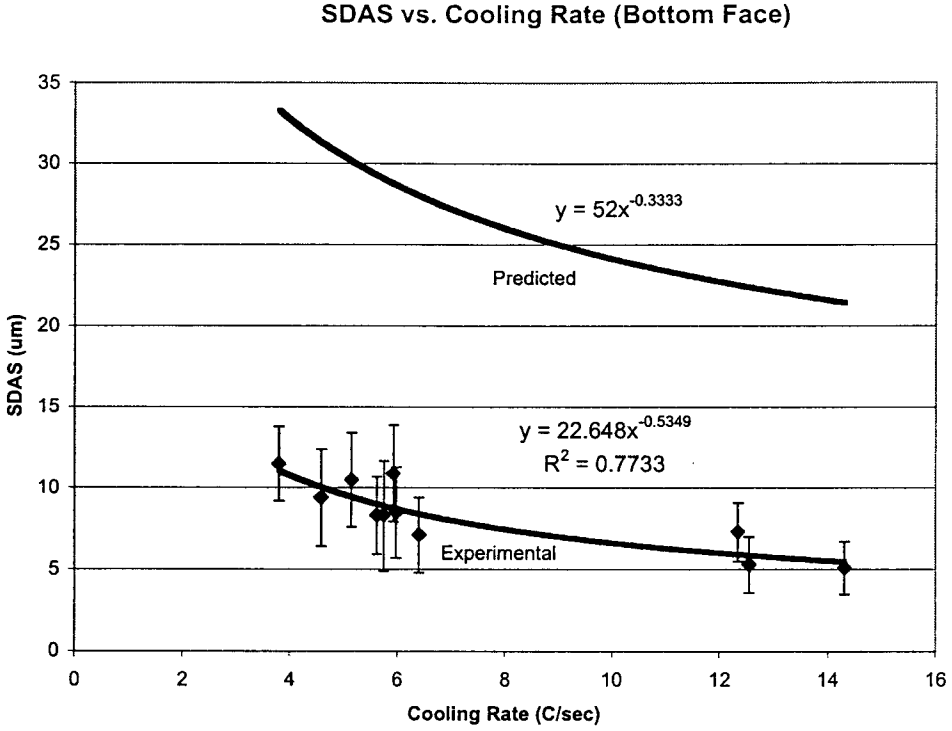

Figure 22: Comparison of predicted and experimental curves

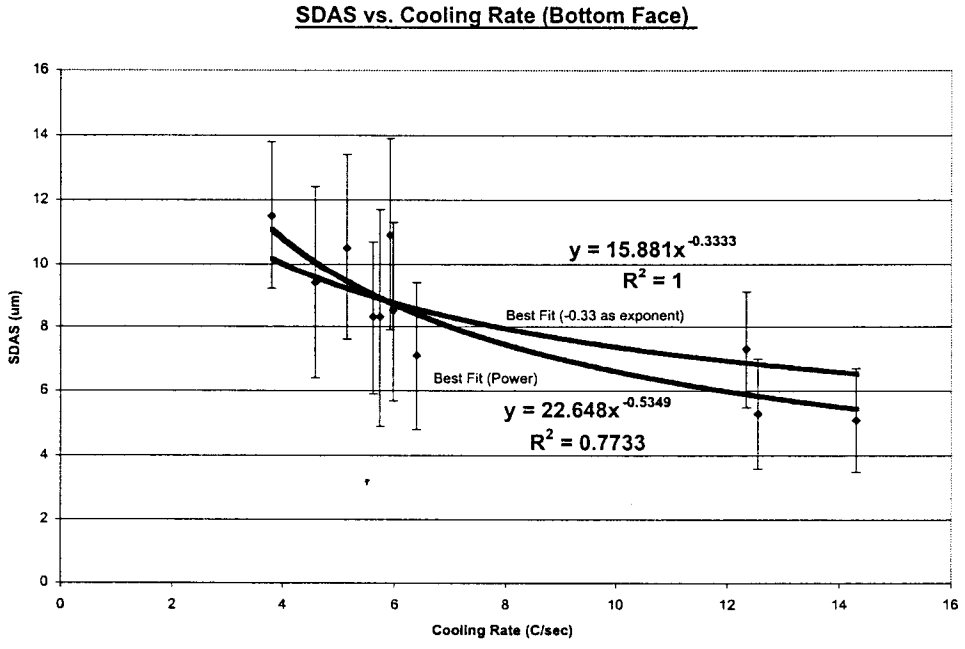

Figure 23: Comparison of the best fit of data points between power law and -0.33 as exponent.

8. EXPERIMENTAL STUDY AT AMCAST AUTOMOTIVE

A wheel-like shaped casting (Figure 24) was made in a low-pressure PM casting machine at Amcast Automotive, in which molten metal from a pressurized furnace is pushed into the mold via a feed tube, called a stalk. The air pressure inside the furnace is increased to pressurize the metal to feed porosity as the casting solidifies. 26 thermocouples were embedded in the die cavity to monitor the cooling behavior of the casting and to record the temperature history using the associated data acquisition system. The pressure levels, along with the time required to achieve complete filling, are microprocessor controlled in the casting machine.

Low pressure PM experimental trials with the wheel-like test mold were conducted by Amcast Automotive on December 28, 1999 at their Fremont plant in Indiana with the following specifications: -

Name of the casting produced: *Wheel-like shaped casting* (Maximum diameter at rim: 17" and height: 7.8") as shown in Figure: 24.
Machine: *Programmable Logic Controlled (PLC)* low-pressure caster with a center filled mold.
Alloy: A356; Die material: H13; Pouring Weight: 7970 g.
Bath temperature (°C): 718
Temp. of liquid metal before entering the die (measured from a previous test) (°C): 690

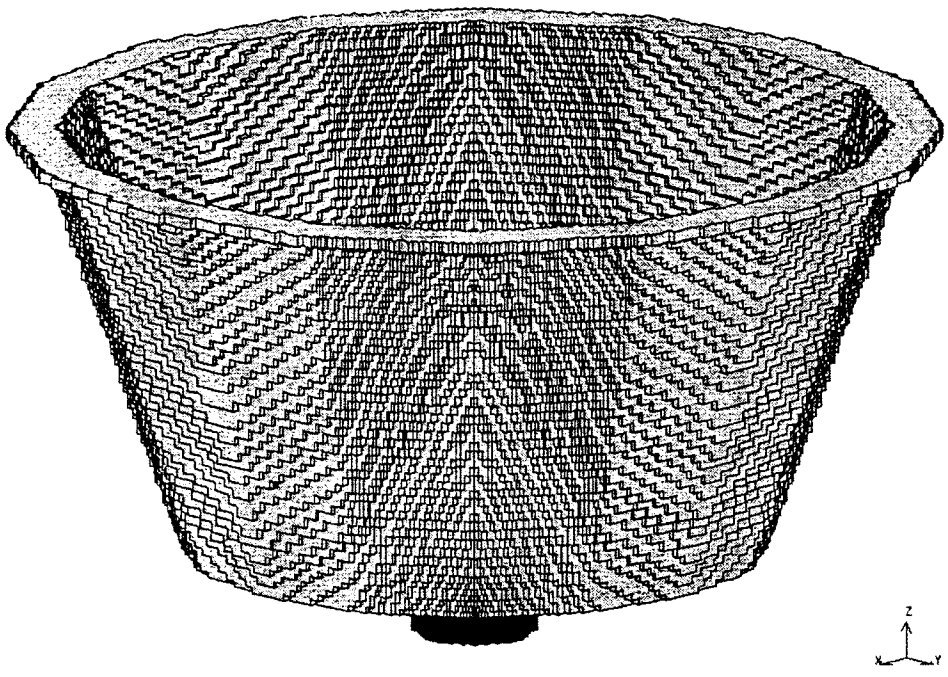

Figure 24: Finite Difference mesh of the Wheel-like casting

Initial mold temperature (°C): 500
Pressurization: 10 mbar/sec. during the pressure range 0~379 mbar and increased to 17 mbar/sec. until a pressure of 1034 mbar.
Time lapsed from start of shot to end of pressure: 324 sec.
Time lapsed from end of pressure to mold open: 47 sec.
Mold opening time: 17 sec.
Number of warm up shots: 10

Amcast has reported that the entire die was first coated with *Pyrostan*, a base coating with little insulation and then with *Concote 200*, which is a surface finish coating, and that only the top die was finally coated with *Ceramcote 252* which is an insulation coating containing refractory fillers. These were the standard die coatings normally applied to a typical wheel die. No cooling of the dies was used in the experiments conducted.

The locations of 26 thermocouples placed in the mold for accurate recording of temperature history are illustrated in Figure: 25. Two thermocouples (No.25 and No.26), permanently embedded in the flange of the wheel-like casting, were used to identify the completion of mold filling. Temperature recorded by a mold thermocouple (No.18), mounted close to the sprue bushing, was used to control the injection cycle. The temperature data from the remaining 23 thermocouples were recording using the associated data acquisition system.

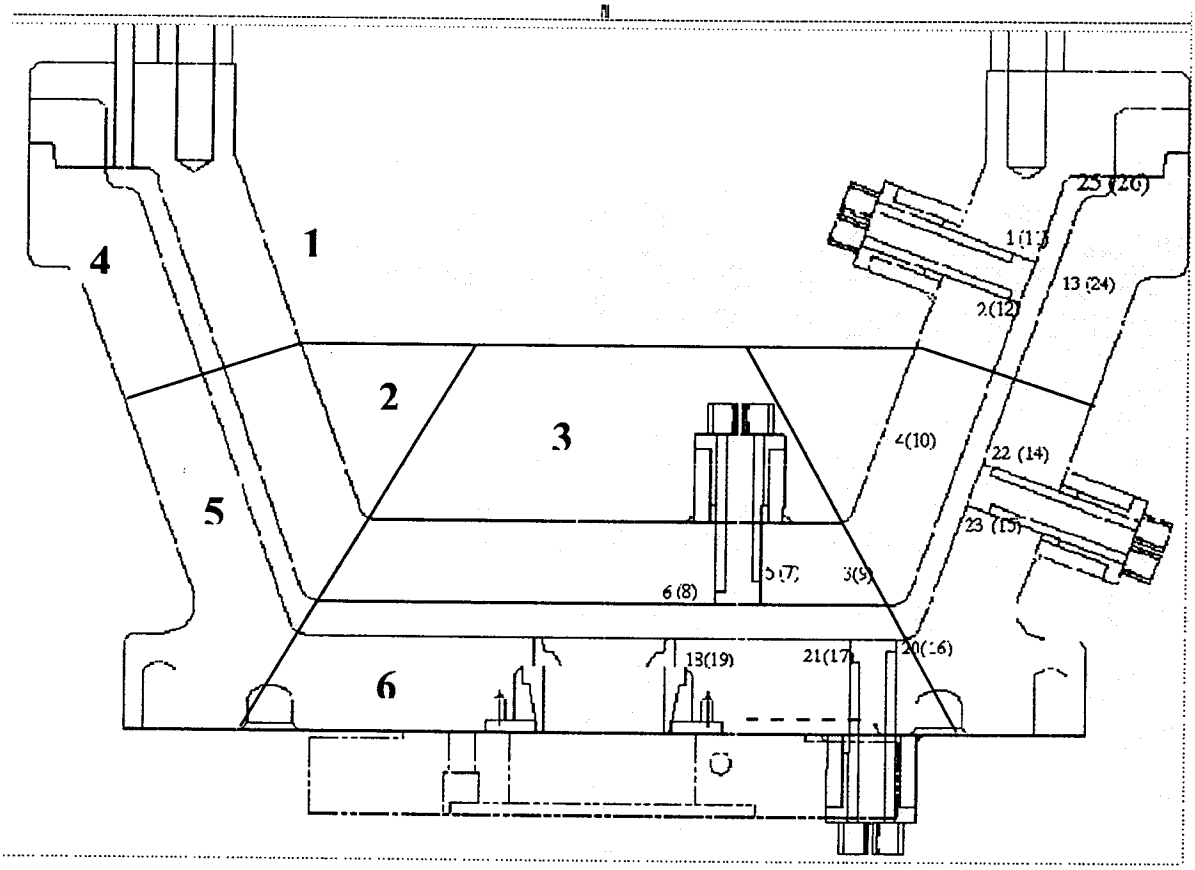

Figure 25: Relative positions of various thermocouples in the segmented wheel-like test mold.

The LPPM experiments conducted at Amcast generated a vast amount of temperature data, which were used to arrive at the experimental cooling curves at various locations of the casting. These curves were later matched with the simulated cooling curves to estimate the interfacial heat transfer coefficient at every location of the casting.

No measurements of pressure or air gap were made during these experimental trials. Casting samples from these tests were sent to UM for metallographic inspection.

Table VI: *Thermocouples located in each of the six die segments*

Description of location	***Segment number as per Figure 4***	***Thermocouple number***
Top-inner	1	1, 2, 11, 12
Top-outer	4	13, 24
Middle-inner	2	4, 10
Middle-outer	5	14, 15, 22, 23
Bottom-inner	3	3, 5, 6, 7, 8, 9
Bottom-outer	6	16, 17, 18, 19, 20, 21

9. LPPM SOLIDIFICATION SIMULATION AT UM

The 3D geometric data file in the *stl* format was imported into MAGMAsoft, a commercial solidification software package, for enmeshment. A total of 2,000,000 control volumes were used to enmesh the wheel-like shaped casting shown in Figure 24. Several simulations were run for the 3D solidification of the casting using MAGMAsoft ver.4.0 with various interfacial heat transfer coefficients in order to identify which HTC values closely matched the experimental data. Virtual thermocouples were placed in the die halves corresponding to their actual positions in the test mold as per Figure 25, to output simulated cooling profiles at those locations. During the initial warm up cycles with a uniform mold temperature, the cavity is assumed to be filled and simulation is carried out in a cyclic mode. Once the mold reaches an equilibrium temperature, the temperature distribution at the start of that cycle is used as the initial temperature distribution for running further simulations with filling and solidification (Tan R.K., et al., 1998)[13]. In our case, we have observed that at the end of the tenth cycle, the mold closely approached the equilibrium temperature and all the simulation results are extracted after completion of the eleventh cycle.

Several preliminary simulations were run with various interfacial heat transfer coefficients in order to identify which HTC values closely matched with the experimental data supplied by Amcast. In each simulation run, a time dependent HTC distribution was assumed with five peak HTC values of 500, 1000, 1700, 2400 and 3000 W/m^2 K. At the completion of every simulation, the average cooling rate for each HTC distribution was calculated for each thermocouple location and plotted against the corresponding peak HTC value. A curve was fitted for all such points, a total of five, corresponding to the five HTC values. Figure 26 shows the variation of the average cooling rates with peak HTC values at various thermocouple locations. Five curves are plotted on this figure corresponding to the five pairs of thermocouple locations inside the mold. These initial simulations helped to identify the maximum and minimum limits of the Interfacial Heat Transfer Coefficients (IHTC) for this casting process. IHTC' s for this process were found to vary from a minimum value of about 500 W/m^2 K to a maximum value of about 3000 W/m^2 K, depending on location.

The original geometry file of the wheel-like mold was sectioned into six segments by defining two section planes, one close to the middle of the mold assembly and the other close to the mold bottom. Figure 25 shows a schematic diagram of the segmented mold. Thermocouples mounted in each segment are presented in Table IV. Segmentation was done to improve heat flow simulation from the dies using MAGMAsoft and to take into account the effect of geometry and regional air gap in estimating interfacial heat transfer coefficients (Ransing and Lewis, 1997)[14]. The relationship for the overall heat transfer coefficient, h, neglecting the effects of radiation heat transfer (negligible for aluminum alloys) is as given below:

$$\frac{1}{h} = \frac{1}{h_{gap}} + \frac{1}{h_{coating}} + \frac{1}{h_{oxide}}$$ Equation 1

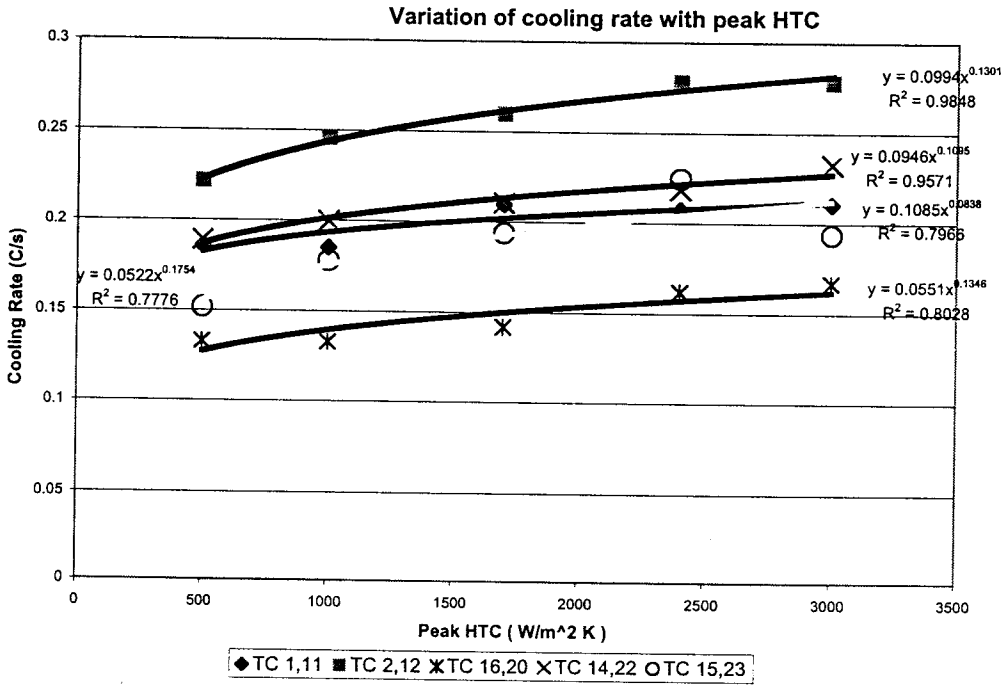

Figure 26 : Variation of local cooling rates at various thermocouple locations, when HTC values are varied from 500 to 3000 W/m^2 K

where h_{gap} is the heat transfer coefficient due to any air gap formed between the mold and casting; $h_{coating}$ is the heat transfer coefficient to account for thermal resistance of the die coating material layer; h_{oxide} is the heat transfer coefficient to account for the thermal

resistance of any oxide layer on the solidifying alloy. The last term in the above equation 1 is neglected because no information is available on this very, very thin oxide layer.

Michael Trovant and Argyropoulos Stavros (Trovant and Stavros, 2000)[15] have developed a semi-empirical inverse equation to characterize the heat transfer coefficient-air gap relationship across the various stages of solidification from their experiments with a cylindrical aluminum casting in a copper mold. The form of the equation that correlates both the experimental data from their study, as well as the data available from the literature, is reported as:

$$HTC = \frac{1}{k.A + r} + C \qquad \text{Equation 2}$$

where the above equation takes into account variations in surface roughness, radiation and other uncontrolled variables present among differing literature studies to be absorbed by the constants k, r and C. 'A', is the variable air gap in mm and k, r and C are input with the units of $W^{-1}m^2$ K mm^{-1}, $W^{-1}m^2$ K and Wm^{-2} K^{-1}, respectively. The correlation from their experiments is shown in Figure 27.

Based on the coating thickness and thermal conductivity data from the literature, simulations were run with the segmented mold geometry in MAGMAsoft. Separate HTC values were assigned for each of the six interfacial segments (Figure 25) of the wheel-like mold. HTC distribution was chosen based on the air gap formation and the HTC due to die coating for an average die coating thickness of 50 μm. HTC due to air gap was calculated based on equation 2. A linear distribution of air gap with solidification time was assumed (Trovant and Stavros, 2000)[15] in order to calculate the HTC due to air gap formation.

The interfacial HTC distributions for mold segments 1, 2 and 3 are shown in Figures 28-29. Figure 28 compares the HTC distribution for segments 1 and 2 for all the nine simulation versions. Figure 29 compares the HTC distributions for segment 3. Comparison of the experimental and theoretical curves for temperature distribution at various thermocouple locations in the mold are shown for mold segments 1, 3, 5 and 6 in Figures 30-33. Only a few representative cooling curves are presented in this report. Thermocouple locations referred to in these curves are described in Table VI. It should be noted that temperature distribution for versions 4 and 5 are almost identical as depicted in Figures 30-33.

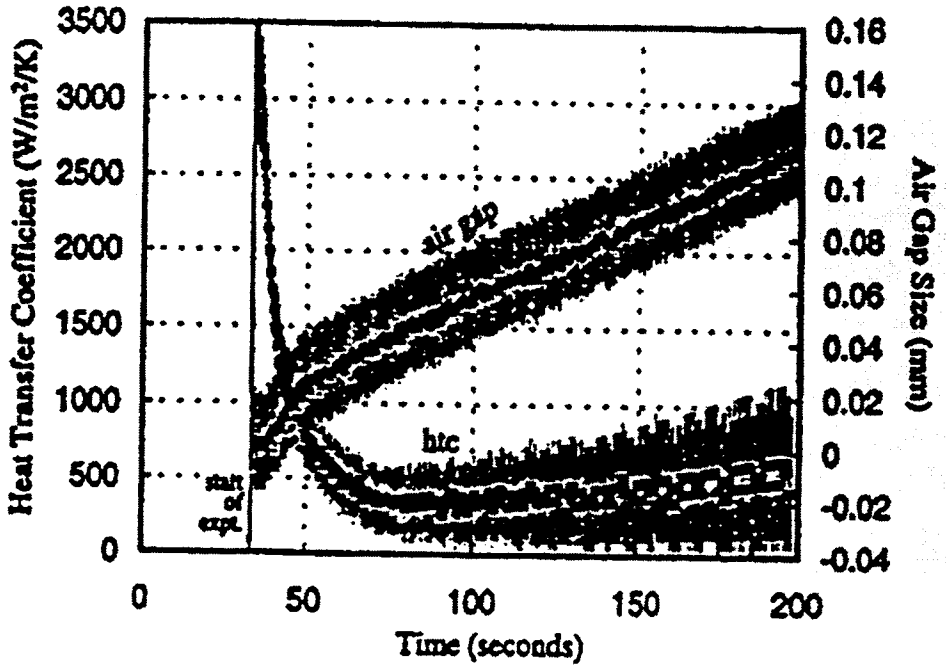

Heat transfer coefficient and air gap size measurements for the A356-copper system.

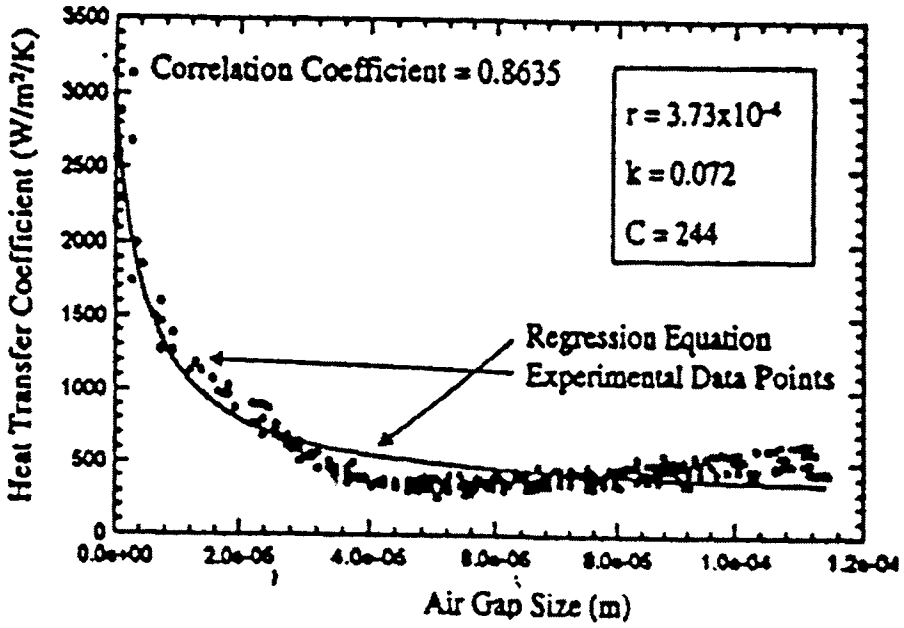

Correlation plot for A356 aluminum alloy cast in a copper mold.

Figure 27: Courtesy of Michael Trovant and A.Stavros, Metallurgical and Materials Transactions B, Vol. 31B, pp. 75-96, February 2000. (15)

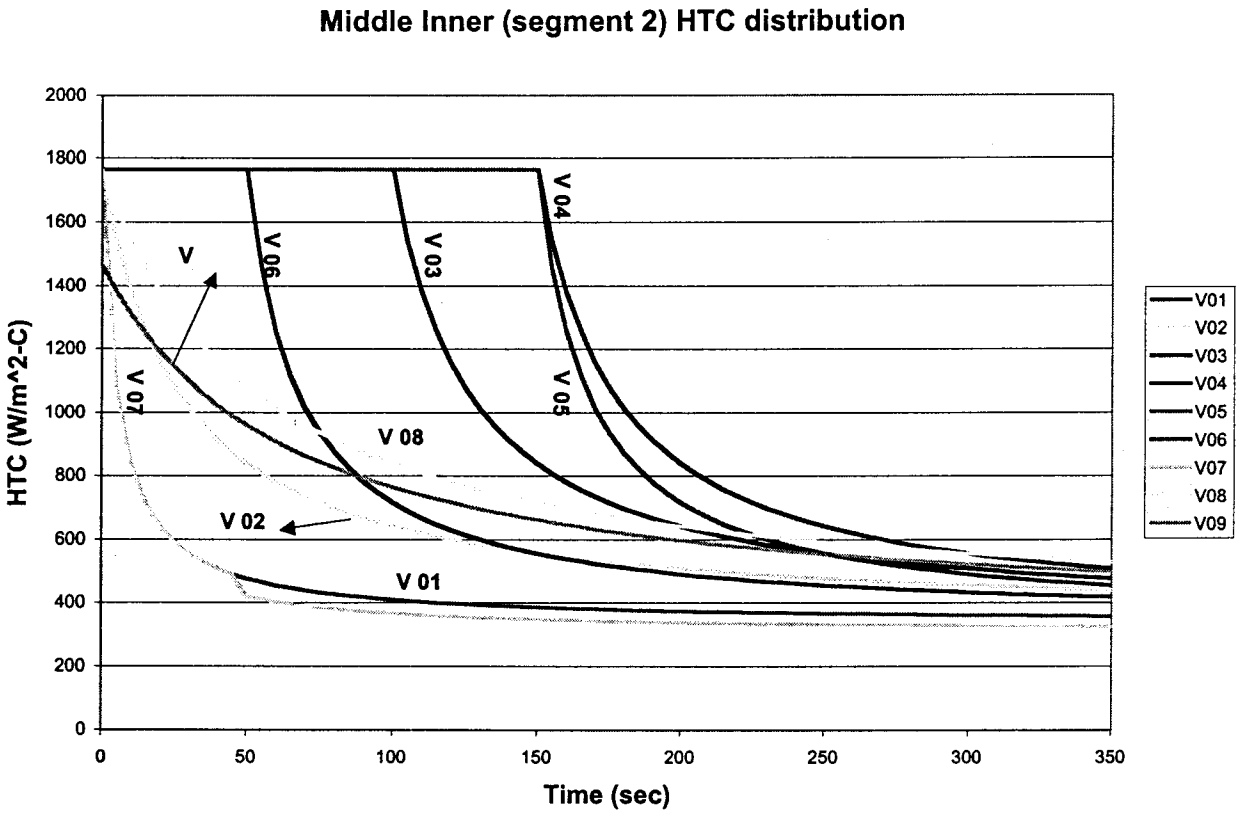

Figure 28: HTC distribution for segments 1 and 2

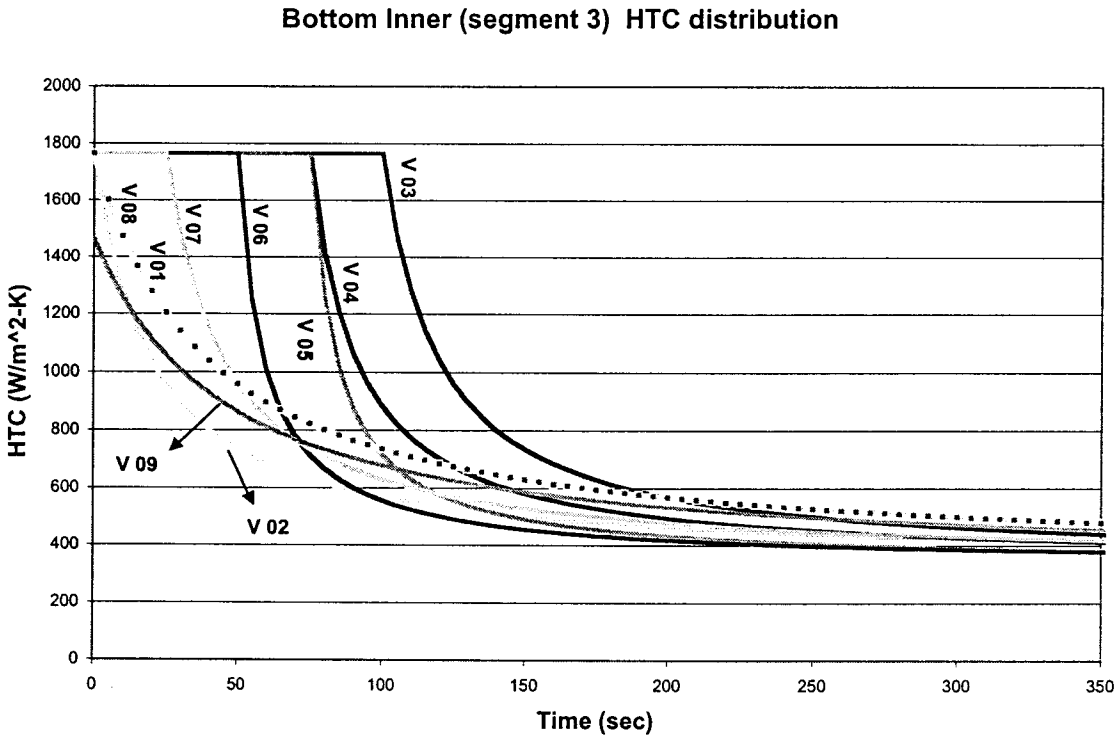

Figure 29: HTC distribution for segment 3

It is readily seen from the curves of Figures 30-33 that experimental temperature distributions at symmetrical thermocouple locations (e.g.: 1-11, 23-15, 5-7 and 21-17) are very similar as expected. It was seen that simulated curves have a lower starting temperature for the same time when compared to that of the experimental curves. This might have been caused either by variations in the actual geometrical locations of the thermocouple junctions in the die halves, delay in thermocouple response, or due to a calibration error. However, as we are interested in estimating appropriate interfacial HTC values in each die segment, it is sufficient to match the cooling rates of both of the curves. Hence, all the original simulated curves were moved to their new positions, thereby adjusting for the thermocouple error. The simulated curves presented in all the above figures are compared with the experimental curves after this adjustment.

The HTC distribution for the bottom face core-casting interface (segment 6) is kept unchanged in all the simulation versions as it results in a very good match with the experimental data. Figure 31 confirms this fact. All the nine simulation versions shown in the figure show a good match for the mold segment 6. A higher value of HTC in this case is due to the perfect contact aided by gravity between the wide base of the casting and the bottom die and the absence of an air gap.

It is observed that the overall HTC for segments 1-3 in all the simulations drops from 1765 W/m^2 K to about 400 W/m^2 K, except for version 9, the time required being dependent on the air gap. The coating thermal conductivity was decreased from 0.46 to 0.3 W/m K for version 9. The difference in the HTC distributions for segments 1 and 2 and for segment 3 is related to the air gap, where for segment 3, a larger air gap has been assumed than for segment 2, except for version 7. A larger air gap of 500 μm at segments 1 and 2 for version 7 resulted in a better match, as illustrated in Figure 33. The HTC for version 7 decreases from 1765 W/m^2 K to 500 W/m^2 K in about 40 seconds because of this larger air gap. A good matching of the simulated and experimental curves is the result of this modified HTC distribution as illustrated in Figure 33. This leads to the conclusion that the air gap formed at the middle and top inner interfacial segments (i.e. segments 1 and 2) are larger than the earlier assumption.

In the case of segments 1 and 2, it is seen that the usual time dependent distribution of HTC used for the other segments do not result in a good match of the simulated and experimental curves. In the case of segments 3, 4 and 5 the distribution of HTC is more complex due to the formation of an air gap, as well as the geometric variations in the casting. It is observed that at the middle and top segments 1, 2, 4, and 5, the casting seems to make and break contact with the mold, depending on the balance between the shrinkage force and gravitational pull.

It is observed in all the HTC distributions shown in Figures 28-29 that the HTC approaches a constant value of about 400 W/m^2 K, after the lapse of about 300 seconds, no matter whatever may be the air gap. This clearly shows that at this point, the HTC is no longer influenced by the air gap, but depends on the thermal conductance at the metal-mold interface. The interfacial thermal conductance depends on the thermal properties of the coating material and mold and coating thicknesses, as well as the surface roughness of the interfaces.

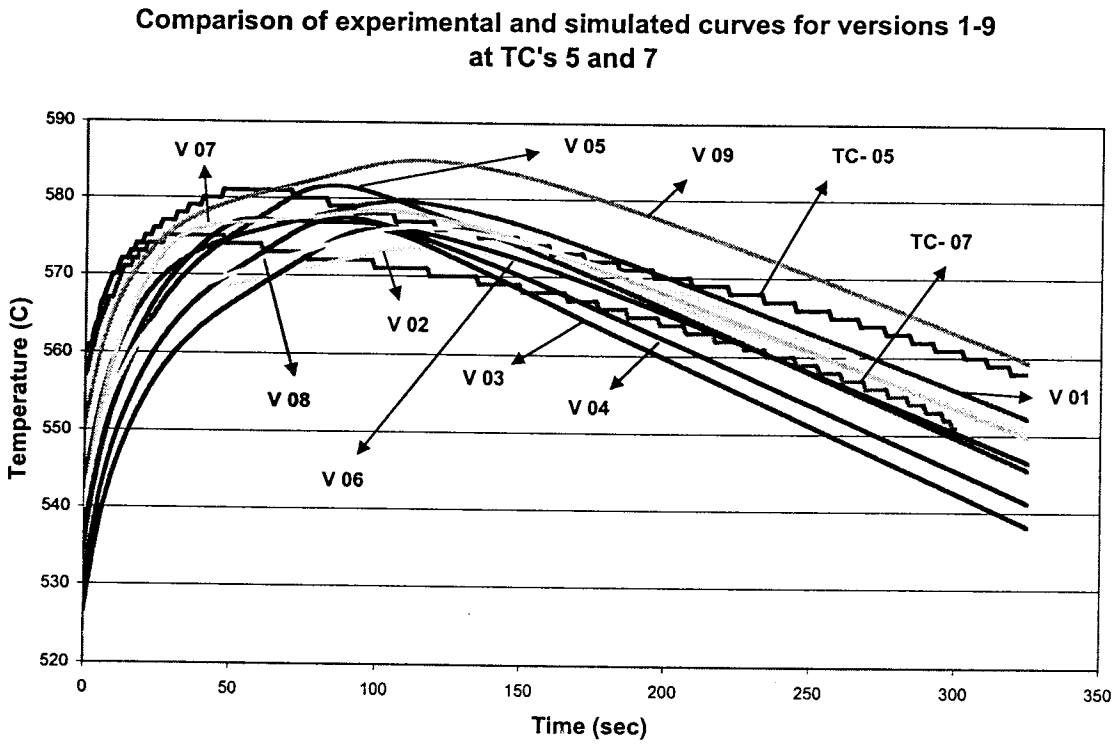

Figure 30: Comparison of experimental and simulated temperature distribution at segment 3

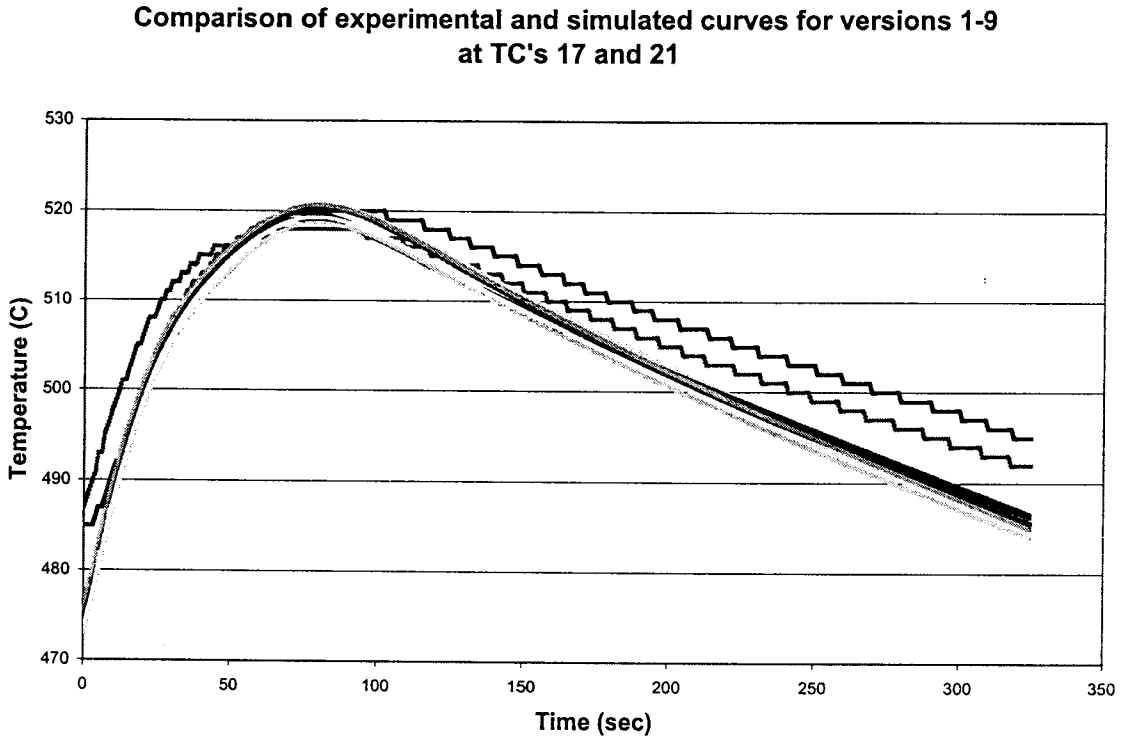

Figure 31: Comparison of experimental and simulated temperature distribution at segment 6 with a constant HTC of 2000 W/m^2 K

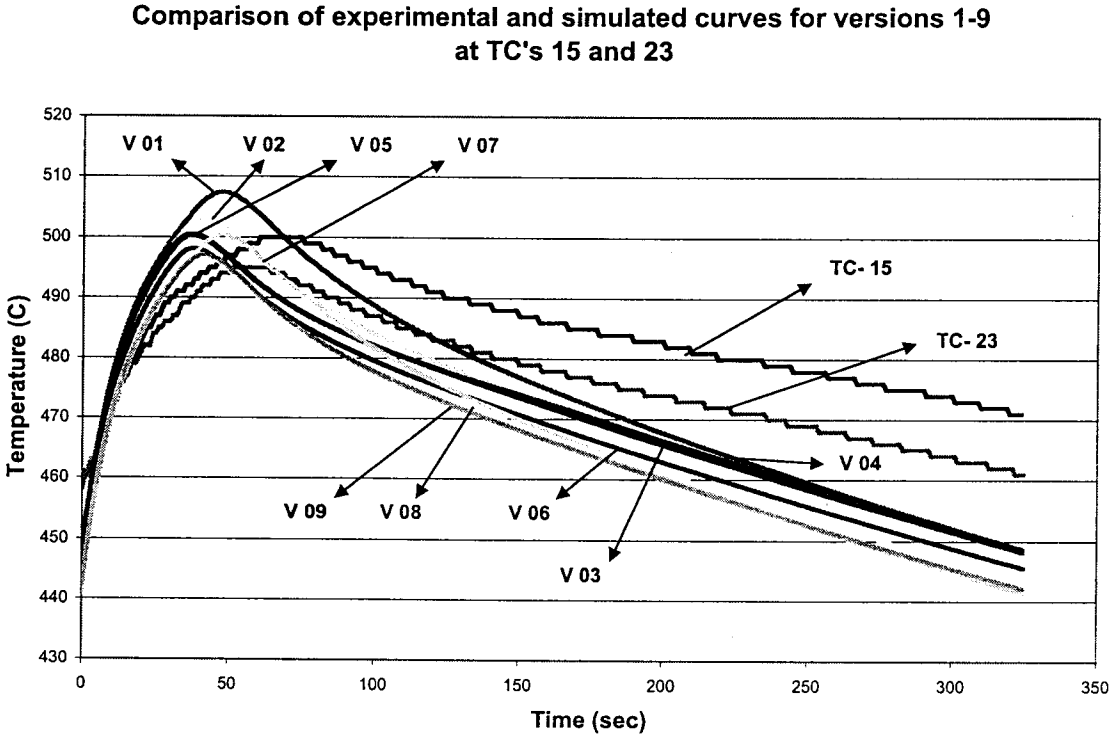

Figure 32: Comparison of experimental and simulated temperature distribution at segment 5

Note: ***Although the HTC distributions for segments 4 and 5 are assumed to be the same, the temperature distribution shown in the above figure is for segment 5 only. This is due to the fact that no experimental temperature data is available for segment 4, because of the absence of thermocouples at that mold segment.***

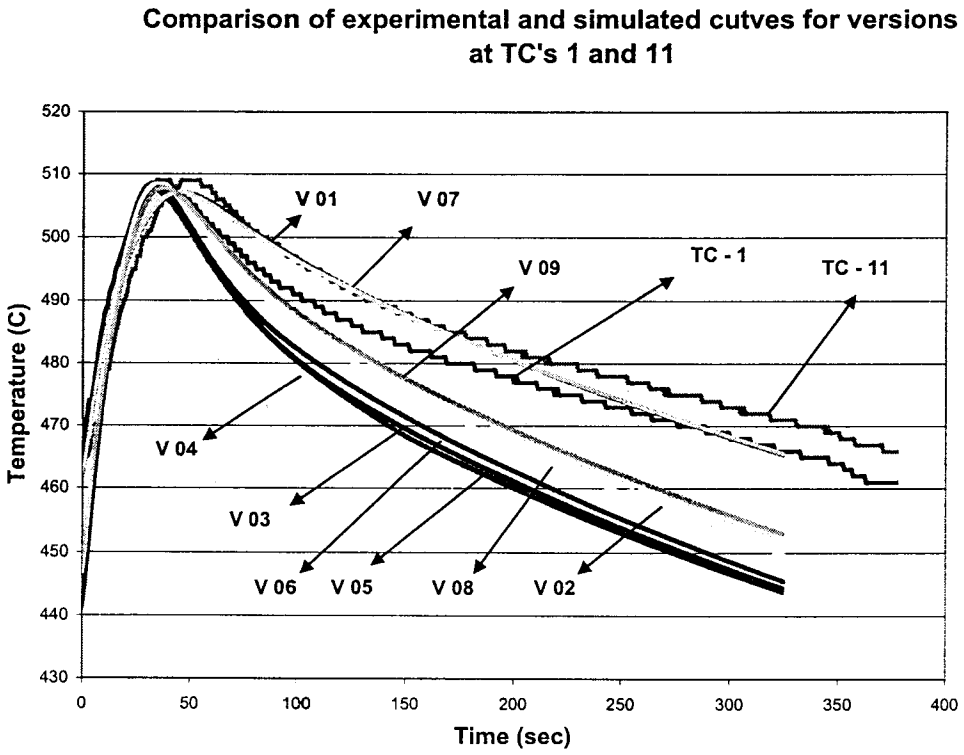

Figure 33: Comparison of experimental and simulated temperature distribution at segment 1

Note: ***Although the HTC distributions for segments 1 and 2 are assumed to be the same, as shown in Figure 7, the temperature distribution shown in the above figure is for segment 1 only. This is due to the fact that no experimental temperature data is available for segment 2, because of the absence of thermocouples at that mold segment.***

10. DIE COATING ANALYSIS AT UM

The thermal conductivity values from the literature (16-19) for white die coatings were used to account for the decrease in HTC values at mold-metal interfaces. Amcast has sent

UM some data, received from one of their coating vendors, relating to the thermal conductivity values of their coating materials. UM also received some data on conductance of coatings summarized by Franco Chiesa, et al. (16,17) and some literature on low pressure casting processes. Thermal conductivity estimation of a thick (about 6 mm) commercial heat insulting-type mold coating by Wei, S, et al (19) found the value to vary from 0.50 to 0.30 W/m K for the temperature range of 25-600 ^{0}C. A sensitivity analysis by the same authors showed that, a 20-25 % variation of the coating material thermal conductivity does not affect the heat transfer through the mold. Nyamekye, K., et al., (18) reported a thermal conductivity of 0.12- 0.33 W/m K depending on the refractory filler material and porosity of the coatings. Since the thickness in our case for the white coatings was very small, we used an average thermal conductivity value of 0.2 W/m K for the top mold and 0.3 W/m K for the bottom mold.

A total of five coating samples was sent to UM from Amcast, each representing the actual coating condition on the top and bottom die halves and the respective layers of coating, insulating as well as non-insulating. Table-VII, given below, shows the coating material on each of the sample pieces received.

Table -VII: *Coating material on each of the sample pieces from Amcast*

Sample No.	Color	Coating material	Remarks
1	red	Pyrostan	low insulation
2	green	Concote 200	medium insulation
3	blue	Ceramcote 252	high insulation
4	green	Pyrostan + Concote 200	
5	blue	Pyrostan+Concote 200+Ceramcote 252	

All the five coating samples were sectioned, mounted, ground and polished.
Figures 34-36 show optical micrographs taken from the coating samples received from Amcast. The coatings were applied manually using a spray gun on mild steel sample plates. Micrographs from sample 1 with only a very thin layer of *Pyrostan* (a base die coating) did not reveal any information about the thickness of the coating. Similarly, micrographs taken from sample 5 with three layers of coating did not reveal a clear picture where each layer can be clearly distinguished from the other. However, using the measured coating thickness of samples 2, 3 and 4, the thickness of coatings for samples 1 and 5 were estimated. The thickness data are presented in Table VIII. It is observed that the average thickness of an insulating die coating is close to 43 μm compared to the earlier assumed value of 100 μm.

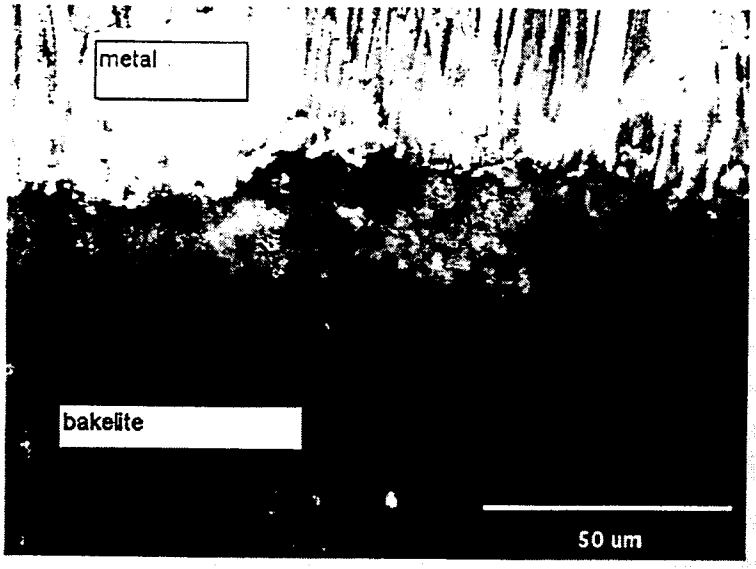

Figure 34: Optical micrograph showing a layer of *Concote 200* between the metal and the Bakelite mount

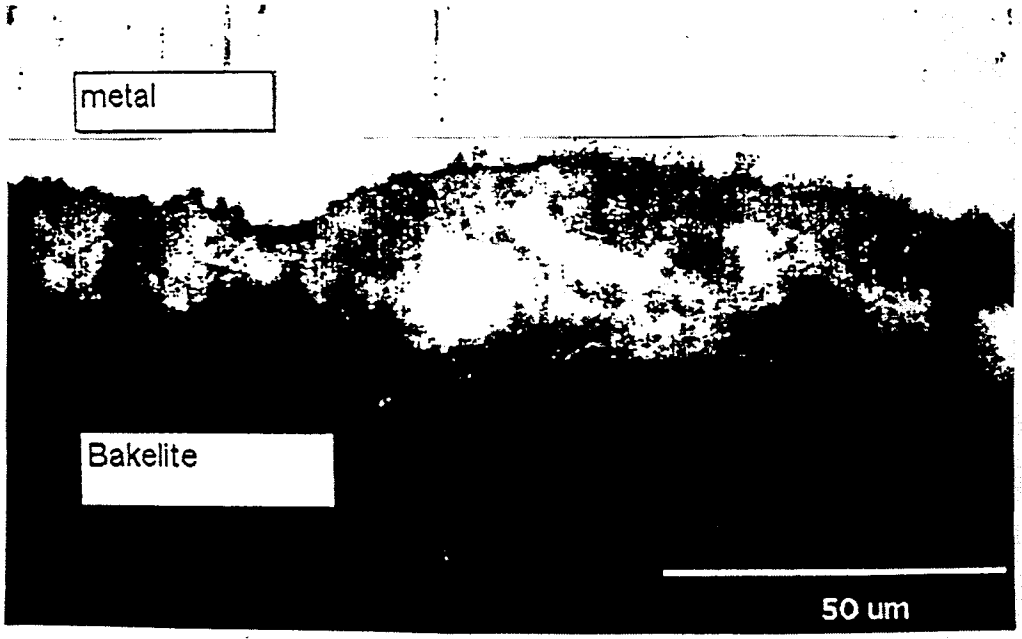

Figure 35: Optical micrograph showing a layer of *Ceramcote 252* between the metal and the Bakelite mount

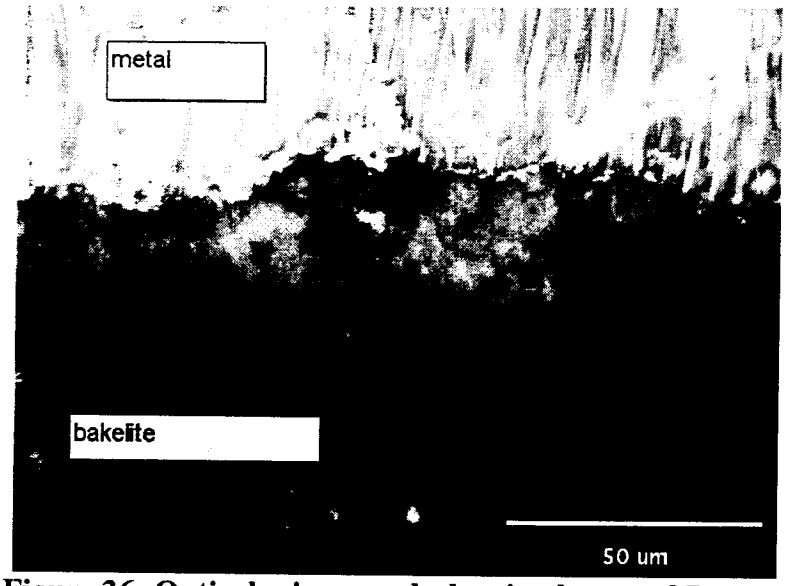

Figure 36: Optical micrograph showing layers of *Pyrostan* and *Ceramcote 252* between the metal and the Bakelite mount

Table VIII: Measured die-coating thickness from the micrographs

Coating sample no.	Coating material	Measured Thickness in μm			
		Max.	Min.	Mean	Std.deviation
2	*Concote 200*	35.5	4.13	16.3	7.23
3	*Ceramcote 252*	26.4	9.9	19.9	5.5
4	*Pyrostan+ Ceramcote*	46.3	11.6	22.9	8.1

Six simulations, 10-15, with varied coating parameters and different constant period HTC's were run and these results are compared.

As in the case of the earlier simulations, a linear distribution of air gap with solidification time was assumed in order to calculate the HTC due to air gap formation. Figures 37, 38, and 39 compare the HTC distributions applied in versions 10-15 for segments 1-5. HTC distribution for segment 6 was kept at a constant value of 2000 W/m^2 K, except for version 15, where a small decrease in HTC with time is applied, as shown in Figure 40. Comparison of the experimental and simulated curves for temperature distributions at various thermocouple locations in the mold are shown for mold segments 1, 3, 5 and 6 in Figures 41-46. Thermocouple locations referred to in these curves are presented in Table VI and their positions in the actual mold halves, illustrated in Figure 25 (see page 74).

The HTC distribution at the interface between the top core and casting has been modified in these versions by varying the constant HTC period and coating parameters (thickness and thermal conductivity) to better fit the experimental data. The coating thermal conductivity was kept constant in versions 10 and 11 and assumed to be 0.3 W/m K. For version 12, coating thermal conductivity at segment 3 was reduced from 0.3 to 0.2 W/m K and further reduced to 0.1 W/m K for version 13. Coating thickness was reduced from 100 μm to 50 μm in the case of segments 1 and 2 in version 11, while keeping the thermal conductivity unchanged. The coating thermal conductivity at segment 3 (see figure 38) for version 14 was kept the same as that of version 13 and further reduced to 0.08 W/m K for version 15. The coating thicknesses and constant HTC time periods were unchanged at these locations. A reduction in $h_{coating}$ (HTC of die coat) from 2000 W/m^2 K to 1000 W/m^2 K and even to 800 W/m^2 K in the case of version 15, seems to result in a better match, as shown in Figure 41. Since the time-dependent HTC distributions in the earlier simulations did not result in a good match at thermocouple locations 1,11 and 2, 12 in segment 1, a temperature-dependent HTC distribution was applied at these locations for simulations 12-15. The HTC was reduced from 1800 W/m^2 K to about 400 W/m^2 K when the metal temperature decreased from the liquidus (613^{0}C) to the solidus (542^{0}C) for version 12 and 13 and was reduced from 1900 to 300 W/m^2 K for subsequent simulations. Using temperature distributions from the metal-mold interface from a virtual thermocouple, the corresponding time dependent HTC distributions were derived and are

shown in Figure 37. The distributions shown in Figure 37 indicate a larger air gap of about 200 μm at segments 1 and 2. A better match is observed in Figures 45 and 46.

A different HTC distribution with an air gap assumption at segments 4 and 5 (see figure 39) is used in the present simulations to better fit the experimental data at these mold segments. With the air gap and coating thickness unchanged, the coating thermal conductivity was reduced from 0.3 to 0.2 W/m K for version 13, 0.1 W/m K for version 14 and 0.08 W/m K for version 15. A constant HTC time period of 50 seconds was applied in simulations 12-15 at these locations. A better fit of data is observed using these HTC distributions, as illustrated by Figures 43 and 44.

When versions 10 and 11 are compared, it is concluded that the HTC distributions assumed for version 10 for all the regions resulted in a better fit than for version 11. It is observed that an addition of a constant HTC period of 25 seconds for the HTC distribution of segments 3 and 5 for version 11 did not improve the matching of curves. When versions 14 and 15 are compared, it is concluded that the HTC distributions assumed for version 15 for all the regions resulted in a better fit than for version 14, except at segment 3. It is observed that a low coating thermal conductivity, and hence a lower overall HTC value at mold segments 3-5, seems to yield a relatively closer fit for the simulated version 15. A small decrease in IHTC with time applied at segment 6 for version 15 only, which was assumed to be constant in all the earlier simulations, helped to result in a closer fit, as shown in Figure 42. Thus the simulated version 15 helps to identify the IHTC's for the present case study.

It is important to note the influence of coating parameters on the cooling behavior of the casting after an air gap has been formed. Thus as mentioned in our earlier reports, the interfacial heat transfer after the air gap formation is primarily controlled by the coating parameters.

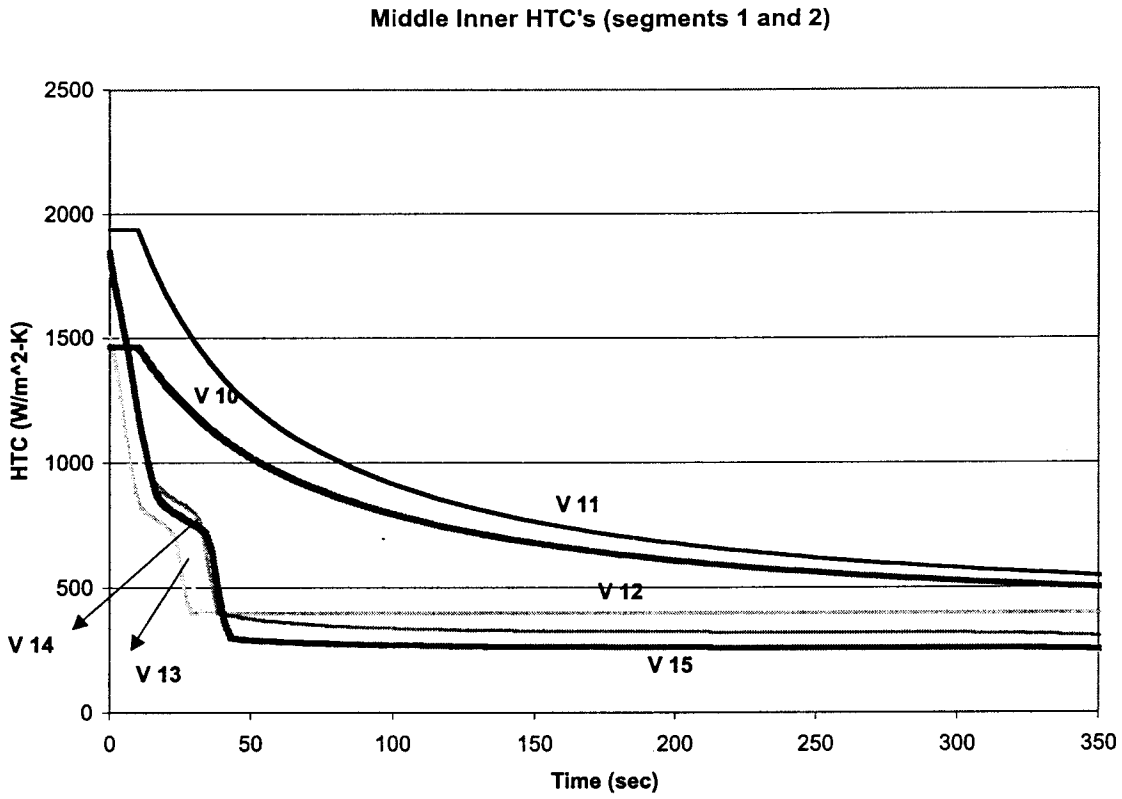

Figure 37: HTC distributions for segments 1 and 2 for versions 10-15

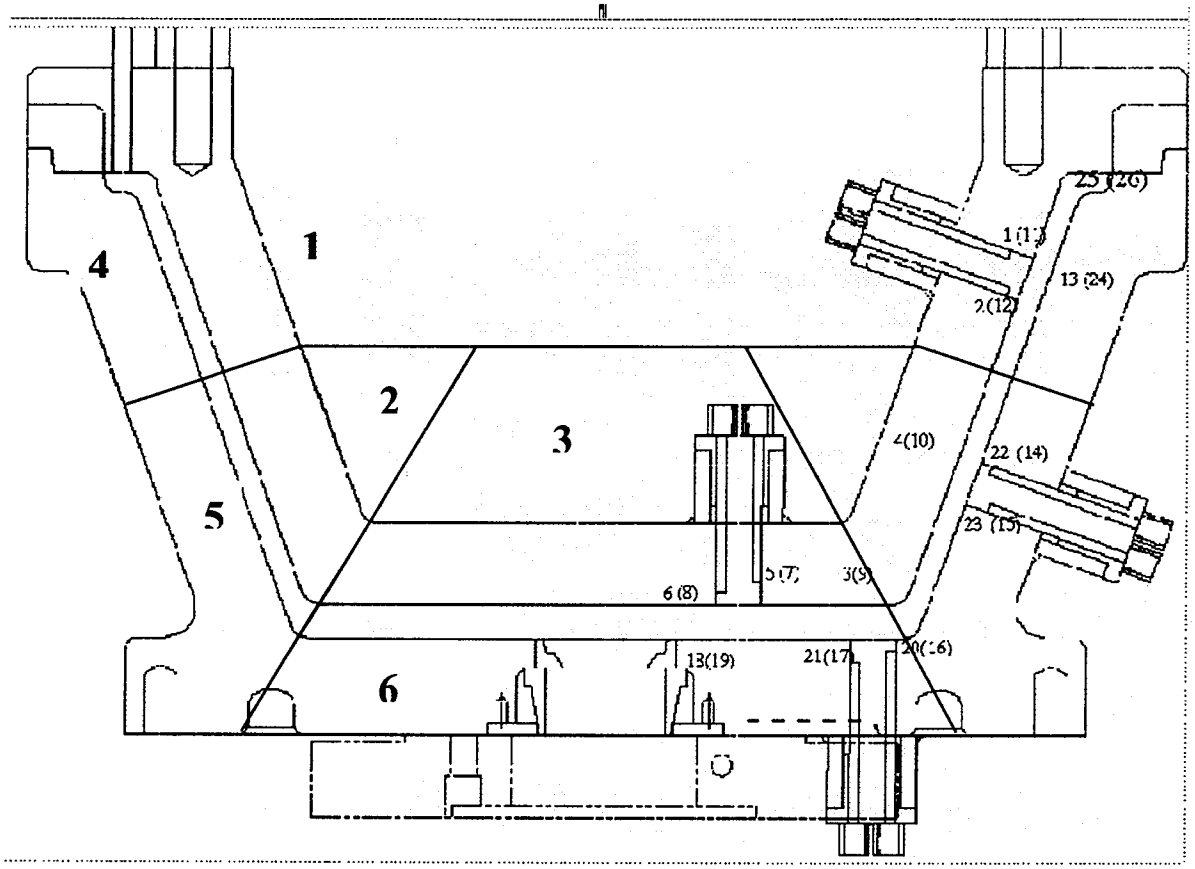

For reference, Figure 25 is shown again.

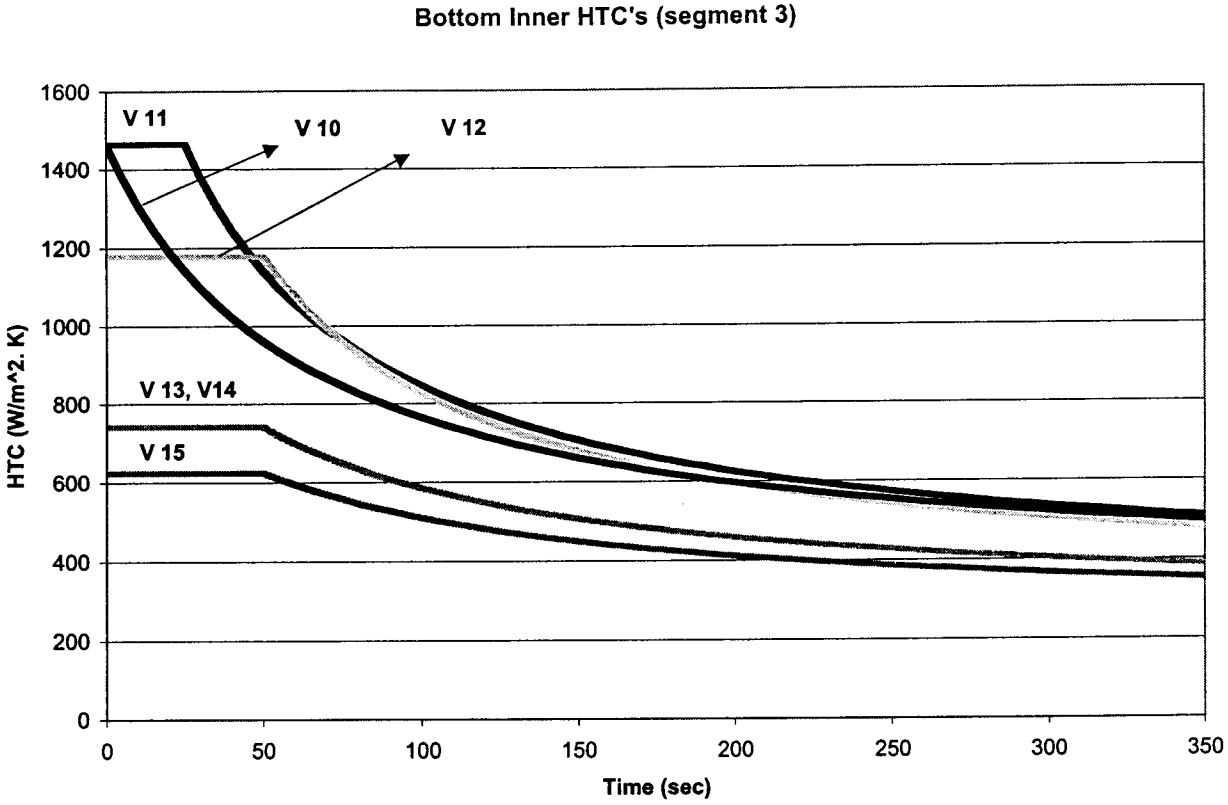

Figure 38: HTC distributions for segment 3 for versions 10-15

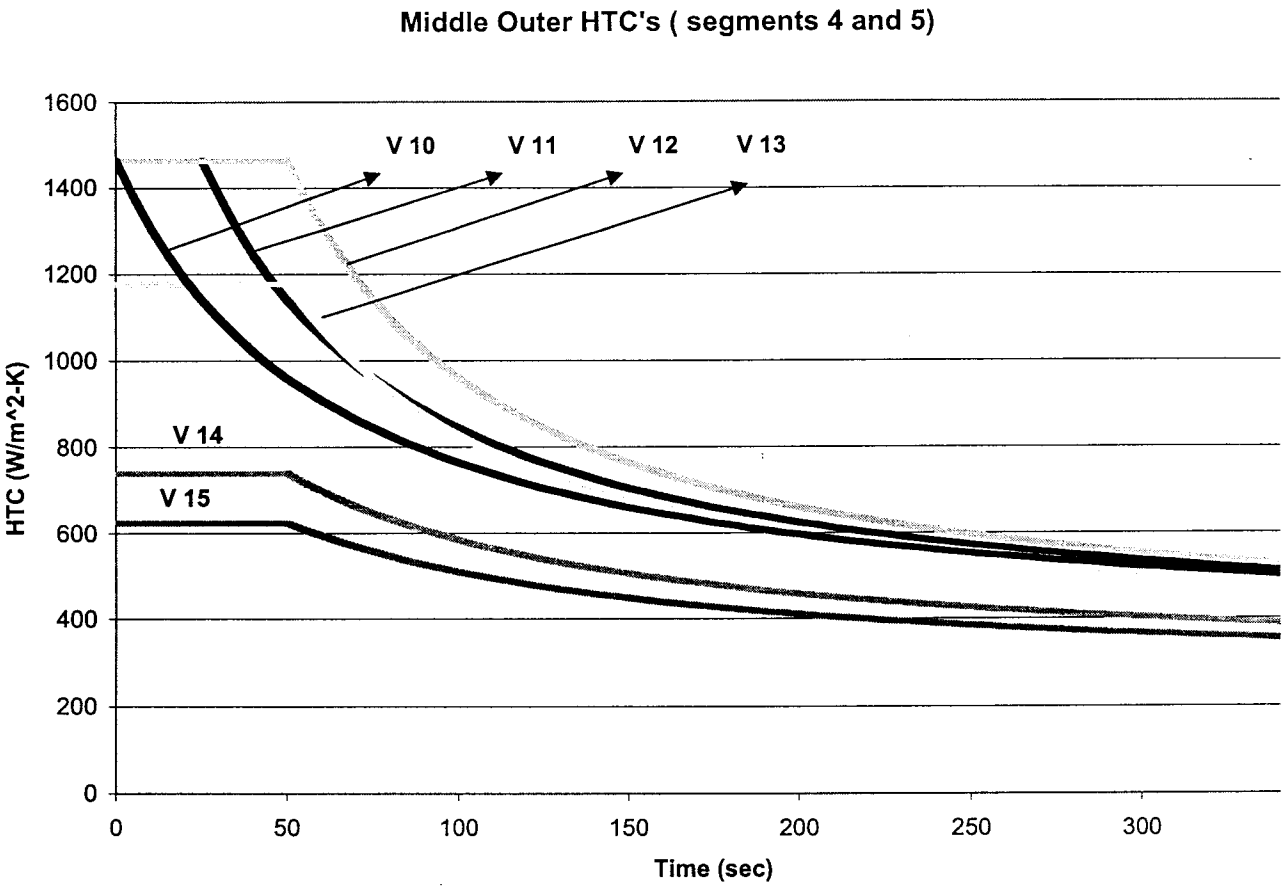

Figure 39: HTC distributions for segments 4 and 5 for versions 10-15

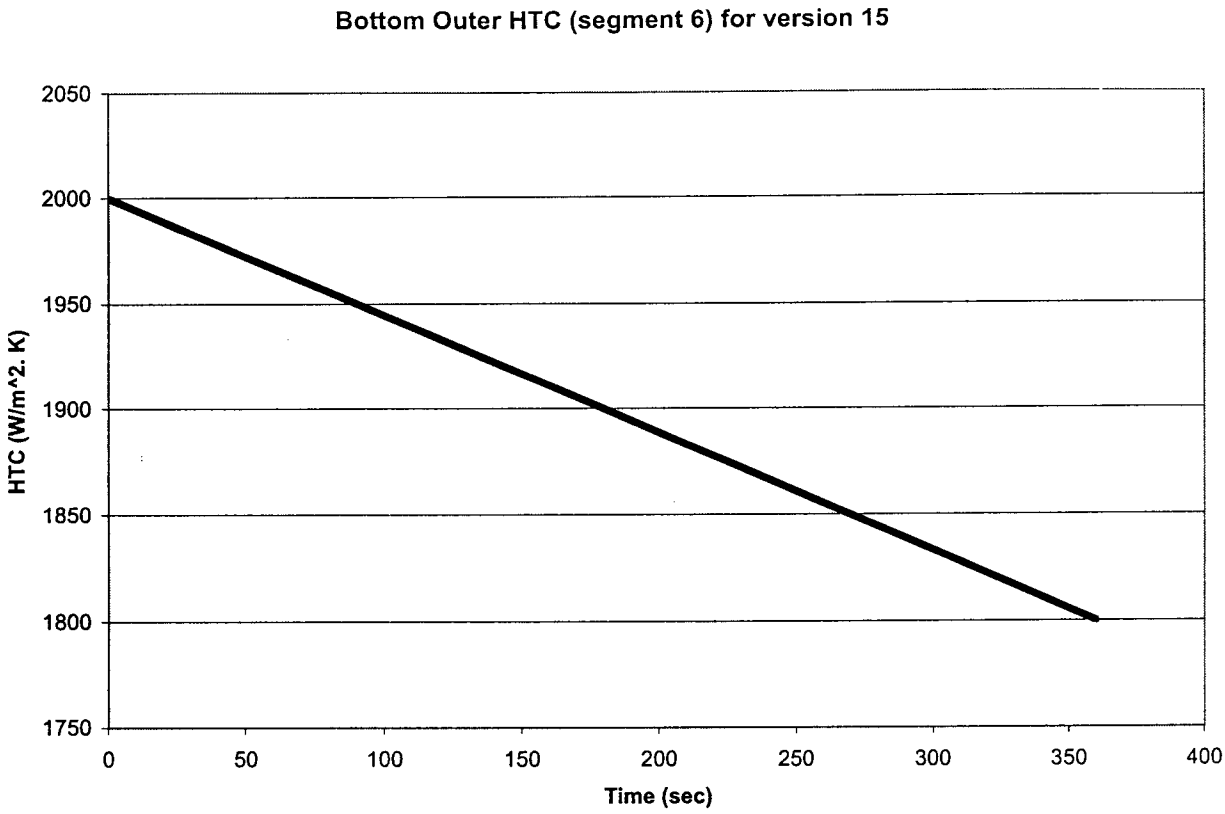

Figure 40: HTC distribution for segment 6 for version 15

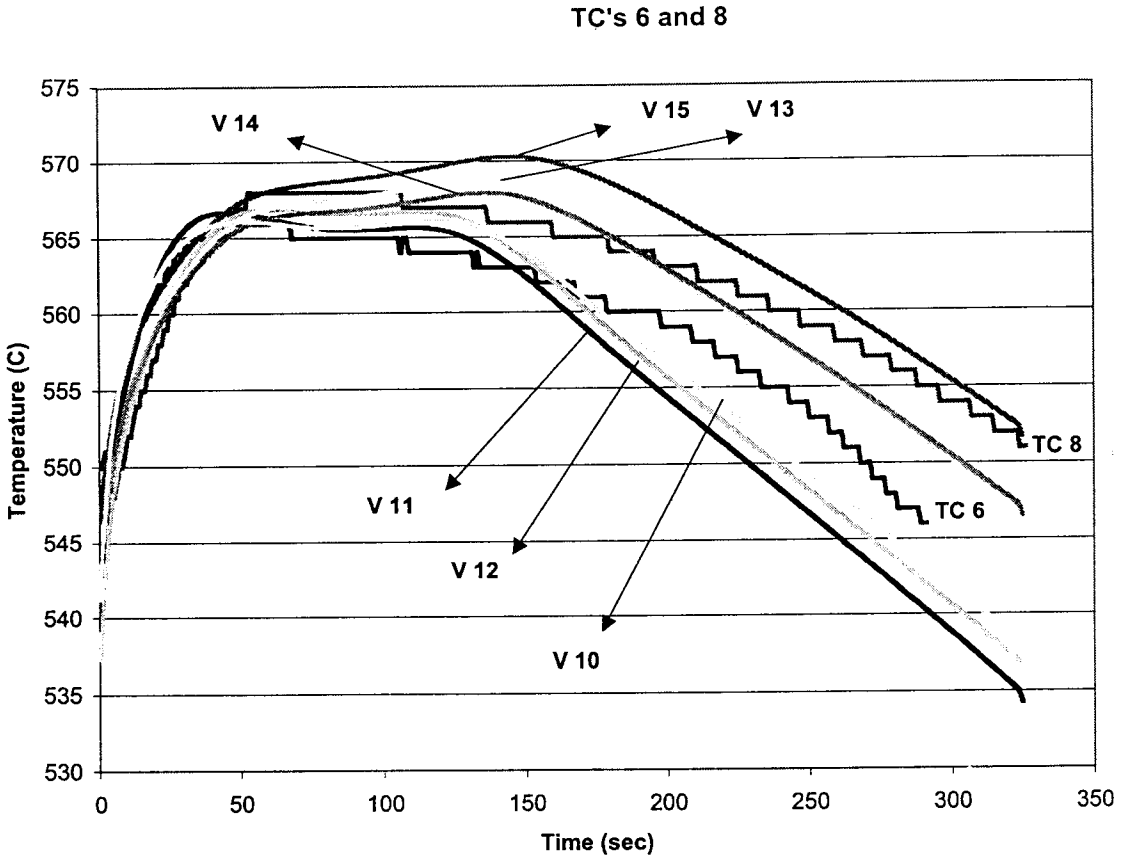

Figure 41: Comparison of experimental and simulated temperature distributions at TC's 6 and 8 for versions 10-15

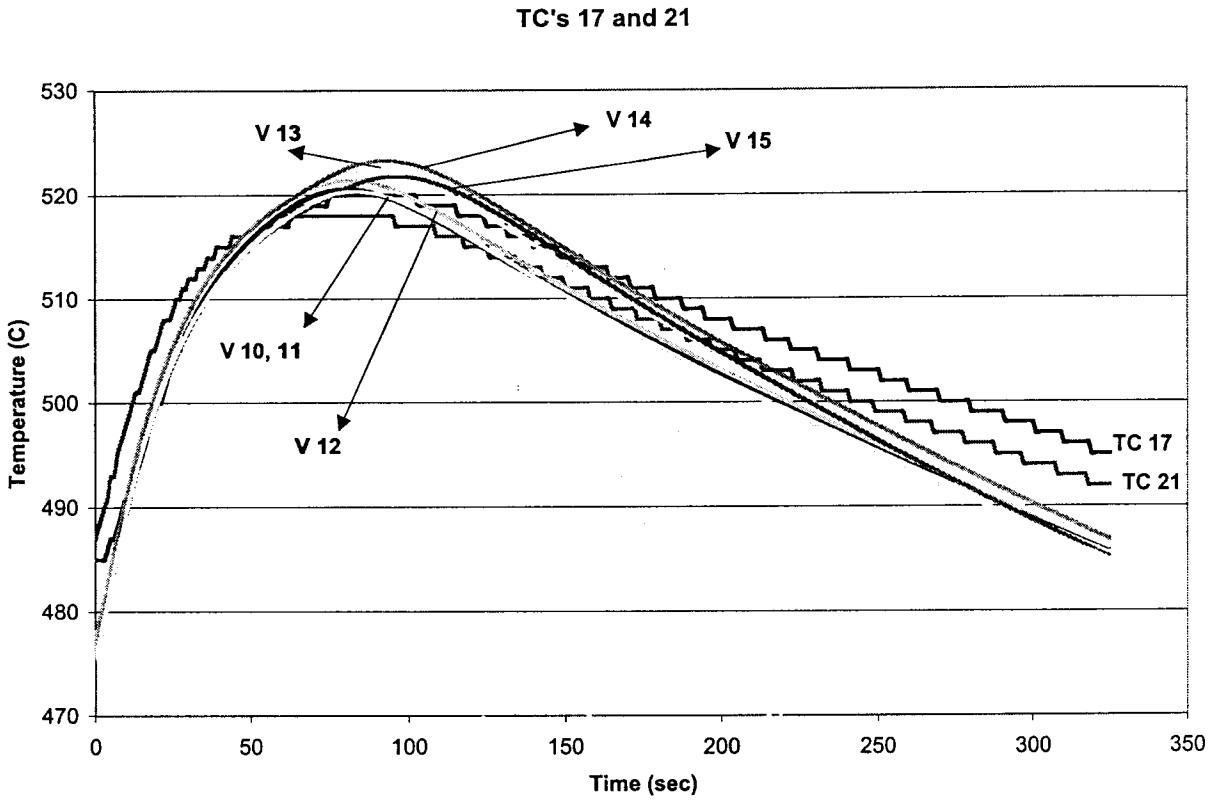

Figure 42: Comparison of experimental and simulated temperature distributions at TC's 17 and 21 for versions 10-15

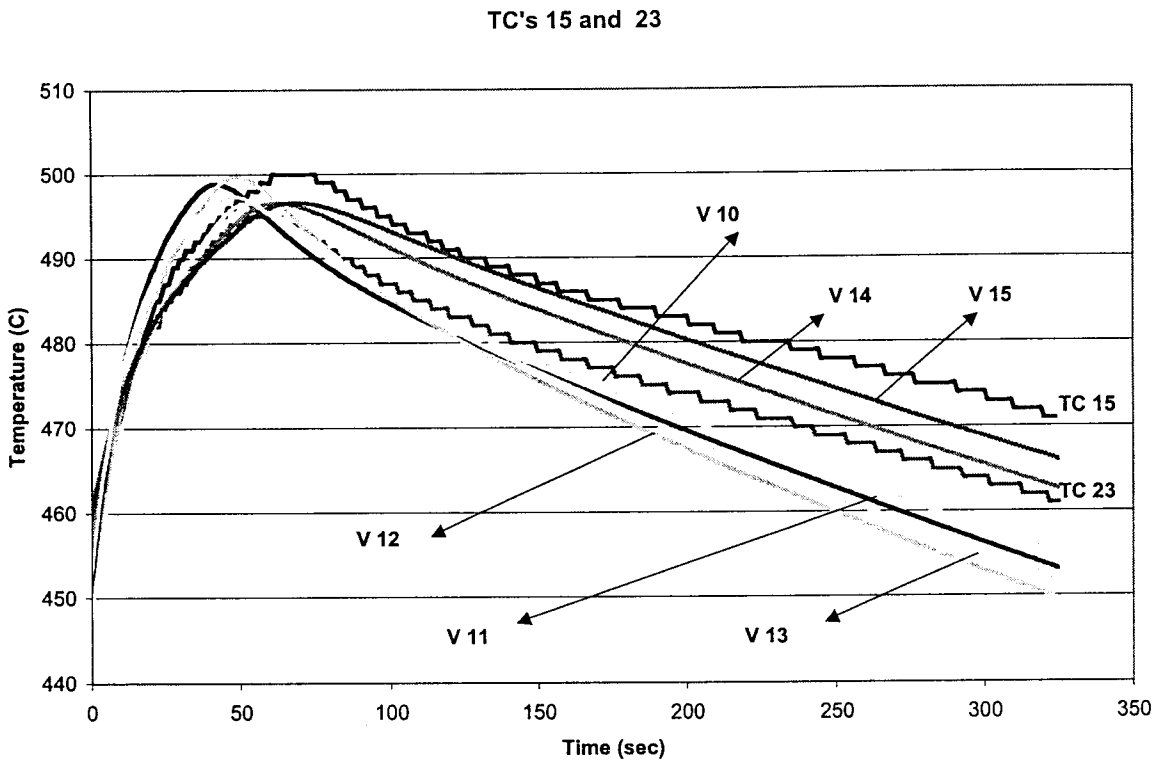

Figure 43: Comparison of experimental and simulated temperature distributions at TC's 15 and 23 for versions 10-15

Note: ***Although the HTC distributions for segments 4 and 5 are assumed to be the same, as shown in Figure 39, the temperature distribution shown in the above figure is for segment 5 only. This is due to the fact that no experimental temperature data are available for segment 4, because of the absence of thermocouples at that mold segment.***

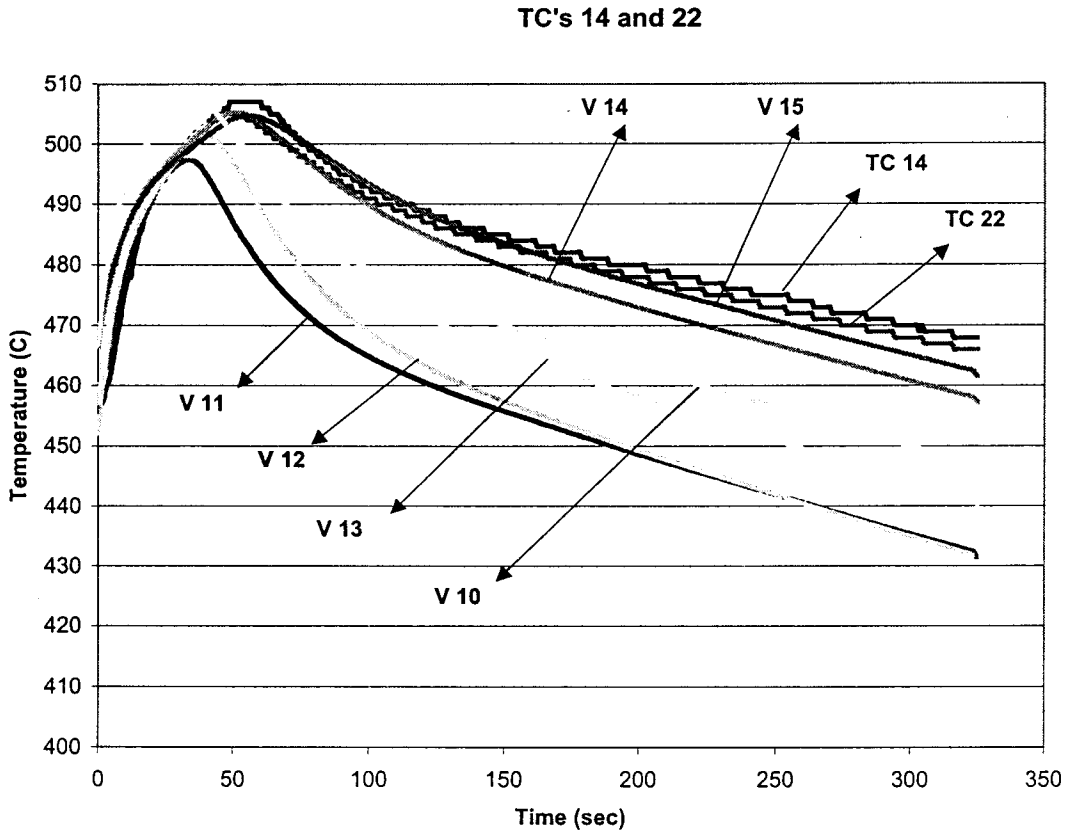

Figure 44: Comparison of experimental and simulated temperature distributions at TC's 14 and 22 for versions 10-15

Note: ***Although the HTC distributions for segments 4 and 5 are assumed to be the same, as shown in Figure 39, the temperature distribution shown in the above figure is for segment 5 only. This is due to the fact that no experimental temperature data are available for segment 4, because of the absence of thermocouples at that mold segment.***

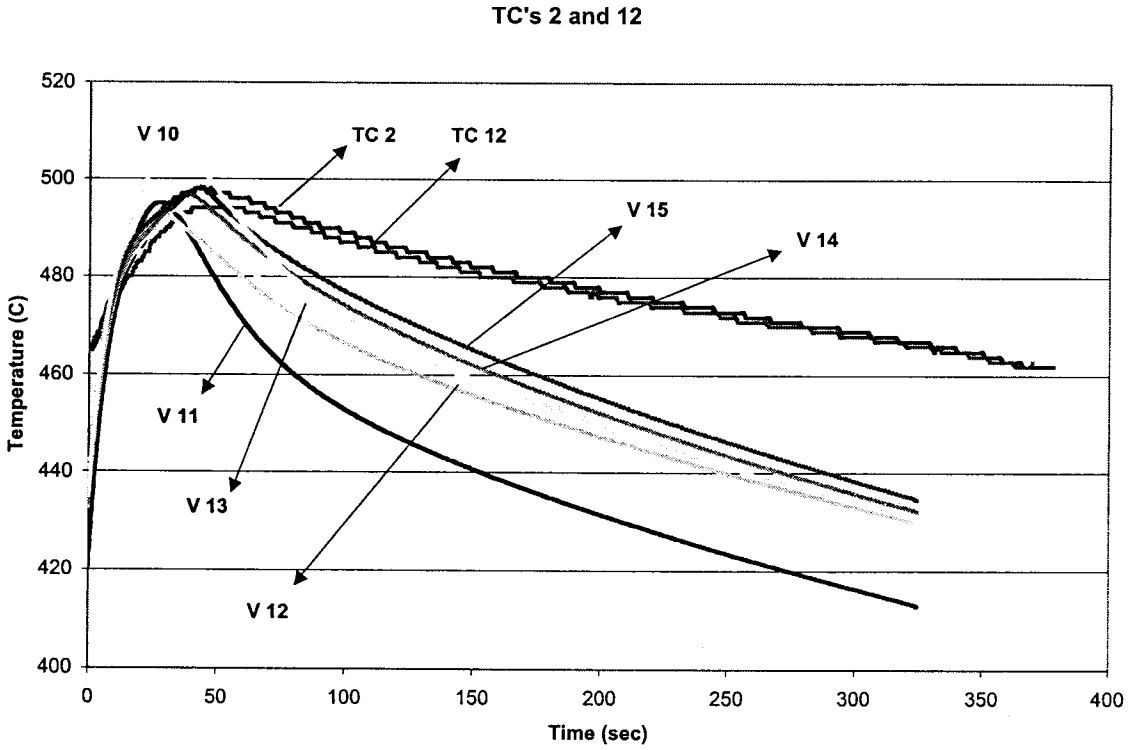

Figure 45: Comparison of experimental and simulated temperature distributions at TC's 2 and 12 for versions 10-15

Note: ***Although the HTC distributions for segments 1 and 2 are assumed to be the same,, the temperature distribution shown in the above figure is for segment 1 only. This is due to the fact that no experimental temperature data are available for segment 2, because of the absence of thermocouples at that mold segment.***

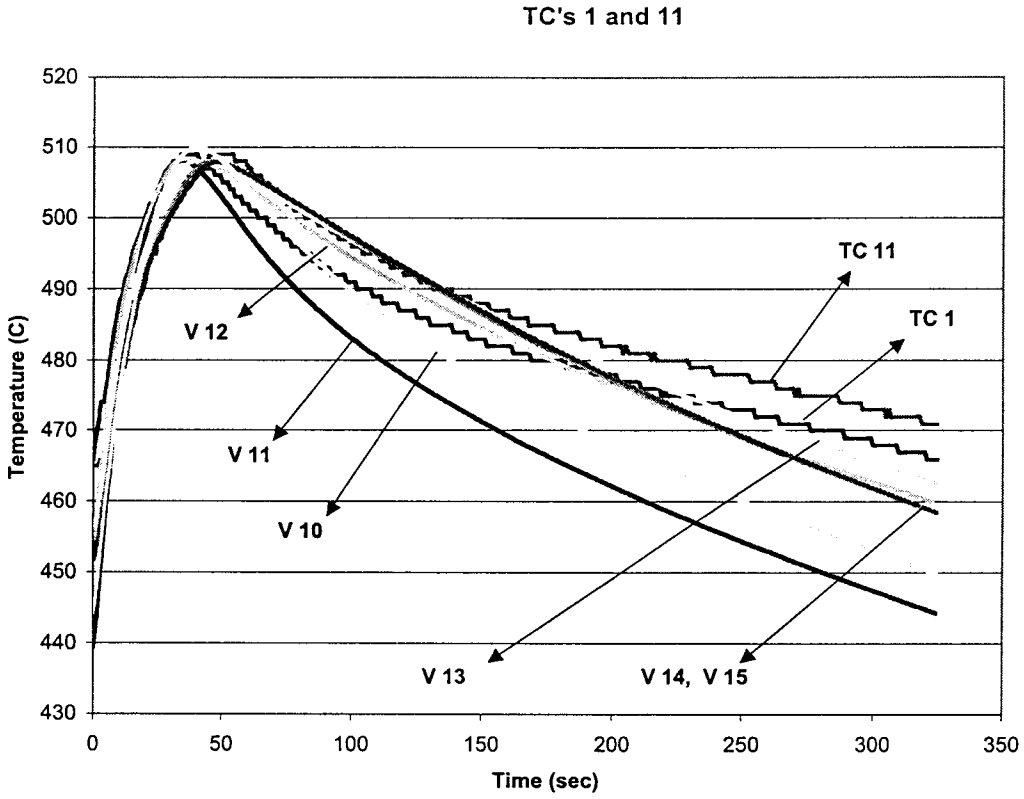

Figure 46: Comparison of experimental and simulated temperature distributions at TC's 1 and 11 for versions 10-15

Note: ***Although the HTC distributions for segments 1 and 2 are assumed to be the same, as shown in Figure 37, the temperature distribution shown in the above figure is for segment 1 only. This is due to the fact that no experimental temperature data are available for segment 2, because of the absence of thermocouples at that mold segment.***

11. METALLOGRAPHIC INSPECTION OF WHEEL-LIKE CASTING

One low pressure cast sample was sectioned, ground, and polished as per the usual grinding and etching procedure for cast aluminum alloys. Sections were taken from the flange, top, middle and bottom of the wheel-like casting as shown in Figure 47. The optical micrographs corresponding to the Flange, Top, Middle and Bottom are presented in Figures 48 (a)-(d). For each section, micrographs close to the inner surface of the wheel, close to the outer surface of the wheel, as well as from the middle region are shown. While finer dendritic structures were observed for the flange and top sections of the casting, coarser structures were seen at the bottom sections of the casting as anticipated.

Secondary Dendrite Arm Spacing (SDAS) from various locations of the sample were measured using the well-known line intercept method and are presented in Table IX. It is easily verified that the LPPM process results in an intermediate microstructure and SDAS values between the gravity die casting and the squeeze casting processes.

Table IX: Secondary Dendrite Arm Spacing for LPPM Casting Samples

Sample # 2A (LPPM)	Min. SDAS (μm)	Max. SDAS (μm)	Average SDAS (μm)
Flange	19.2	31.8	26.6
Top	23.6	36.4	28.3
Middle	28.4	51.5	38.2
Bottom (Outer)	41.2	57.1	47.7
Bottom (Inner)	62.6	88.2	69.9

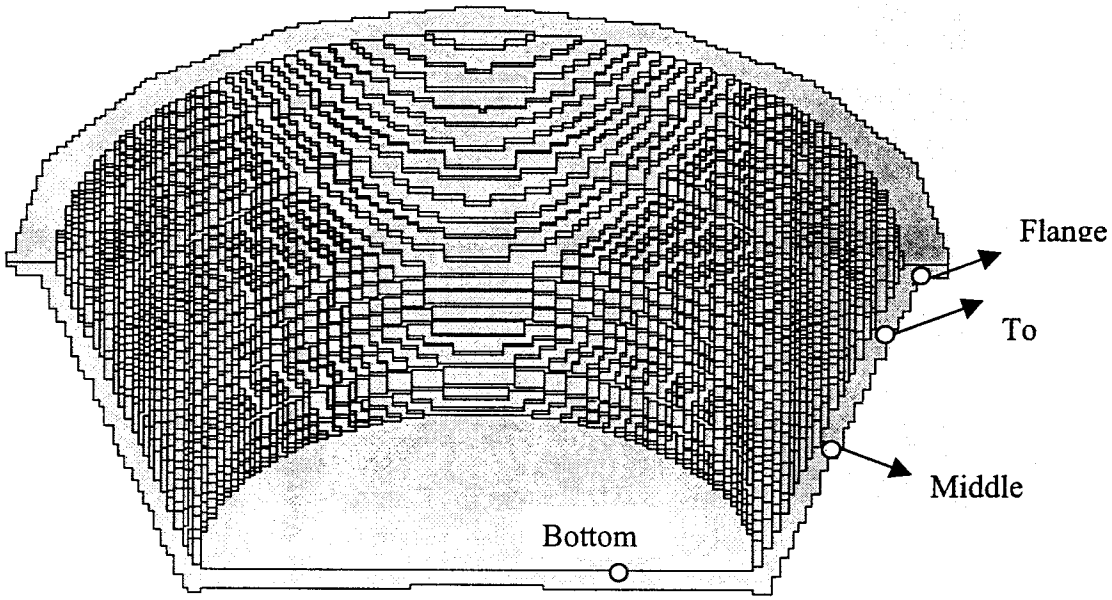

Figure 47: A Section of the Wheel-like Casting Showing Locations where Microstructures were taken.

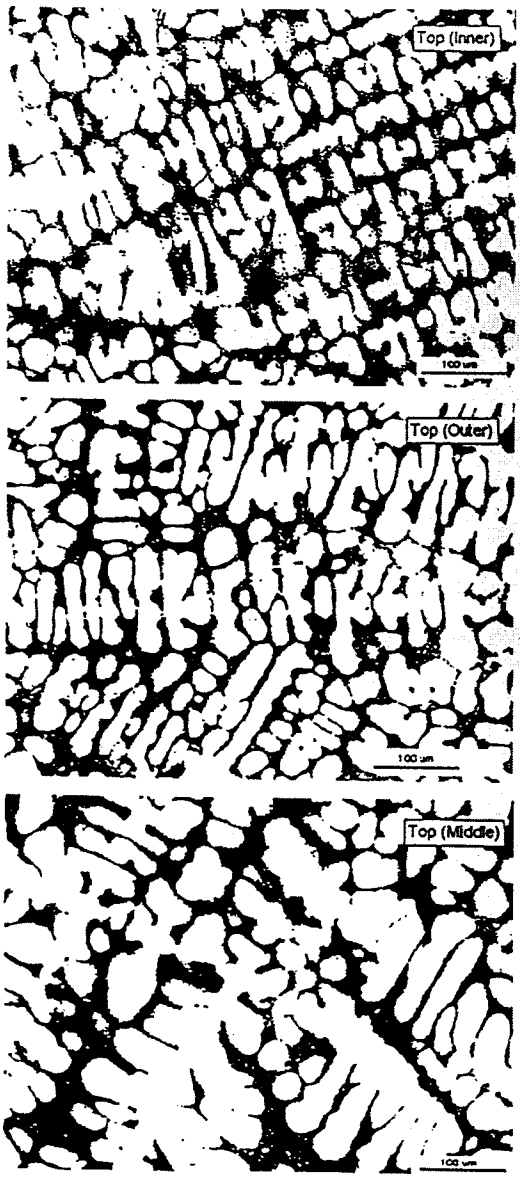

Figure 48 (a): Micrographs from the Flange Section

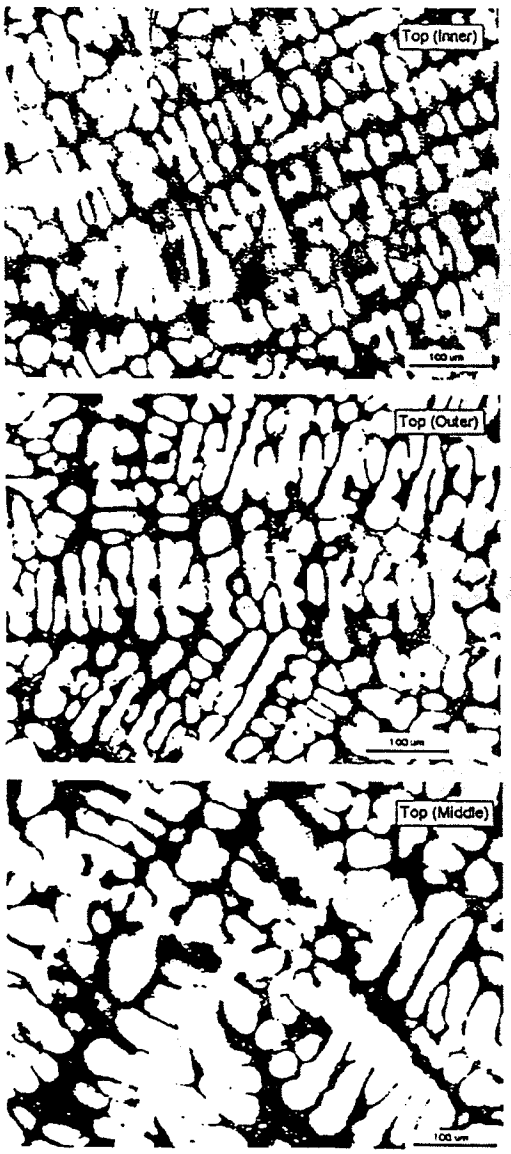

Figure 48 (b): Micrographs from the Top Section

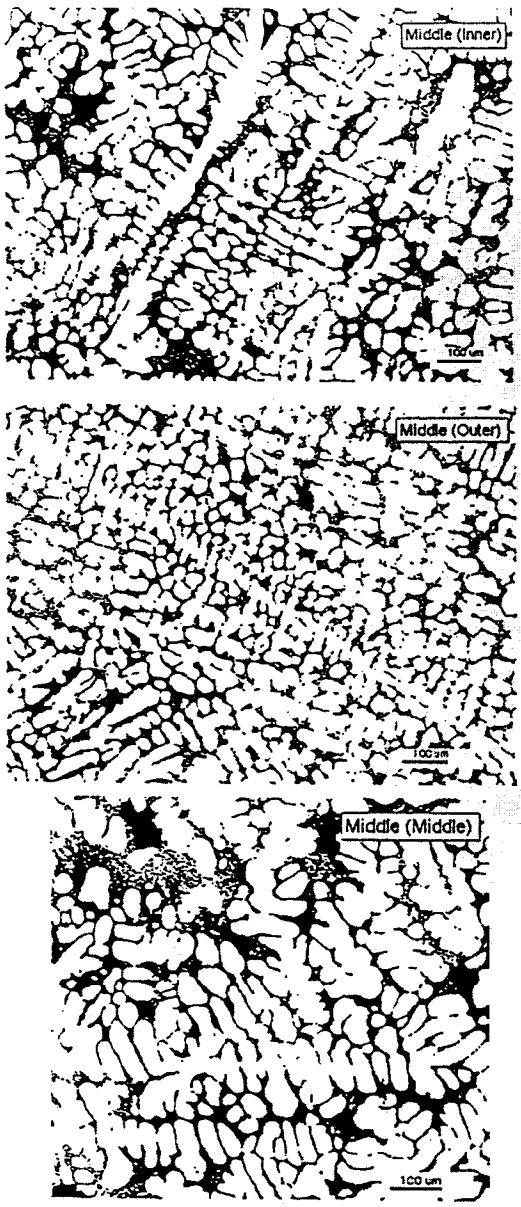

Figure 48 (c): Micrographs from the Middle Section

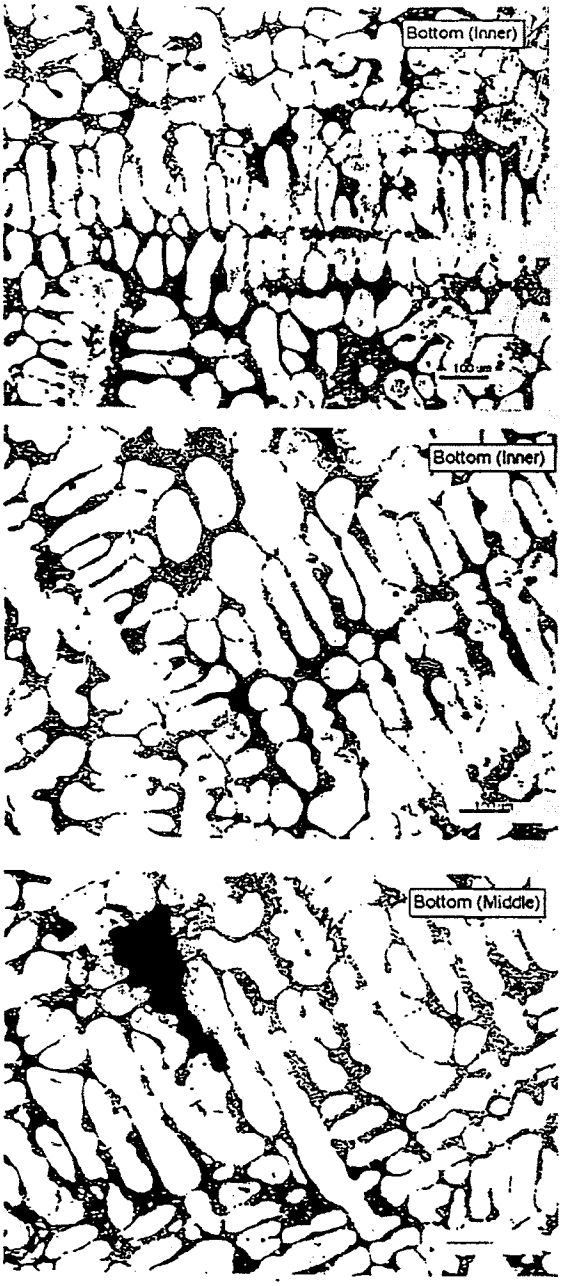

Figure 48 (d): Micrographs from the Bottom Section

SDAS-Cooling Rate Correlation

SDAS values were also calculated based on the empirical relation reported in the literature for A356 alloys. The SDAS-local solidification time relationship reported from the literature is SDAS = (11.03) $t^{0.33}$, where 't' is the local solidification time. The local solidification time was found from the MAGMA display of 'LiqtoSol' (Solidification time) shown in Figure 49. The MAGMA post-processor display of SDAS by inserting the above relationship as a 'composed' solidification criterion function, is shown in Figure 50. The measured and calculated, as well as MAGMAsoft displayed, SDAS values are compared in Figure 51. The comparison is good at most of the locations except at the top region (section 4) of the casting. A correlation plot was drawn between the measured SDAS values and the calculated cooling rates and is presented in Figure 52. Figure 52 also shows the best power law fit for these calculated points and the developed SDAS-Cooling Rate correlation with a correlation coefficient R= 0.97 is SDAS (μm)= (40.7) $(t^*)^{-0.4663}$ where t^* is the cooling rate in °C/sec. The empirical relationship often quoted in the literature for A356 alloys is SDAS= (52) $(t^*)^{-0.33}$ and is also plotted in Figure 52 for the purpose of comparison. It was seen that deviations from the literature curve were much smaller than that for the squeeze casting case.

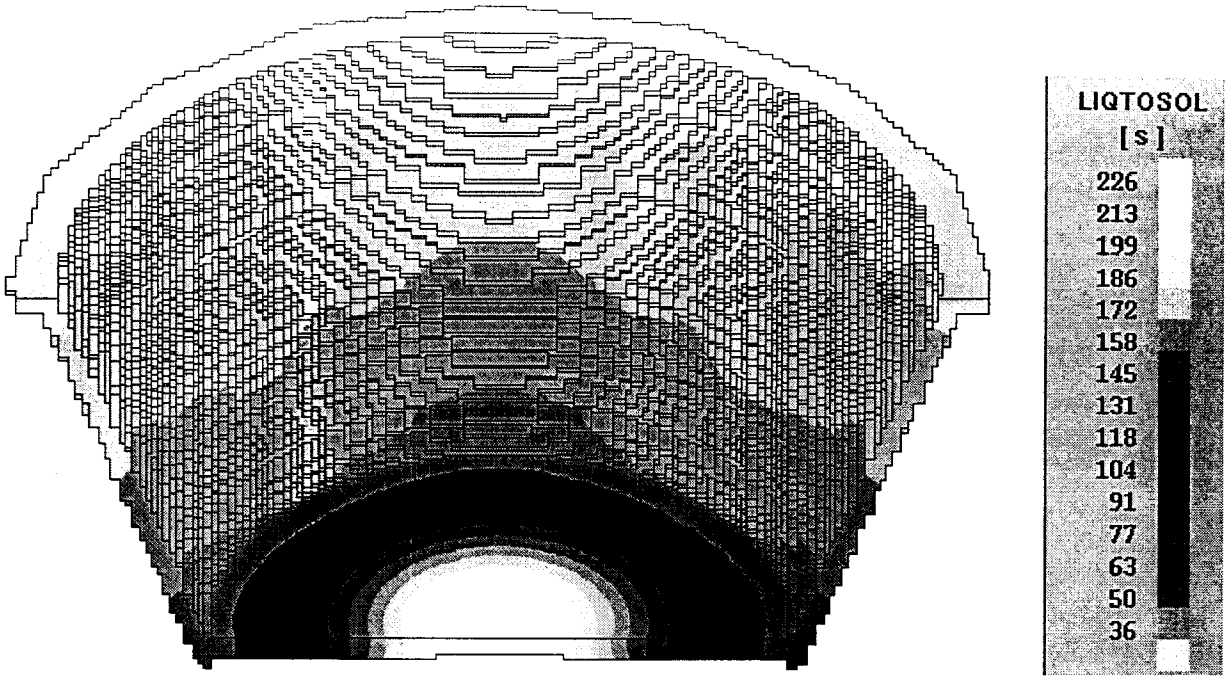

Figure 49: MAGMAsoft Display of the Solidification Time Distribution for the Wheel-like Casting

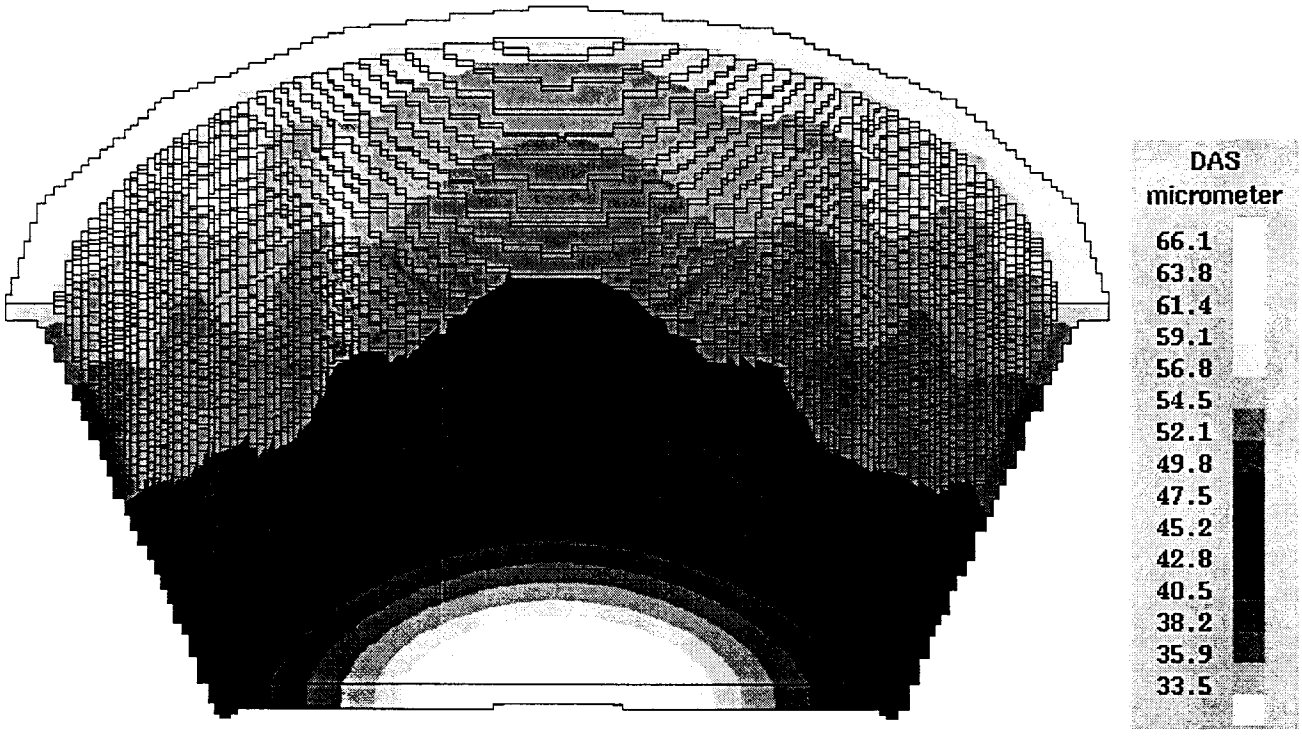

Figure 50: Display of SDAS from MAGMAsoft Based on the Criterion Function SDAS= $(11.03)\ t^{0.33}$, where 't' is the Solidification Time

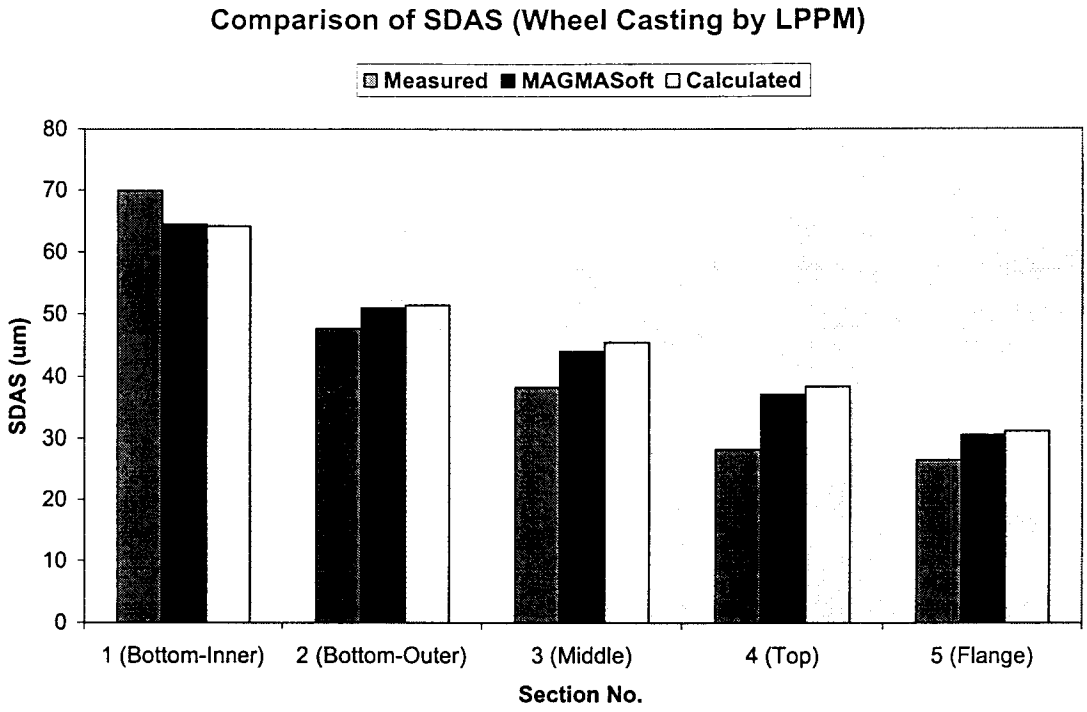

Figure 51: Comparison of SDAS values from the Wheel-like Casting by Three Methods

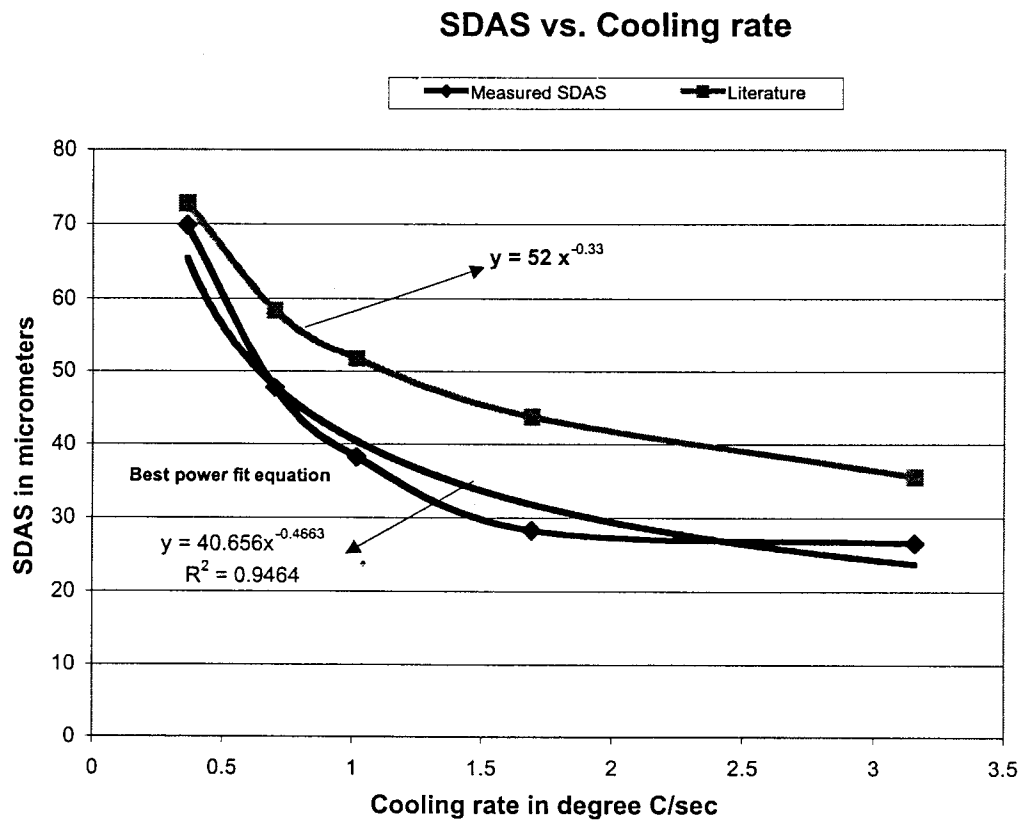

Figure 52: Comparison of SDAS-Cooling Rate Correlation, Measured vs. Literature

12. INFLUENCE OF MOLD COATING PARAMETERS ON INTERFACIAL HEAT TRANSFER IN THE LPPM CASTING PROCESS

Based on the results of the fifteen simulation runs described in earlier reports, the following conclusions were made on the influence of coating parameters and air gap formation on Interfacial Heat Transfer in the LPPM Casting Process.

The overall thermal resistance at the metal-mold interface, R_{total} (reciprocal of which is the overall HTC) during solidification in the LPPM process is the sum of the thermal resistance due to the mold coating, $R_{coating}$ and the thermal resistance due to air gap formation, R_{gap}. Considering conduction as the primary mode of heat transfer (radiation heat transfer can be neglected for metal mold casting of aluminum alloys), $R_{coating}$ is determined by the ratio of coating thickness to the thermal conductivity of the coating material. Although several studies have been reported in the literature [16-26] on the measurements of coating thermal conductivity, such measurements do not represent the actual conditions existing at the metal-mold interface, and hence cannot be used in the simulation of the process [26]. The conductivity is also found to vary with temperature and with the thickness and porosity of the coating as well. The compositional variations among different manufacturers of coating materials, as well as the influence of grain size, porosity and method of spraying the coating, influence the insulating performance, and further complicate the applicability of estimated thermal properties of the coating. One die coating manufacturer [27] reported thermal conductivity values of their coating materials ranging from 0.09 (best insulator) to 33.60 W/m K (best chill coating). Maintaining a uniform coating thickness on the mold surface is another problem. Frequent touch up of the mold surfaces in between shots and the different methods of applying the coating materials on the mold surfaces result in large variations of coating thickness. As reported earlier, the measurements of coating thickness of the samples provided by Amcast showed large variations in thickness and a very small layer of coating, on the order of 43 μm. Considering all the above factors, the influence of coating parameters (thickness and thermal conductivity) on the cooling behavior of the casting were studied by varying these parameters in the simulations and analyzing the mold temperature history resulting from that change. To analyze the effect of thermal conductivity of the coating, K, on the overall HTC, values of K were varied from a maximum value of 0.46 to a minimum value of 0.08 W/m K, while keeping a constant thickness of 100 μm and a maximum air gap of 50 μm. The effect is shown in Figure 53. The HTC values shown in the figure are the maximum values. The HTC eventually decreases to a minimum value of 300-400 W/m^2 K during the solidification process. When the coating thickness was varied from 50 to 100 μm, keeping K=0.3 W/m K, the overall HTC decreased from 1938 W/m^2 K for a thickness of 50 μm to 1465 W/m^2 K for a thickness of 100 μm.

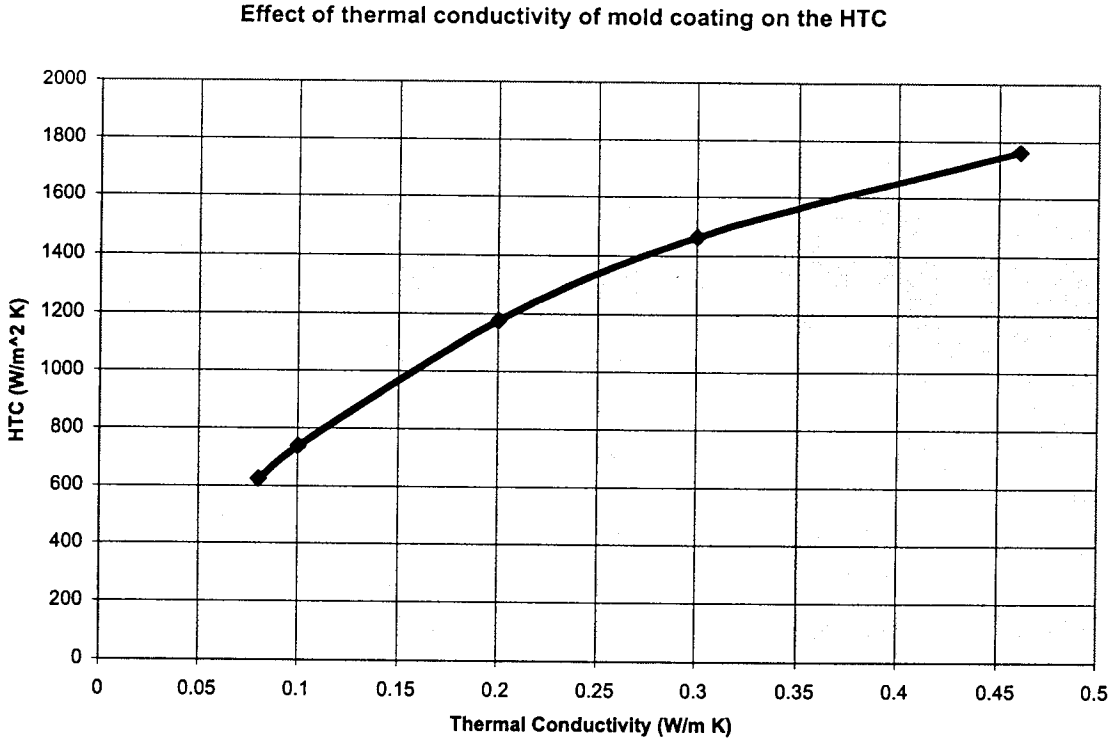

Figure 53: Effect of Thermal Conductivity of Mold Coating on the HTC (Coating Thickness= 100 μm and Maximum Air Gap=50 μm)

13. INFLUENCE OF AIR GAP FORMATION ON INTERFACIAL HEAT TRANSFER IN THE LPPM CASTING PROCESS

The importance of measuring and characterizing air gap formation in permanent mold casting processes need not be overemphasized. As reported earlier, in the absence of measurement of the formation of an air gap at the interface, the correlation developed by Trovant, M. and Argyropoulos, S.[15]for A356 alloys was used to relate the HTC with the air gap. The equation gives an initial h_{gap} value (with no air gap) of about 2900 W/m^2 K. With a mold coating of K= 0.46 W/m K and thickness=100 μm, the overall HTC is calculated as 1765 W/m^2 K. Thus at the onset of an air gap formation, if the coating properties remain unchanged, the overall HTC will be limited to a maximum value of 1765 W/m^2 K, no matter what may be the air gap. Assuming a linear distribution of air gap with the progress of solidification, the maximum assumed air gap in each simulation was distributed over a total period of about 400 seconds. To study the influence of air gap formation on the overall HTC distribution with time, different air gap thickness values ranging from 50 μm to 500 μm were used, keeping the coating parameters constant. The effect is presented in Figure 54. Thus it can be seen that the air gap determines the rate at which the overall HTC decreases with time. A larger air gap at the interface will result in a rapid decrease of the HTC to a minimum value of 300-400 W/m^2 K. It is also observed

from Figure 54 that the HTC approaches a minimum value of 350-400 W/m^2 K, independent of the air gap thickness. HTC at this stage is governed by the coating properties.

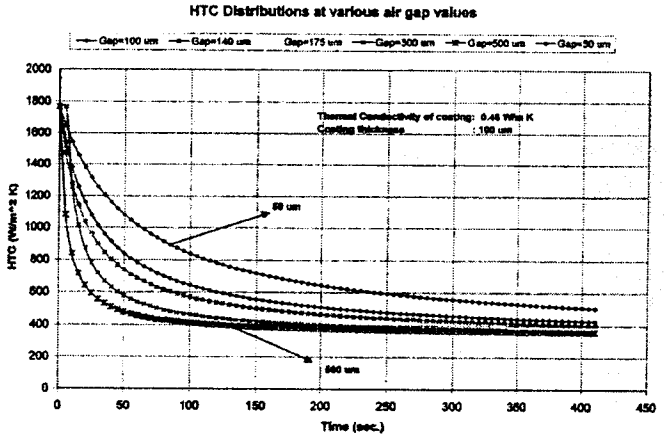

Figure 54: Influence of Air Gap Thickness on the HTC Distribution

14. CMM MEASUREMENT RESULTS AT HAYES-LEMMERZ TECH CENTER

It was decided to perform dimensional measurements of one whole wheel-like casting received from Amcast using the CMM (Coordinate Measuring Machine) facility at Hayes-Lemmerz Tech Center. The objectives of these measurements are to:

- Identify form errors, especially cylindricity error.
- Measure variation of rim thickness along the length of the casting.
- Measure variations of the above thickness at various clock positions around the casting to get an estimate of the total contraction. This will be done for various planes normal to the wheel axis.

A preliminary report received from Hayes-Lemmerz Tech Center on the wheel casting measurements is presented below:

An aluminum casting sample was received from the University of Michigan the week of January 21, 2001 in the metrology laboratory of the Hayes Lemmerz Technical Center. The sample was dimensionally laid out with a Coordinate Measuring Machine (CMM) under rigid atmospheric and calibration conditions. The layout shows wall thickness results of specific areas on the sample casting.

Laboratory Equipment

The measurement was performed with a DEA Beta 2305 gantry type Coordinate Measuring Machine (CMM). Last calibration date, September 14, 2000.

- Linear accuracy: X .00071mm
  Y .00093mm
  Z .00010mm
- Volumetric accuracy: .0018mm
- Repeatability: .00009mm
- Room and sample temperature: 70 deg. F

Layout Sample Setup

The sample was placed on the coordinate measuring machine table with the bottom (such as a bowl) surface down and parallel to the XY plane or table surface. The top surface, or rim, was also parallel to the XY plane.

The sample was aligned by taking measurements within the cone shape. Using the CMM's least squares algorithms for averaging the measurements, a vertical centerline was created through the middle of the sample. The centerline was named the Z-axis and the XY origin.

The sample was then aligned around the Z-axis by measuring the two small holes on the top of the rim. The two-hole alignment created the Y-axis. The X-axis was created perpendicular to the Y-axis.

The Z origin was created by measuring and averaging three places on the top surface of the rim.

Inside Diameter Measurements

From the top rim surface as the vertical origin, the inside was measured, as shown, in nine places. Each diameter is measured at a depth of 20mm increments beginning at 10mm from the top to ending at 170mm from the top surface.

Sample Wall Thickness measurements

From the top rim surface as the vertical origin, the first wall thickness measurement in each zone was measured at 10mm deep. From that measurement down, the wall thickness was measured at 20mm increment depths parallel to the wall. Therefore the measurements were taken at 20mm incremented depths at 20 degrees to the Z-axis.

The wall thickness was measured in 30-degree increments around the circumference of the sample. The zero point or the line drawn through the 12:00 and 6:00 locations is the X-axis, Y origin. This line is visually found to be the bisector between the

two small holes on top of the rim. The first measurement zone is 30 degrees, or 1:00 from this line. Nine wall thickness measurements were taken in each zone. A total of 108 wall thickness locations were measured.

Wall Thickness Results

Immediate observation shows the cone wall thickness to increase from bottom to top. The exception is the surface wall measurements at 12:00. This zone increases in width up to the area 50mm from the top surface. Then the thickness begins to decrease. The overall range of increase is from approximately 0.1mm to 0.35mm differences. The layout shows the overall range is from 8.519mm thick to 9.301mm thick. Detailed results are shown in the following tables:

	"Dimensions Taken In These Zones"								
	10 mm.	30 mm.	50 mm.	70 mm.	90 mm.	110 mm.	130 mm.	150 mm.	170 mm.
Inside Dimensions:	381.287	366.629	351.961	337.444	322.868	308.275	293.697	279.081	264.503

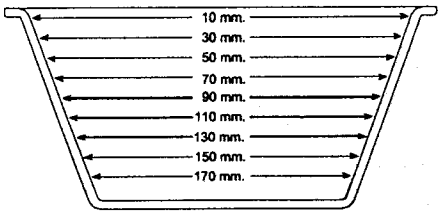

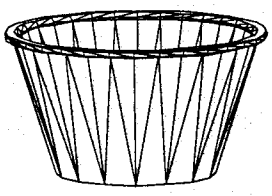

All Dimensions in the tables are in 'mm'

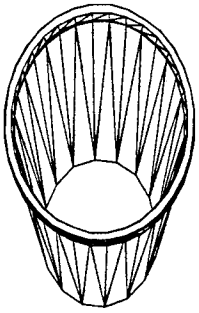

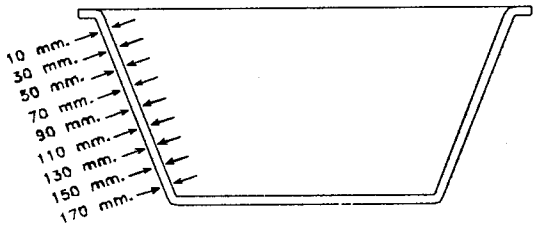

Dimensions Every:	"Dimensions Taken In These Zones"											
	1:00	2:00	3:00	4:00	5:00	6:00	7:00	8:00	9:00	10:00	11:00	12:00
10 mm.	9.249	9.301	9.186	9.103	8.953	8.828	8.785	8.799	8.821	8.884	9.038	8.871
30 mm.	9.168	9.19	9.103	9.019	8.874	8.695	8.703	8.744	8.763	8.894	8.973	9.088
50 mm.	9.139	9.142	9.031	9.133	8.835	8.662	8.654	8.898	8.758	8.89	8.976	9.126
70 mm.	9.105	9.055	9.02	8.922	8.751	8.624	8.622	8.665	8.755	8.873	8.981	9.116
90 mm.	9.091	9.056	8.99	8.877	8.736	8.573	8.595	8.65	8.776	8.885	8.954	9.089
110 mm.	9.101	9.052	8.959	8.844	8.723	8.574	8.592	8.642	8.732	8.87	8.952	9.07
130 mm.	9.093	9.052	8.953	8.696	8.697	8.589	8.555	8.563	8.704	8.82	8.941	9.018
150 mm.	9.074	9.061	8.947	8.821	8.694	8.58	8.558	8.604	8.708	8.824	8.95	9.066
170 mm.	9.048	9.018	8.888	8.795	8.637	8.541	8.519	8.564	8.652	8.793	8.956	9.009

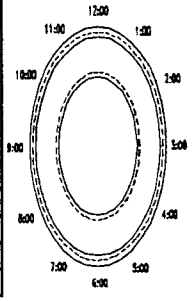

15. REFERENCES

Some Collected Relevant References:

V. Panachanathan, M.R. Seshadri & A. Ramachandran "Thermal Behavior of Metallic Molds with Long Freezing Range Alloys", AFS Transactions, v. 72, (1964), pp. 65-71.

C.W. Nelson "Nature of Heat Transfer at the Die Face", Paper 63, Die Casting Congress, (1970).

E.S. Tillman & J.T. Berry "Influence of Thermal Contact Resistance on the Solidification Rate of Long freezing Range Alloys", AFS Cast Metals Research Journal, (1972), pp. 1-6.

M. Prates, J. Fissolo & H. Biloni "Heat Flow Parameters Affecting the Unidirectional Solidification of Pure Metals", Met Trans., v.3, (1972), pp. 1419-1425.

M. Prates & H. Biloni "Variables Affecting the Nature of the Chill Zone", Met Trans., v. 3, (1972), pp. 1501-1510.

S. Engler, D. Boenisch & B. Kohler "Metal and Mold Wall Movements During Solidification of Cast Iron", AFS Cast Metals Research Journal, (1973), pp. 20-30.

D.R. Durham & J.T. Berry "Role of the Interface During Solidification of a Pure Metal Against a Chill", AFS Transactions, v. 82 (1974), pp. 101-110.

L.J.D. Sully "The Thermal Interface Between Castings and Chill Molds", AFS Transactions, v. 84 (1976), pp. 735-744.

Y. Nishida & H. Matsubura "Effect of Pressure on Heat Transfer at the Metal -Mould Interface", British Foundaryman, v. 69, (1976), pp. 274-278.

S. Hong, D.G. Backman & R. Mehrabian "Heat Transfer Coefficient in Aluminum Alloy Die Casting", Met. Trans. B, vol. 10B, (1979), pp. 299-301.

V. de L. Davies "Heat Transfer in a Gravity Die Castings", British Foundryman, v. 73, (1980), pp. 331-334.

K. Ho & R.D. Pehlke "Transient Methods for Determination of Metal - Mold Interfacial Heat Transfer", AFS Transactions, v. 91, (1983), pp. 689-698.

K. Ho & R.D. Pehlke "Mechanisms of Heat Transfer at a Metal - Mold Interface", AFS Transactions,
v. 92 (1984), pp. 587-598.

K. Ho & R.D. Pehlke "Metal-Mold Interfacial Heat Transfer", Met Trans., 16 B (1985), pp.585-594.

M. Bamberger & M.M. Stupel "Influence of Different Chill Materials on HeatFlux & Dendrite Arm Spacing of 356 Aluminum Casting", Giessereiforshung, v.38, (1986) pp. 77-80

T.X. Hou & R.D. Pehlke "Determination of Mold - Metal Interfacial Heat Transfer & Simulation of Solidfication of an Al 13% Si Casting", AFS Transactions, v. 96, (1988), pp. 129.

M.R. Tadayon & R.W. Lewis "A model of Metal - Mould Interfacial Heat Transfer for Finite Element Simulation of Gravity-Diecasting", Cast Metals, v. 1, n. 1, (1988), pp. 24-28.

H. Huang & J.T. Berry "Solidification Heat Transfer in Aluminum Investment Castings", ASME Heat Transfer Conf., (1988), pp. 93-99.

M.C. Lukens, T.X. Hou, R.D. Pehlke " Mold/ Metal Gap Formation of Al 356 Cylinders Cast Horizontally in Dry & Green Sand", AFS Transactions, v. 98, (1990), pp. 63-70.

F. Chiesa " Measurement of the thermal conductance at the Mold/Metal Interface of Permanent Molds", AFS Transactions, v. 98, (1990), pp. 193.

T.S.P. Kumar & K.N. Prahbu "Heat Flux Transients at the Casting/Chill Interface during Solification of Aluminum Base Alloys", Met. Trans., v. 22B, (1991), pp.717-727.

M.A. Taha et al. "Effect of Melt Superheat & Chill Material on Interfacial Heat-Transfer Coefficient in end - chill Al & Al - Cu Castings", Journal of Material Science, v. 27, (1992), pp. 3467-3473.

S. Das & A. Paul "Determination of Metal - Mold Interfacial Heat Transfer Coefficients for Castings using a Solution Technique for Inverse Problems based on the Boundary Element Method", Modelling of Casting, Welding and Advanced Solification ProcessesVI, TMS, (1993), pp. 647-656.

S. Das & A. Paul "Determination of Interfacial Heat Transfer Coefficients in Casting and Quneching using a Solution Technique for Inverse Problems based on the Boundary Element Method", Met Trans., v. 24B, (1993), pp. 1077-1086.

P. Schmit "Heat Transfer during Filling in Die Casting Processes", Materials Science & Engineering, v. A173 (1993), pp. 271-274.

J.C. Hwang, H.T. Chuang, S.H. Jong & W.S. Hwang "Measurement of Heat Transfer Coefficient at Metal/Mold Interface during Casting" AFS Transactions, v. 102, (1994), pp. 877-883.

H. Huang, O. Gurdogan, H.U. Akay, W.W. Fincher " Thermal Transport Phenomena in Metal Casting Simulations", AFS Transactions, v. 103, (1995), pp.243-252.

A. Poitron, C. Gerometta, J.M. Plun, Y. Caratini & C. Rigaut " Determination of Heat Transfer Coefficient for Cooling Devices in Permanent Molds", in Modelling of Casting, Welding and Advanced Solification Processes VII, TMS, (1995).

F. Chiesa " Influence of some Processes and Metallurgical Factors on Production of Cast Aluminum Wheels", AFS Transactions, v. 103, (1995), pp. 547-554.

C.A. Muojekwu, I.V. Samarasekara & J.K. Brimacombe " Heat Transfer & Microstructure during the Early Stages of Solidification", Met Trans., v. 26B, (1995), 361-382.

D. R. Gunasegaram, J. van der Touw & T.T. Nguyen "Heat Transfer at Metal -Mould Interfaces", Proc. of IMMA/ADCA Int. Conf. on Casting and Solification of Light Alloys, Gold Coast, Australia (1995) pp. 91-96.

D. R. Gunasegaram & T.T. Nguyen "Comparison of Heat Transfer Parameters in Two Permanent Molds", AFS Transaction, v.105, (1997).

A.M. Assar "Mould surface roughness and interfacial heat transfer using heat flow model", Materials Science & Technology, v. 13, (1997), pp.702-704.

J.T. Anderson, D.T. Gethin, R.W. Lewis & J.T. Cross "Experimental investigation and finite element modelling in gravity die casting", Proc. Instn. Mech. Engrs., v. 211, Part B, (1997), pp. 93-107.

References:

1. J.A.Sekhar *et al.*, "Effect of Pressure on Metal-Die Heat Transfer Coefficient during Solidification"- *Materials Science and Engineering*, 40(1979) 105-110.
2. S.Rajagopal, "Squeeze Casting: A Review and Update"-*Journal of Applied Metalworking*, 1(4) 1981, 3-14.
3. Bell, F., D.T. Gethin and J.T. Anderson, "A Foundry-based Experimental Investigation into the Effect of Die Coats in the Gravity Casting Process", Cast Metals, Vol. 8, No. 1, 1996, pp. 51-56.
4. Cho, I.S. and C.P. Hong, "Evaluation of Heat Transfer Coefficients at the Casting/Die Interface in Squeeze Casting", Int. J. Cast Metals Res., Vol. 9, 1996, pp. 227-232.
5. P.K.Rohatgi *et al.*, Journal of Materials Science 29 (1994) 5357-5366.
6. Banghong Hu and Hang Li ,"*Grain Refinement of DIN226S alloy at lower titanium and boron addition levels*", Journal of Materials Processing Technology, V. 74, pp. 56-60, 1998.
7. P.S.Mohanty and J.E.Gruzleski, "*Mechanism of Grain Refinement in Aluminum*", Acta metall. Mater., Vol.43, No. 5, pp. 2001-2012, 1995.
8. Banghong Hu, "*Comparison of effects of master alloys containing titanium and or boron on the grain size and dendrite arm spacing of DIN226S aluminum alloy*", Journal of Materials Science Letters, V. 16, issue 21, pp. 1750-1752, 1997.
9. Spittle, J.A, Keeble, J.M and Al Meshhedani, M, "*The Grain Refinement of Al-Si Foundry Alloys*", 126th TMS Annual Meeting, Florida, Feb 9-13, 1997.
10. Kearns, M.A, Thistlethwaite, S.R and Copper, P.S. "*Recent Advances in Understanding the Mechanism of Aluminum Grain Refinement by TiBAl Master Alloys*", 125th TMS Annual Meeting, Anaheim, CA, USA, 19960204-19960208.
11. M.M.Hariedy, A. Niazi and A.A. Nofal, "*Thermal Analysis of Aluminum Alloys as a tool to Evaluate Grain Refiners Efficiency*", 125th TMS Annual Meeting, Anaheim, CA, USA, 19960204-19960208.
12. T.Sritharan and H.Li, *"Influence of Titanium to Boron Ration on the ability to grain refine Aluminum-Silicon alloys*". Journal of Materials Processing Technology, Vol. 63, pp. 585-589, 1997.
13. Tan R.K. et al., *Computer Aided Design of a Semi-Permanent Mold for the Casting of an Aluminum Spool*, Proceedings from Materials Solutions Conference' 98 on Aluminum Casting Technology, pp. 85-93, 1998.

14. Ransing, R. S., and Lewis, R.W., *Optimal Design of die coating thickness using Lewis-Ransing Correlation*, Int. J. Cast Metals Res., Vol.9, pp. 269-277, 1997.
15. Trovant Michael and A. Stavros., *Finding Boundary Conditions: A coupling Strategy for the Modeling of Metal Casting Processes: Part I and II*, Metallurgical and Materials Transactions B, Vol. 31B, pp. 75-96 February, 2000.
16. Chiesa, F and Mucciardi, F., *Thermal Behavior of Permanent Molds during Production of Aluminum Castings*, AFS Transactions, 93-90, pp. 459-467, 1993.
17. Chiesa, F., *Measurement of the Thermal Conductance at the Mold/Metal Interface of Permanent Molds*, AFS Transactions, 98, pp. 193-200, 1990.
18. Nyamekye, K et al., *A Review of Permanent Mold Coatings and Their Effect on Heat Transfer in the Mold*, AFS Transactions, 94-143, pp. 869-876, 1994.
19. Wei, S et al., *Influence of Mold Coating on Heat Transport in Permanent Mold Casting process*, AFS Transactions, 96-90, vol. 104, pp. 251-262, 1996.
20. Prabhu, K.N. et al., *"Effect of Coating/mold Wall/Casting Thickness on Heat Transfer and Solidification of Al-Cu-Si alloy (LM21) in Cast Iron Molds"*, AFS Transactions, 94-109, (1994), pp. 827-832.
21. Giannos, M. et al. *"A Comparison of Sodium Silicate Bonded Die Coats with Thermally Sprayed Coatings for Permanent Mold Castings"*, Proc. From Materials Solution Conference '98 on Aluminum Casting Technology, (1998), pp. 175-181.
22. Schmidt, Pal, *"Heat Transfer in Permanent Mould Casting"*, Ph.D. thesis, Royal Institute of Technology, Sweden, 1994.
23. Dillingham, J. et al., *"Literature Review for Tenacious Coatings for Aluminum Permanent Mold Casting Process"*, AFS Transactions, 96-162, (1996), pp. 1079-1095.
24. Chiesa, F. and Trottier, J., *"Mechanics of the die coating application in the permanent mold casting process"*, Int. J. Cast Metals Res., (1996), Vol. 9, pp. 145-152.
25. Chiesa, F. and Boisvert, A., *"Factors Affecting Drying conditions of Coatings Sprayed on permanent Molds"*, AFS Transactions, 96-23, (1996), pp. 769-775.
26. Chiesa, F., *"Quantifying Permanent Mold Coatings Functional Properties"*, AFS Transactions, 98-39, (1998), pp. 589-594.
27. Thermal Conductivity data received from a die coating vendor, 1997.

Appendix: List of technical articles sent to AFS

CONTINUOUS CASTING			
Title	**Author(s)**	**Journal**	**Date**
Transient Thermal Model of the Continuous Single-Wheel Thin-Strip Casting Process	Guowei Li, Brian G. Thomas	Metallurgical and Materials Transactions B, V. 27B, June, pp. 509-525	1996
Simulation of Continuous-Casting Processes (Reconsideration of Heat Balance and Improvement of Efficiency in Continuous-Casting Process)	Akio Saito, Seiji Okawa, Kentaro Kaneko, Hideo Kaneko	Heat Transfer - Japanese Research, V.23, No. 1, pp. 35-51	1994
Thermal Modeling of the Continuous Casting Process	B.H. Kang, Y. Jaluria	Journal of Thermophysics and Heat Transfer, V. 7, No. 1, pp. 139-147	1993
Thermal Calculation of a Mold for Continuous Casting of Metal Strip	A.N. Abramenko, A.S. Kalinichenko, Yu. K. Krivosheev	Translated from Inzhenerno-Fizicheskii Zhurnal, V. 61, No. 1, pp. 26-32	1991

HIGH PRESSURE DIE CASTING			
Title	**Author(s)**	**Journal**	**Date**
A New Method for Thermal Analysis of Die Casting	M.R. Barone, D.A. Caluk	Transactions of the ASME, V. 115, May, pp. 284-293	1993
Heat Transfer coefficient in Aluminum Alloy Die casting	S. Hong, D.G.Backman and R.Mehrabian	Metallurgical Transactions B, V. 10B, June, pp. 299-301	1979

IHTC			
Article Title	**Author(s)**	**Journal**	**Date**
Numerical Modeling of Casting Solidification: The Concept of Problem Linearization	B. Mochnacki, J.S. Suchy	AFS Transactions 96-11, pp 203-209	1996

Computer Simulation of Mould Filling for Horizontal Castings and Its Experimental Validation	Z.A. Xu, F. Mampaey	European Journal of Mechanical Engineering, Vol. 40, No. 2, pp 89-101	1995
Cooling Properties of Various Cooling Methods for Aluminium Semicontinuous Casting	Masanori Tsunekawa, Nobuyuki Muto, Norifumi Hayashi, Teruo Uno	Japanese Journal, Vol.35, No.1, No.2	1994
Determination of Interfacial Heat Transfer Coefficients in Casting and Quenching Using a Solution Technique for Inverse Problems based on the Boundary Element Method	S. Das, A.J. Paul	Metallurgical Transactions B, V. 24B December, pp. 1077-1086	1993
A variable property analysis of alloy solidification using the anisotropic porous medium approach.	S.K. Sinha, T. Sundararajan	International Journal of Heat Mass Transfer, V35, No. 11 pp 2865-2877	1992
Unidirectional solidification of a binary alloy and the effects of induced fluid motion	D.G. Neilson, F.P. Incropera	International Journal of Heat Mass Transfer, V. 34, No. 7, pp 1717-1732	1991
Identification of heat transfer between the casting and the mold in ingotless rolling	S.L. Balakovskii, E.F. Baranovskii, N.V. Diligenskii, P.V. Sevast'anov	0022-0841/89/5701-0823 pp. 823-827	1990
Metal-Mold Interfacial Heat Transfer	K. Ho, R.D. Pehlke	Metallurgical Transactions B, V. 16B, September	1985
Mechanisms of Heat Transfer at a Metal-Mold Interface	K. Ho, R.D. Pehlke	AFS Transactions 84-61, pp 587-598	1984
Transient Methods for Determination of Metal-Mold Interfacial Heat Transfer	K. Ho, R.D. Pehlke	AFS Transactions 83-80, pp 689-698	1983
Influence of Thermal Contact Resistance on the solidification Rate of Long Freezing Range Alloys	E.S. Tillman, J.T. Berry	AFS Cast Metals Research Journal, March, pp. 1-6	1972

INVESTMENT CASTING

Title	Author(s)	Journal	Date
Gap Formation and Interfacial Heat transfer in Alloy 718 Investment Castings	Vivek Sahai, Ruel A. Overfelt	Modelling of Casting, Welding, and Advanced Solidification Processes VII, TMS, pp. 417-425	1995
Application of Inverse Methods to the Estimation of boundary Conditions and Properties	M. Rappaz, J.L. Desbiolles, J.M. Drezet, Ch. A. Gandin, A. Jacot, Ph. Thevoz	Modelling of Casting, Welding, and Advanced Solidification Processes VII, TMS, pp. 449-457	1995
Solidification Heat Transfer in Aluminum Investment Castings	H. Huang, J.T. Berry	Collected Papers in Heat Transfer, Presented at the winter annual meeting of ASME, pp. 93-99	1988

NUMERICAL METHODS IN SOLIDIFICATION PROCESSING

Title	Author(s)	Journal	Date
Time-varying heat transfer coefficients between tube-shaped casting and metal mold	T.G. Kim, Z.H. Lee	International Journal of Heat and Mass Transfer, V. 40, No. 15, pp. 3513-3525	1997
Effects of Coating Thickness and Pouring Temperature on Thermal Response in Lost Foam Casting	R. Venkataramani, C. Ravindran	AFS Transactions, 96-93, pp. 281-290	1996
Three Dimensional Solidification Analysis of the Initial State of D.C.Casting Process	Yoshio Watanabe, Norifumi Hayashi	Sumitomo Light Metal Technical Reports, V. 37, No. 1,2 pp. 44-49	1996
Application of the BEM in the thermal theory of foundry	E. Majchrzak	Engineering Analysis with Boundary Elements, V. 16, pp. 99-121	1995
Modelling of temperature losses in liquid metal during casting formation in expendable pattern casting process	S. Shivkumar	The Institute of Materials, pp. 986-992	1994

Solidification Pattern of an Aluminum Alloy in Step-Plate Castings	H.S. Chiou, R.H. Yen, M.D. Chu, Y.N. Pan	Journal of the Chinese Society of Mechanical Engineers, V. 14, No. 1, pp. 53-62	1993
Determination of Metal-Mold Interfacial Heat Transfer Coefficients for Castings Using a Solution Technique for Inverse Problems Based on the Boundary Element Method	S. Das, A.J. Paul	Modeling of Casting, Welding and Advanced Solidification Process VI, pp. 647-655	1993
Solidification of arbitrarily shaped casting in mold-casting system	R.Y. Tzong, S.L. Lee	International Journal of Heat and Mass Transfer, V. 35, No. 11, pp2795-2803	1992
Effect of melt superheat and chill material on interfacial heat-transfer coefficient in end-chill Al and Al-Cu alloy castings	N.A. El-Mahallawy, M.A. Taha, A.M. Assar, R.M. Hamouda	Journal of Materials Science, V. 27, July 1992, pp. 3467-3473	1992
A finite element model for the simulations of mould filling in metal casting and the associated heat transfer	A.S. Usmani, J.T. Cross, R.W. Lewis	International Journal for Numberical Methods in Engineering, V. 35, pp. 787-806	1992
Interfacial Heat Transfer Coefficient in End - Chill Al and Al-Cu Castings	N.A. El-Mahallawy, M.A. Taha, A.M. Assar, R.M. Hamouda	Seventh International Conference on Numerical methods in Thermal problems, Volume VII. I , July 1991, pp. 340-345	1991
Heat Flux Transients at the Casting/Chill Interface during Solidification of Aluminum Base Alloys	T.S. Prasanna Kumar, K. Narayan Prabhu	Metallurgical Transactions B, V. 22b, October 1991, pp. 717-727	1991
Simulation of Heat Transfer at Casting Metal-Mold Interface	D.G.R. Sharma, M. Krishnan	AFS Transactions, 91-81, pp. 429-438	1991
Mathematical Modelling of the Semi-Permanent Mould Casting of Aluminium Alloy Cylinder Heads and Engine Blocks	L. Hofmann, H. Hlock, P. Lee	SAE International Congress and Exposition-New engine and advanced component Design,SAE special publications, n 823, 1990	1990
Numerical Solutions to an Inverse Problem of Heat Conduction for Simple Shapes	G. Stoltz, Jr.	Transactions of the ASME, Feb. pp. 20-26	1960
Research Developments in the Low Pressure	T.T. Nguyen, G. R. de	CSIRO Division of Manufacturing Technology and	

Die Casting of Automotive Components	Looze, M.T. Murray, R.J. Esdaile	CRC for Alloy and Solidification Technology (CAST), Melbourne, Austraillia.	
The effects of thermal resistance at metal/mold interface on casting solidification	Chung-Whee Kim	A Report	

PERMANENT MOLD CASTING			
Title	**Author(s)**	**Journal**	**Date**
Comparison of Heat Transfer Parameters in Two Permanent Molds	D.R. Gunasegaram, T.T. Nguyen	CRC for Alloy and Solidification Technology (CAST) and CSIRO Division of Manufacturing Technology	1997
Experimental investigation and finite element modelling in gravity die casting	J.T. Anderson, D.T. Gethin, R.W. Lewis, J.T. Cross	Proc Instn Mech Engrs V. 211 Part B pp. 93-107	1997
Mould surface roughness and interfacial heat transfer using heat flow model	A.M. Assar	The Institute of Materials,1997, pp. 702-704	1997
A foundary-based experimental investigation into the effect of die coats in the gravity casting process	F. Bell, D.T> Gethin, J.T. Anderson	Cast Metals V. 8, No. 1, pp 51-56	1996
Determination of Heat Transfer Coefficient Between Casting and Chill in Unidirectional Heat Flow	M. Krishnan, D.G.R. Sharma	AFS Transactions 94-16, pp. 769-774	1994
Effect of Coating/Mold Wall/ Casting Thickness on Heat Transfer and Solidification of Al-Cu-Si- Allow (LM-21) in Cast Iron Molds	K.N. Prabhu, S.A. Kumar, N. Venkataraman	AFS Transactions, 94-109, pp. 827-832	1994
Thermal Expansion of Gases at the Metal/Mould Interface in Permanent-mould Casting	I.L. Svensson, P. Schmidt	Cast Metals V. 6, No. 3, 1993 pp 127-130	1993
Solidification of Pure Metal in Imperfect Contact with a Mold	Eisuke Niyama, Koicki Anzai	Metallurgical Transactions B, V. 24B, June pp. 542-544	1993

On the interfacial heat transfer coefficient for cylindrical ingot casting in a metal mould	Abdel-Wahed M. Assar	Journal of Materials Science Letters, V. 11 pp. 601-606	1992
Measurement of the thermal Conductance at the Mold/Metal Interface of Permanent Molds	F. Chiesa	AFS Transactions 90-10, pp. 193-200	1990
Solidification of Castings in Motallic Moulds	H.B. Naik, A.K. Dave	Communications in Applied Numerical Methods, V. 5, pp. 467-472	1989
Gating of a Permanent Mold Aluminum Plate Casting	Franco Chiesa, Gilles Asselin	Modern Casting, December pp. 24-25	1988
Variables Affecting the Nature of the Chill Zone	M. Prates, H. Biloni	Metallurgical Transactions, V. 3, June, pp. 1501-1510	1972
Heat Flow Parameters Affecting the Unidirectional Solidification of Pure Metals	M. Prates, J. Fissolo, H. Biloni	Metallurgical Transactions, V. 3, June, pp. 1419-1425	1972
Solidification and Heat Transfer In Permanent Mould casting	P. Schmidt, I. Svensson	Dept. Casting of Metals, Royal Institute of Technology, Stockholm, Sweeden	
Heat transfer in gravity die castings	V. de L. Davies		
Heat Transfer at Metal-Mould Interfaces	D.R. Gunasegaram, T.T. Nguyen, J. van der Touw	CRC for Alloy and Solidification Technology (CAST) and CSIRO Division of Manufacturing Technology pp. 91-96	

SAND CASTING			
Title	**Author(s)**	**Journal**	**Date**
Study and Application of Mold Filling Simulation of Shaped Casting	Baicheng Liu, Wei Qiu, Houfa Shen, Zhiqiang Gao	Journal of Materials Science Technology, V. 13, pp. 107-112	1997
Thermal Transport Phenomena in Metalcasting Simulations	H. Huang, O. Gurdogan, H.U. Akay	AFS Transactions, 95-95, pp. 243-252	1995
Heat transfer in moulds during continuous production of metal castings	D.GT. Thomas, G.A. Davies, D.J. Bell	Math. Engng. Ind., V. 5, No. 2, pp. 113-128	1995

Mould Filling and Solidification Simulation of the Bench Mark Casting	Z.A. Xu, F. Mampaey	Modelling of Casting, Welding and Advanced Solidification Processes VII, TMS, pp. 963-970	1995
A Mathematical Model for Air-gap Formation at the Metal-Mould Interface in the Computer Simulation of the Solidification of Al-12%Si in a Sand Mould	H.R. Shahverdi, F. Farhadi, A. Karimitaheri, P. Davami, K. Asgari	Cast Metals, V. 6, No. 4, pp. 231-237	1994
Measurement of heat Transfer Coefficient at Metal/Mold Interface During Casting	J.C. Hwang, H.T. Chuang, S.H. Jong, W.S. Hwang	AFS Transactions, 94-144, pp. 877-883	1994
Utilization of the Boundary Element Method for Numerical Analysis of Thermal Processes in the Casting-Mould System	E. Majchrzak	Proc 1, Intl. Conference on Computational Modeling of Free and Moving Boundary Problems, Computational Mechanics Publ, July 1991, pp. 223-237	1991
Mold/Metal Gap Formation of Aluminum Alloy 356 Cylinders Cast Horizontally in Dry and Green Sand	M.C. Lukens, T.X. Hou, R.D. Pehlke	AFS Transactions, 90-03, pp. 63-70	1990
Geometric Modeling of Casting Solidification	Teng-Shih Shih, Meng-Yen Li	Journal of the Chinese Society of Mechanical Engineers, V. 11, No. 1, pp. 75-84	1990
Metal and Mold Wall Movements During Solidification of Cast Iron	S. Engler, D. Boenisch, B. Kohler	AFS Cast Metals Research Journal, March 1973, pp. 20-30	1973

SQUEEZE CASTING

Title	Author(s)	Journal	Date
Evaluation of heat Transfer coefficients at the casting/die interface in squeeze casting	I.S.Cho and C.P.Hong	Int. J. Cast Metals Res., 1996, 9, 227-232	1996
A Finite Element Approach for modeling Metal flow and pressurized solidification in the Squeeze casting process	D.T.Gethin, R.W.Lewis and M.R.Tadayon	Int. J. for Num. Meth. In Eng.,vol.35, 939-950	1992